**Earth Sciences**
2019; 8(5): 235-267
http://www.sciencepublishinggroup.com/j/earth
doi: 10.11648/j.earth.20190805.11
ISSN: 2328-5974 (Print); ISSN: 2328-5982 (Online)

# Contrasting $TiO_2$ Compositions in Early Cenozoic Mafic Sills of the Faroe Islands: An Example of Basalt Formation from Distinct Melting Regimes

**Jógvan Hansen[1, *], Jon Davidson[1], Dougal Jerram[2, 3, 4], Christopher Ottley[1], Mike Widdowson[5]**

[1]Department of Earth Sciences, Durham University, Durham, United Kingdom

[2]The Centre for Earth Evolution and Dynamics (CEED), Oslo University, Oslo, Norway

[3]Dougalearth Ltd., Solihull, United Kingdom

[4]Earth, Environmental and Biological Sciences, Queensland University of Technology, Brisbane, Australia

[5]School of Environmental Science, University of Hull, Hull, United Kingdom

## Email address:

jogvanha@olivant.fo (J. Hansen), jogvan.hansen@dunelm.org.uk (J. Hansen), dougal@dougalearth.com (D. Jerram), c.j.ottley@durham.ac.uk (C. Ottley), m.widdowson@hull.ac.uk (M. Widdowson)

[*]Corresponding author

## To cite this article:

Jógvan Hansen, Jon Davidson, Dougal Jerram, Christopher Ottley, Mike Widdowson. Contrasting $TiO_2$ Compositions in Early Cenozoic Mafic Sills of the Faroe Islands: An Example of Basalt Formation from Distinct Melting Regimes. *Earth Sciences.* Vol. 8, No. 5, 2019, pp. 235-267. doi: 10.11648/j.earth.20190805.11

**Received**: August 14, 2019; **Accepted**: September 23, 2019; **Published**: October 9, 2019

**Abstract:** The Paleocene lava succession of the Faroe Islands Basalt Group (FIBG), which is a part of the North Atlantic Igneous Province (NAIP), is intruded by numerous basaltic sills. These can be grouped into three main categories according to their geochemical characteristics: A low-$TiO_2$ sill category ($TiO_2$ = 0.7-0.9), a relatively high-$TiO_2$ sill category ($TiO_2$ = 1.95-2.6) and an intermediate-$TiO_2$ sill that displays major element compositions lying between the other two categories. Mantle normalised plots for the high-$TiO_2$ and low-$TiO_2$ sills display relatively uniform flat LREE trends and slightly steeper HREE slopes for high-$TiO_2$ relative to low-$TiO_2$ sills. The intermediate-$TiO_2$ Morskranes Sill is LREE depleted. Mantle normalised trace elements of low-$TiO_2$ sill samples define positive Eu and Sr anomalies, whereas high-$TiO_2$ sill samples display negative anomalies for these same lements. Different Nb and Ta anomalies (positive versus negative) in many high-$TiO_2$ versus low-$TiO_2$ sill samples suggest various metasomatism of their sources prior to partial melting. The intermediate-$TiO_2$ sill displays noticeably lower $^{87}Sr/^{86}Sr$, $^{206}Pb/^{204}Pb$ and $^{208}Pb/^{204}Pb$ ratios relative to both the high-$TiO_2$ and the low-$TiO_2$ sill samples. Pb isotope compositions displayed by local co*ntaminated basaltic lavas imply that some of these assimilated distinct crustal material from E Greenland or basement from NW Britain, while others probably assimilated only distinct E Greenland type of crustal material. A third crustal source of E Greenland or Rockall-type basement could be required in order to explain some of the range in lead isotopes displayed by the intermediate-$TiO_2$ Morskranes Sill. Geochemical modelling suggest that Faroese high-$TiO_2$ sills, could have formed by ~4 to 7.5% batch melting of moderately fertile lherzolites, while 16 to 21% batch melting fertile mantle sources could explain geochemical compositions of Faroese low-$TiO_2$ sills. The intermediate-$TiO_2$ sill samples could have formed by a range of 6 to 7% batch melting of a depleted mantle source, probably with a composition comparable to sources that gave rise to local low-$TiO_2$ and intermediate-$TiO_2$ host-rocks. Most Faroese sill samples probably developed outside the garnet stabilitry field and probably formed by batch melting of mantle materials comparable in composition to those reported for the sub-continental lithospheric mantle (SCLM) previously at depths of ≤ 85 km. Relative enrichments in LREE (and LILE in general), and their varying Nb and Ta anomalies point to sources affected by metasomatism.

**Keywords:** North Atlantic, Faroe Islands, Flood Basalts, Sill Intrusion, Partial Melting, Fractional Crystallisation, Mineral Accumulation, Crustal Contamination

# 1. Introduction

Numerous hypotheses on the petrogenetic evolution of large basaltic igneous provinces (LIPs) such as the North Atlantic Igneous Province (NAIP) have been proposed earlier [1-2]. In order to distinguish between various units/suites within LIPs in general and flood basalts in particular, $TiO_2$ contents are commonly described [3-9]. Formation of low-$TiO_2$ basalts have at times been attributed to relatively large-degree melting of enriched material from the continental lithospheric mantle or else developed in response to melting of other mantle sources contaminated with subducted crust/sediments and/or associated expulsion of fluids [10-12]. Alternatively, they could also result from relatively large-degree melting (~20%) of depleted mantle sources [7-8]. By contrast, high-$TiO_2$ basaltic magmas probably form by relatively low-degree mantle melting from sources that may reside at relatively deeper mantle levels [9, 13, 14], or else the sources may originate from mantle plumes, perhaps owing some of their geochemical characteristics to recycled oceanic crust [8-11].

Within the NAIP, $TiO_2$ compositions have been widely used to distinguish their mainly basaltic compositions. Early Cenozoic high-$TiO_2$ basaltic rocks from W Greenland are interpreted to have developed by periodical replenishment-tapping-fractionation (RTF) processes from local low-$TiO_2$ basaltic melts, with plagioclase and clinopyroxene as the main fractionating assemblages and relatively high (16 to 20%) degrees of partial melting of a moderately depleted mantle have also been invoked [15]. Early Cenozoic basaltic rocks from E Greenland, which gave rise to high-$TiO_2$ basalts, presumably resulted from ~4 to ~8% mantle melting [16-17] compared to the 19 to 20% mantle melting probably needed to generate primary magmas that produced the low-$TiO_2$ basalts in parts of this region [17]. Compositional differences between their respective mantle sources likely affected the ultimate geochemistry of low-$TiO_2$ versus high-$TiO_2$ basaltic rocks of this region [17-18]. Heterogeneous mantle sources have been inferred for basaltic rocks from E Greenland [19-22]; W Greenland [15]; Iceland [21], NW Britain [22] and the Faroe Islands [7, 8, 9, 23]. In addition to geochemical variations of magma sources, variations in lithospheric thicknesses could in theory explain some of the spatial variations of $TiO_2$ magma types within the lava sequences of the Faroes [9]. Assimilation of crustal material during evolution of igneous products of the NAIP have been inferred to have contributed to the petrogenesis of basaltic rocks from E Greenland [19, 18, 24], W Greenland [15], NW Britain [25] and the Faroe Islands [7-26].

The lava successions of the Faroe Islands have been intruded by a number of sills. These provide insight to some of the later stages of magma generation. Although these sills have previously been characterised in terms of their geometries and stratigraphic relationships within the lava sequences [27], limited information exists regarding their petrogenesis, and in particular the likely sources of melting and how they may or may not relate to the lava sequences that they intersect. Understanding the later stages of magma generation during the evolution of the NAIP is desirable to better understand the wider temporal and spatial evolution of the province as a whole [2, 28, 29].

Accordingly, we focus on the compositions of primary magmas that ultimately evolved to the sills of the Faroe Islands. The sill samples are categorised according to major element compositions (especially $TiO_2$), trace elements (including REE) and isotopic compositions (Pb, Sr and Nd). The sills are then grouped into three main units defined primarily by their $TiO_2$ compositions. Their evolution is examined by partial melting modelling in order to help characterise their formation and mantle sources in terms of the degrees of melting and source rock compositions. The petrogenetic interpretations presented for the Faroese sills in this study are considered in the context of late-stage magmatic processes during the formation of the NAIP, and in particular we look at the effects of partial melting at relatively shallow mantle levels during the waning stages of basaltic magmatism in this LIP.

# 2. Geological Framework

The Faroe Islands Basalt Group (FIBG) was emplaced at the NW European margin as a central part of the contemporaneous NAIP magmatism [3, 30, 31, 32]. Geophysical studies suggest that the basaltic rocks of the Faroese block lie on ~30 km thick stretched ancient continental crust [33, 34, 35, 36], with total stratigraphic thickness of exposed and drilled lavas of this region of ~6.6 km [3, 32, 37, 38, 39] (Figure 1). The total extent onshore and offshore of these basaltic rocks have been estimated at ~120000 $km^2$ [32]. The Faroese lava succession was previously grouped into Upper, Middle and Lower Series basalts [3-38], but a revised nomenclature with seven formations was proposed recently [32]. From the bottom to top of the lava succession these are: the ~1075 m thick Lopra Formation; the ~3250 m thick Beinisvørð Formation; the ~9 m thick Prestfjall Formation; the 40-50 m thick Hvannhagi Formation; the 1250-1350 m thick Malinstindur Formation; the ~30 m thick Sneis Formation and finally the ~900 m thick Enni Formation [32-39] (Stratigraphic column Figure 1). Individual lava flows within the Beinisvørð, Malinstindur and Enni formations are often separated by thin volcaniclastic lithologies or weathering surfaces measuring a few centimetres, a few tens of centimetres and occasionally a few metres in thickness [32, 38, 39]. Basalts of the Beinisvørð Formation are generally aphyric whereas those of the Malinstindur and Enni formations include both olivine and plagioclase phyric rocks in addition to aphyric basalts [3, 32, 37]. Dating by the $^{40}Ar/^{39}Ar$ method has yielded ages of ~61 Ma for a lava sequence within the Beinisvørð Formation [42] and ~55 Ma for another lava sequence belonging to the Enni Formation [43]. An additional study on age(s) of Faroese lavas based on local palynoflora stated that the entire lava succession was deposited in the time span from 57.5 to 60.56 Ma [44].

Dykes are ubiquitous throughout the exposed parts of the lava succession while 'saucer-shaped' sills are confined to the uppermost parts of the Malinstindur Formation, the Sneis Formation and the lowermost parts of the Enni Formation [27, 32, 38, 39, 41] (Figure 1). High-$TiO_2$ lavas ($TiO_2$ >1.5 wt%) make up most of the volume in the lowermost ~5.5 km of the Faroese lava succession, while low-$TiO_2$ lavas ($TiO_2$ <1.5 wt%) become increasingly common in the remaining upper parts [3, 8, 9, 32, 37, 45, 46]. High-$TiO_2$ dykes and lavas of the Malinstindur and Enni formations are exposed throughout the archipelago, while low-$TiO_2$ dykes and lavas of these formations are most common in the northern parts of the islands [8-47]. Low-$TiO_2$ sills are exposed in the central parts of the Faroe Islands whereas high-$TiO_2$ sills are exposed in the N and NE parts of the archipelago [7-47]. A few lava flows of the Malinstindur Formation display anomalously high $SiO_2$ contents of ~54.0 wt% [26]. In the Beinisvørð Formation, clear stratigraphic trends of MgO and TiO2 contents are recorded and associated with large scale magma pulses [48]. However, in the Malinstindur and Enni Formations, the chemical stratigraphy is more erratic between individual lava flows irrespective of stratigraphic levels [8, 45, 46], and this has recently been demonstrated to relate to multiple inter-digitating lava flow packages fed from distinct magma batches [9].

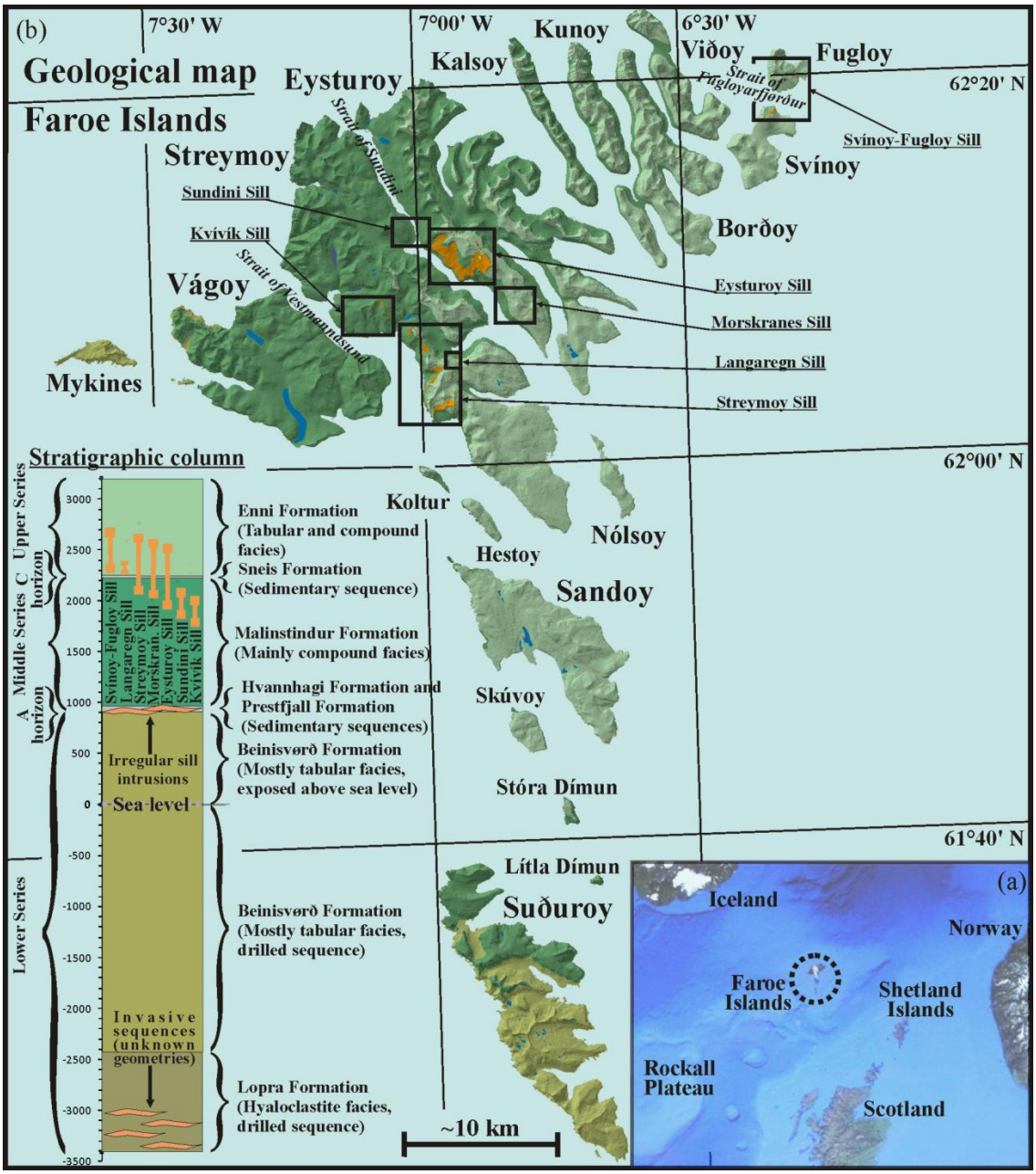


***Figure 1.*** *North Atlantic maps. (a) Relative location of the Faroe Islands. (b) The geological map shows the main basaltic formations of the Faroe Islands and sites of sill exposures. The stratigraphic column indicates the vertical extents of the actual sills and of local geological formations. Initial nomenclature from [3, 38, 40] is indicated to the left of the stratigraphic column, while the revised nomenclature from [39] is shown to the right. (The figure is modified from [27]).*

# 3. Previous Petrogenetic Models on Faroese Magmatism

Primary magmas that gave rise to high-$TiO_2$ basaltic dykes and lavas of the Faroe Islands are thought to have formed in response to 2.5 to 3.5% mantle melting compared to ~20% melting during production of primary magmas that yielded local low-$TiO_2$ rocks [7]. Relatively primitive samples of Faroese dykes and lavas fall on olivine control lines in plots of e.g. MgO versus $TiO_2$ [7]. Internal geochemical variations amongst relatively evolved basaltic rocks represented by local low-$TiO_2$ dykes have previously been interpreted in terms of low-pressure fractional crystallisation of olivine, plagioclase and clinopyroxene previously [47]. A scenario that also involved melting of a North Atlantic end-member mantle component (NAEM) was envisaged for Faroese basaltic lavas in a more recent study [8]. These authors further argued in favour of distinct sources for the low and high-Ti Faroese lavas. Most recently, a ne study identified four mantle sources to high-$TiO_2$ lavas of the Enni and Malinstindur formations and an additional source to low-$TiO_2$ lavas of the same formations [9].

Compositional variations in high-$TiO_2$ versus low-$TiO_2$ mantle sources have also been inferred for E Greenland [18-20] and Iceland [49]. Other authors have argued in favour of a depleted asthenospheric source to local LREE-depleted (low-$TiO_2$) basalts and a sub-continental lithospheric mantle or a deep mantle plume source to local LREE-enriched (high-$TiO_2$) basalts [23]. Coherent up-section variations in MgO, $TiO_2$, Y and Zr compositions within rocks of the Beinisvørð Formation led some authors to infer magma supplies from at least two independent volcanic systems [45]. Combined geochemical and isotopic characteristics of local contaminated basaltic lavas (~54 wt% $SiO_2$) have previously been explained in terms of contamination with Lewisian-type amphibolite facies gneisses [7-23]. While attributed non-linear isotopic trends of "common" tholeiitic Faroese lava/dyke samples could result from mild crustal contamination [23]; other authors have ascribed such insignificant variations to slight isotopic heterogeneities originating within their mantle sources [7]. Some authors have argued in favour of a trans-Atlantic chemostratigraphic correlation between units of the Nansen Fjord area in the central parts of E Greenland and sections of the Faroese lava pile [46-50]. However, a more recent study suggests that albeit the dominant progression of high-$TiO_2$ basaltic rocks in these regions appears broadly equivalent, these characteristics are not necessarily a direct indication of such a correlation, since Faroese high-$TiO_2$ lava flows can be chronostratigraphically constrained only on local (~10's km) scale [9]. They [9] argue that low-$TiO_2$ lava flows in these two regions could have been fed across a broader area of still relatively thick lithosphere associated with a strike-slip zone between the FIBG and Blosseville Kyst region of East Greenland.

The new data sets introduced in this paper present additional constraints on the nature of mantle sources and petrogenetic processes involved during the final known phases of magmatism in the Faroese region that ultimately resulted in the emplacement of sills within the volcanic successions. Our study provides both propositions regarding igneous processes acting during waning stages of NAIP formation and more general implications for LIP formation.

# 4. Petrography, Geochemistry and Isotope Geology of the Faroese Sills

### *4.1. Petrography*

Samples were collected from 7 Faroes sills, as well as from a number of selected local dykes and irregular intrusions in order to further constrain the petrogenesis of the magmas: Previous work [27-41] outline locations of sills and collected samples. Petrographically, the Faroese sills comprise ca. 40 to 55% plagioclase, 40 to 45% clinopyroxene, 5 to 10% olivine and 3 to 10% Fe/Ti oxides. More specifically, the Streymoy and Kvívík sills are feldspar-phyric; the Langaregn Sill is feldspar- and olivine-phyric; the Eysturoy and Sundini sills display intergranular texture, but clinopyroxene oikocrysts are also common within these; the Svínoy-Fugloy and Morskranes sills both display ophitic to sub-ophitic textures. Late clinopyroxene crystallisation is suggested by the ophitic/subophitic texture in the Svínoy-Fugloy and Morskranes sills in particular, but also to some degree in the Eysturoy Sill. Early olivine crystallisation is suggested by the occurrences of partly altered large olivine phenocrysts in the Streymoy and Kvívík sills and by the presence of olivine microphenocrysts occurring as inclusions within larger plagioclase grains of the Langaregn Sill. The occurrences of plagioclase grains in feeder dykes, which display increasing degrees of resorption with increasing distances from contacts with their host-rocks, seem to suggest that Ca-rich plagioclases were dominating early crystallisation phases, which subsequently reacted with surrounding melts to produce fine grained Na-rich plagioclases and clinopyroxenes. Earlier studies on basalts of the Faroe Islands have indicated olivine compositions of $Fo_{86-88}$ in low-$TiO_2$ basalts and $Fo_{72-73}$ in high-$TiO_2$ basalts whereas $An_{64-70}$ has been measured for plagioclases representing both these rock types [7].

See Supplement 1 [51] for further details on petrography.

### *4.2. Analytical Methods*

Following careful selection, 56 rock samples representing 7 Faroese sills and a number of local dykes and irregular intrusions selected for analysis, then crushed and milled according to standard methods in preparation for analysis. Major elements and selected trace elements representing 44 sill samples (Table 1) and 12 dyke and irregular intrusion samples (Table C in Supplement 3 [51] were determined on rock powder fused to glass discs and pressed powder tablets

respectively using an ARL 8420+ dual goniometer wavelength dispersive XRF spectrometer at the Department of Earth Sciences, Open University, Milton Keynes, UK. Major elements representing 3 additional samples from the Sundini and Morskranes sills were analysed at the Geological Survey of Norway (NGU), using a PANalytical Axios 4 kW. For further details see Supplement 2 [51].

Trace elements and REEs representing 14 sill samples (Table 2) and 8 dyke and irregular intrusion samples (Supplement 3 [51]) were determined on powdered rock samples were carried out on an Elan 6000 Perkin Elmer-Sciex inductively coupled plasma mass spectrometer (ICP-MS) at the Arthur Holmes Trace Element Laboratory, Department of Earth Sciences, Durham University, UK (for preparation and analytical methods see supplement 3 [51]). In addition, trace elements for a further three sill samples (Table 2) were determined using a modified version of the dissolution procedure as described in [52-53]. These analyses were carried out at GEUS, Denmark, by inductively coupled plasma mass spectrometry (ICP-MS) using a Perkin-Elmer Elan 6100 DRC quadrupole ICP-MS instrument. For further details see Supplement 2 [51].

Sr and Nd isotope ratios for 8 selected sill samples and Pb isotope ratios of 7 selected sill samples (Table 3) were determined according to the preparation methods described in [54-55]. Sr and Nd fractions were taken up in 1ml of 3% $HNO_3$ separately and introduced into a mass spectrometer using an ESI PFA50 nebuliser and a dual cyclonic–Scott Double Pass spraychamber. Pb samples were taken up in 1ml of 3% $HNO_3$ and spiked with Tl prior to introduction into a mass spectrometer using an ESI PFA50 nebuliser and a dual cyclonic–Scott Double Pass spraychamber. All isotopes were analysed on a ThermoElectron Neptune Multi-collector Plasma Mass Spectrometer (MC-ICP-MS) at the Arthur Holmes Isotope Geology Laboratory, Durham University, UK.

Whole-rock MC-ICP-MS lead isotope analyses were carried out on 6 additional sill samples on a VG Sector 54-IT TIMS at the Geological Institute, University of Copenhagen, Denmark (Table 3). Dissolution of the powdered samples was achieved in two successive, but identical steps, which consisted of a strong 8 N HBr attack that has been shown to effectively dissolve accessory phosphates [56-57], followed by a concentrated HF-14 N $HNO_3$ mixture, and finally by strong 9 N HCl. Chemical separation of Pb from whole rocks was performed over conventional glass stem and subsequently miniature glass-stem anion exchange columns containing, respectively 1 ml and 200 µl 100–200 mesh Bio-Rad AG 1×8 resin. Lead was analyzed in a static multi-collection-mode where fractionation was controlled by repeated analysis of the NBS 981 standard using values in [58]. For further details see Supplement 2 [51].

### *4.3. Geochemistry*

#### *4.3.1. Major Elements*

The 47 Faroese sill samples analysed for major elements (Table 1; Figure 2) display $SiO_2$ contents ranging from 47.5 to 50.5 wt%, while their combined $Na_2O$ and $K_2O$ contents range from 1.9 to 2.9 wt%, thus indicating subalkaline or tholeiitic composition basalts. The MgO contents for all Faroese sills combined range from ~6.15 to ~8.2 wt%. Here, the range in MgO for the Morskranes Sill is ~7 to ~8.2 wt%, which is a much wider MgO spread than are displayed by any of the other local individual sills. The sills define three main categories according to their $TiO_2$ contents. Here, samples of the Kvívík and Streymoy sills display low $TiO_2$ contents ranging from 0.7 to 0.9 wt%, while samples of the Eysturoy, Langaregn, Sundini and the Svínoy-Fugloy sills exhibit high $TiO_2$ contents spanning from 1.95 to 2.6 wt% (Figure 2). Morskranes Sill samples display intermediate $TiO_2$ contents of ~1.20 wt%. The Kvívík and Streymoy sills display relatively high $Al_2O_3$ and CaO, while the Eysturoy, Langaregn, Sundini and Svínoy-Fugloy sills exhibit relatively high $Na_2O$ and $Fe_2O_3$. Major elements such as $Al_2O_3$, $Fe_2O_3$ and CaO of the intermediate-$TiO_2$ Morskranes Sill plot in between those of the low-$TiO_2$ and the high-$TiO_2$ sill categories (Table 1; Figure 2). Generally, the compositional range of major elements representing the investigated intrusions generally correlate well with published major element data on Faroese lava/dyke samples and with lava/dyke data obtained in this work (Supplement 3 [51]); however, the Streymoy and Kvívík sills in particular display higher $SiO_2$, $Al_2O_3$ and CaO contents and lower $TiO_2$ and $Fe_2O_3$ contents when compared to host-rock lava/dyke samples with comparable MgO contents (insets in Figure 2). More specifically, the published host-rock data show that most local basaltic lavas/dykes display $SiO_2$ contents ranging from ~47 to ~49.5 wt%, their MgO generally range from ~7 to ~9 wt% (their entire MgO range span from ~4.5 to ~23 wt%), while their $TiO_2$ contents range from ~0.6 to ~4.0 wt% [3, 7, 8, 45-47].

***Table 1.*** *Whole rock XRF data on major and selected trace elements representing basaltic sills of the Faroe Islands (Analysed by John Watson, OU, UK, and Ana Banica, NGU, NO).*

| Sample | Sill | | | | | | | |
|---|---|---|---|---|---|---|---|---|
| | 09-JSS-02 | 07-JSS-21 | 07-JSS-23 | 08-JSS-24 | 07-JSS-26 | 07-JSS-28 | 07-JSS-29 | 08-JSS-29 |
| **Wt.%** | **Sill** | **Sill** | **Sill** | **Sill** | **Sill** | **Sill** | **Sill** | **Sill** |
| $SiO_2$ | 49.05 | 49.58 | 49.55 | 50.00 | 49.64 | 49.19 | 49.23 | 49.55 |
| $TiO_2$ | 0.76 | 0.76 | 0.75 | 0.80 | 0.79 | 0.76 | 0.78 | 0.78 |
| $Al_2O_3$ | 17.04 | 16.90 | 17.75 | 16.90 | 16.61 | 17.00 | 17.15 | 16.51 |
| $Fe_2O_3$ | 9.91 | 10.13 | 9.68 | 10.25 | 10.35 | 9.99 | 10.06 | 10.34 |
| MnO | 0.16 | 0.16 | 0.16 | 0.16 | 0.17 | 0.16 | 0.16 | 0.17 |
| MgO | 6.74 | 6.92 | 6.56 | 7.03 | 6.93 | 6.73 | 6.76 | 6.92 |
| CaO | 12.98 | 13.07 | 13.40 | 13.18 | 13.01 | 13.08 | 13.07 | 13.11 |

| Sample | Sill | | | | | | | |
|---|---|---|---|---|---|---|---|---|
| | 09-JSS-02 | 07-JSS-21 | 07-JSS-23 | 08-JSS-24 | 07-JSS-26 | 07-JSS-28 | 07-JSS-29 | 08-JSS-29 |
| **Wt.%** | **Sill** | **Sill** | **Sill** | **Sill** | **Sill** | **Sill** | **Sill** | **Sill** |
| $Na_2O$ | 1.88 | 1.96 | 1.87 | 1.95 | 1.96 | 1.92 | 1.93 | 1.92 |
| $K_2O$ | 0.20 | 0.21 | 0.21 | 0.21 | 0.22 | 0.21 | 0.22 | 0.21 |
| $P_2O_5$ | 0.08 | 0.08 | 0.08 | 0.08 | 0.08 | 0.08 | 0.08 | 0.08 |
| [a]LOI | 0.14 | 0.33 | 0.45 | 0.11 | 0.19 | 0.28 | 0.27 | 0.19 |
| Total | 98.92 | 100.11 | 100.46 | 100.67 | 99.95 | 99.40 | 99.71 | 99.77 |
| ppm | | | | | | | | |
| Sr | 197 | 199 | 205 | 195 | 199 | 196 | 196 | 190 |
| Y | 16 | 18 | 16 | 18 | 18 | 17 | 18 | 18 |
| Zr | 50 | 50 | 49 | 49 | 52 | 49 | 51 | 51 |
| Nb | 3.4 | 2.7 | 2.8 | 2.8 | 3.1 | 3.4 | 3.1 | 2.8 |
| Ba | 64 | 66 | 63 | 67 | 75 | 66 | 66 | 64 |
| Sc | 36 | 37 | 35 | 43 | 39 | 34 | 40 | 38 |
| V | 242 | 228 | 229 | 251 | 247 | 228 | 250 | 252 |
| Cr | 181 | 176 | 166 | 200 | 184 | 170 | 182 | 179 |
| Ni | 80 | 78 | 73 | 86 | 81 | 78 | 76 | 77 |
| Cu | 118 | 110 | 114 | 114 | 122 | 113 | 113 | 106 |
| Zn | 56 | 56 | 53 | 60 | 60 | 54 | 58 | 58 |
| $Y/TiO_2$ | 21.67 | 24.03 | 21.73 | 22.41 | 22.81 | 22.65 | 23.31 | 23.74 |
| Zr/Y | 3.06 | 2.7 | 3.01 | 2.72 | 2.91 | 2.87 | 2.8 | 2.76 |
| Nb/Y | 0.21 | 0.15 | 0.17 | 0.16 | 0.17 | 0.2 | 0.17 | 0.15 |

| Sample Wt.% | Sill | | | | Streymoy | | | |
|---|---|---|---|---|---|---|---|---|
| | 07-JSS-38 | 07-JSS-39 | 07-JSS-40 | 07-JSS-42 | 07-JSS-43 | 07-JSS-44 | 07-JSS-45 | 07-JSS-52 |
| $SiO_2$ | 47.80 | 49.70 | 49.42 | 49.37 | 49.67 | 50.29 | 50.44 | 50.29 |
| $TiO_2$ | 1.13 | 0.78 | 0.73 | 0.76 | 0.76 | 0.77 | 0.82 | 0.82 |
| $Al_2O_3$ | 14.76 | 16.68 | 17.55 | 16.71 | 17.41 | 17.45 | 17.03 | 16.95 |
| $Fe_2O_3$ | 12.05 | 10.27 | 9.65 | 10.27 | 9.93 | 10.01 | 10.34 | 10.42 |
| MnO | 0.19 | 0.17 | 0.16 | 0.16 | 0.16 | 0.16 | 0.17 | 0.17 |
| MgO | 8.46 | 6.94 | 6.74 | 6.86 | 6.83 | 6.83 | 6.92 | 6.86 |
| CaO | 12.96 | 13.09 | 13.31 | 13.22 | 13.40 | 13.25 | 13.13 | 13.22 |
| $Na_2O$ | 1.89 | 1.93 | 1.91 | 1.91 | 1.91 | 1.93 | 1.95 | 2.00 |
| $K_2O$ | 0.06 | 0.19 | 0.20 | 0.19 | 0.20 | 0.20 | 0.22 | 0.20 |
| $P_2O_5$ | 0.09 | 0.08 | 0.07 | 0.07 | 0.08 | 0.08 | 0.08 | 0.09 |
| [a]LOI | 0.43 | 0.11 | 0.18 | 0.23 | 0.32 | 0.26 | 0.46 | 0.14 |
| Total | 99.81 | 99.95 | 99.91 | 99.73 | 100.67 | 101.24 | 101.58 | 101.17 |
| ppm | | | | | | | | |
| Sr | 113 | 197 | 203 | 180 | 198 | 193 | 189 | 198 |
| Y | 27 | 18 | 16 | 18 | 17 | 17 | 18 | 19 |
| Zr | 58 | 52 | 46 | 46 | 47 | 48 | 50 | 53 |
| Nb | 2.2 | 3.1 | 2.8 | 2.9 | 3 | 2.4 | 2.8 | 2.9 |
| Ba | 25 | 69 | 65 | 54 | 63 | 57 | 59 | 72 |
| Sc | 46 | 39 | 36 | 37 | 36 | 38 | 37 | 38 |
| V | 298 | 254 | 228 | 248 | 218 | 247 | 244 | 244 |
| Cr | 359 | 176 | 183 | 174 | 175 | 181 | 178 | 168 |
| Ni | 132 | 79 | 74 | 79 | 85 | 86 | 81 | 74 |
| Cu | 137 | 118 | 107 | 127 | 114 | 114 | 122 | 115 |
| Zn | 74 | 60 | 55 | 60 | 52 | 59 | 59 | 59 |
| $Y/TiO_2$ | 23.89 | 22.59 | 22.25 | 23.31 | 22.72 | 21.39 | 21.46 | 22.57 |
| Zr/Y | ------- | 2.94 | 2.82 | 2.57 | 2.73 | 2.89 | 2.82 | 2.83 |
| Nb/Y | ------- | 0.18 | 0.17 | 0.16 | 0.17 | 0.15 | 0.16 | 0.16 |

| Sample | Streymoy Sill | | | | | | Kvívík Sill | | |
|---|---|---|---|---|---|---|---|---|---|
| | 07-JSS-55 | 07-JSS-57 | 07-JSS-58 | 07-JSS-09 | 09-JSS-09 | 09-JSS-10 | 08-JKS-05 | 08-JKS-18 | 07-JSS-49 |
| **Wt.%** | **Sill** | **Sill** | **Sill** | **F. Dyke** | **F. Dyke** | **F. Dyke** | **Sill** | **Sill** | **Sill** |
| $SiO_2$ | 50.27 | 49.56 | 49.67 | 49.39 | 50.00 | 49.98 | 49.15 | 49.04 | 49.51 |
| $TiO_2$ | 0.75 | 0.80 | 0.71 | 0.79 | 0.81 | 0.79 | 0.79 | 0.76 | 0.76 |
| $Al_2O_3$ | 17.72 | 16.90 | 17.82 | 16.50 | 17.02 | 17.11 | 16.74 | 16.85 | 17.16 |
| $Fe_2O_3$ | 9.68 | 10.37 | 9.53 | 10.57 | 10.41 | 10.36 | 10.47 | 10.20 | 10.11 |
| MnO | 0.16 | 0.17 | 0.15 | 0.17 | 0.17 | 0.17 | 0.17 | 0.17 | 0.17 |

| Sample | Streymoy Sill | | | | | | Kvívík Sill | | |
|---|---|---|---|---|---|---|---|---|---|
| | 07-JSS-55 | 07-JSS-57 | 07-JSS-58 | 07-JSS-09 | 09-JSS-09 | 09-JSS-10 | 08-JKS-05 | 08-JKS-18 | 07-JSS-49 |
| **Wt.%** | **Sill** | **Sill** | **Sill** | **F. Dyke** | **F. Dyke** | **F. Dyke** | **Sill** | **Sill** | **Sill** |
| MgO | 7.21 | 6.70 | 6.79 | 6.63 | 6.75 | 6.65 | 6.60 | 6.68 | 6.81 |
| CaO | 13.35 | 12.86 | 13.50 | 13.31 | 13.38 | 13.27 | 13.07 | 13.46 | 13.42 |
| $Na_2O$ | 1.96 | 2.00 | 1.91 | 1.91 | 1.88 | 1.86 | 1.91 | 1.82 | 1.89 |
| $K_2O$ | 0.22 | 0.23 | 0.20 | 0.14 | 0.09 | 0.18 | 0.20 | 0.10 | 0.18 |
| $P_2O_5$ | 0.08 | 0.09 | 0.08 | 0.07 | 0.08 | 0.08 | 0.08 | 0.07 | 0.07 |
| [a]LOI | 0.39 | 0.17 | 0.20 | 0.36 | 0.28 | 0.17 | 0.27 | 0.50 | 0.24 |
| Total | 101.78 | 99.86 | 100.57 | 99.84 | 100.88 | 100.62 | 99.46 | 99.64 | 100.31 |
| ppm | | | | | | | | | |
| Sr | 195 | 202 | 200 | 176 | 181 | 181 | 185 | 180 | 178 |
| Y | 17 | 19 | 16 | 19 | 18 | 18 | 18 | 18 | 18 |
| Zr | 47 | 52 | 46 | 48 | 51 | 50 | 50 | 46 | 47 |
| Nb | 2.7 | 3 | 2.3 | 2.6 | 3.5 | 4 | 3.6 | 2.8 | 2.7 |
| Ba | 65 | 74 | 64 | 55 | 34 | 55 | 55 | 43 | 60 |
| Sc | 34 | 36 | 33 | 43 | 39 | 37 | 39 | 39 | 37 |
| V | 217 | 236 | 214 | 252 | 250 | 254 | 260 | 252 | 238 |
| Cr | 189 | 159 | 178 | 171 | 162 | 166 | 154 | 170 | 162 |
| Ni | 81 | 75 | 74 | 80 | 83 | 80 | 79 | 79 | 77 |
| Cu | 106 | 117 | 99 | 131 | 133 | 128 | 129 | 127 | 121 |
| Zn | 53 | 57 | 52 | 65 | 64 | 61 | 60 | 62 | 56 |
| $Y/TiO_2$ | 22.82 | 23.57 | 23.02 | 23.82 | 22.61 | 22.19 | 23.15 | 23.94 | 24.05 |
| Zr/Y | 2.71 | 2.77 | 2.81 | 2.54 | 2.77 | 2.82 | 2.71 | 2.55 | 2.59 |
| Nb/Y | 0.16 | 0.16 | 0.14 | 0.14 | 0.19 | 0.23 | 0.2 | 0.15 | 0.15 |

| Sample | Langaregn Sill | | Sundini Sill | | | | [b]Ey. S. |
|---|---|---|---|---|---|---|---|
| | 07-JSS-50 | 07-JSS-51 | 08-JES-01 | 09-JH-01 | 09-JH-05 | 16-JSuS-02 | 08-JES-03 |
| **Wt.%** | **Sill** | **Sill** | **Sill** | **Sill** | **Dyke** | **[c]Sill** | **Sill** |
| $SiO_2$ | 48.86 | 48.84 | 49.44 | 49.43 | 49.11 | 49.20 | 50.28 |
| $TiO_2$ | 2.58 | 2.51 | 2.12 | 2.19 | 2.84 | 2.20 | 2.07 |
| $Al_2O_3$ | 13.80 | 13.81 | 13.43 | 13.40 | 13.83 | 13.10 | 13.54 |
| $Fe_2O_3$ | 14.97 | 14.79 | 15.16 | 14.92 | 14.05 | 15.30 | 14.60 |
| MnO | 0.21 | 0.22 | 0.21 | 0.22 | 0.19 | 0.22 | 0.21 |
| MgO | 6.47 | 6.35 | 6.32 | 6.16 | 6.84 | 6.11 | 6.47 |
| CaO | 10.80 | 10.76 | 11.01 | 10.85 | 10.41 | 10.60 | 11.15 |
| $Na_2O$ | 2.36 | 2.36 | 2.34 | 2.38 | 2.30 | 2.43 | 2.36 |
| $K_2O$ | 0.20 | 0.25 | 0.31 | 0.30 | 0.36 | 0.31 | 0.33 |
| $P_2O_5$ | 0.24 | 0.24 | 0.21 | 0.23 | 0.26 | 0.23 | 0.21 |
| [a]LOI | 0.01 | -0.23 | -0.12 | -0.29 | -0.19 | 0.31 | 0.07 |
| Total | 100.51 | 99.90 | 100.45 | 99.79 | 99.99 | 100.00 | 101.29 |
| ppm | | | | | | | |
| Sr | 255 | 253 | 170 | 176 | ----- | ----- | 169 |
| Y | 34 | 34 | 38 | 38 | ----- | ----- | 37 |
| Zr | 166 | 164 | 139 | 145 | ----- | ----- | 132 |
| Nb | 13 | 13 | 11 | 11 | ----- | ----- | 9.5 |
| Ba | 73 | 66 | 89 | 91 | ----- | ----- | 90 |
| Sc | 41 | 39 | 48 | 41 | ----- | ----- | 47 |
| V | 378 | 392 | 419 | 433 | ----- | ----- | 422 |
| Cr | 148 | 140 | 59 | 52 | ----- | ----- | 65 |
| Ni | 94 | 94 | 68 | 63 | ----- | ----- | 64 |
| Cu | 192 | 216 | 253 | 264 | ----- | ----- | 228 |
| Zn | 104 | 106 | 97 | 100 | ----- | ----- | 94 |
| $Y/TiO_2$ | 13.00 | 13.53 | 17.69 | 17.20 | ----- | ----- | 17.71 |
| Zr/Y | 4.93 | 4.82 | 2.69 | 3.86 | ----- | ----- | 3.6 |
| Nb/Y | 0.38 | 0.37 | 0.29 | 0.29 | ----- | ----- | 0.26 |

| Sample | Eysturoy Sill | | | | | | | |
|---|---|---|---|---|---|---|---|---|
| | 08-JES-04 | 08-JES-07 | 08-JES-08 | 08-JES-10 | 08-JES-11 | 08-JES-19 | 08-JES-20 | 09-JES-08 |
| **Wt.%** | **Sill** | **Sill** | **Sill** | **Sill** | **Sill** | **Sill** | **Sill** | **F.Dyke** |
| $SiO_2$ | 49.67 | 49.27 | 49.69 | 49.23 | 49.59 | 49.33 | 49.28 | 49.13 |
| $TiO_2$ | 2.11 | 1.97 | 2.09 | 2.06 | 2.01 | 2.13 | 2.06 | 2.16 |
| $Al_2O_3$ | 13.47 | 13.26 | 13.22 | 13.41 | 13.39 | 13.31 | 13.34 | 13.54 |

| Sample | Eysturoy Sill | | | | | | | |
|---|---|---|---|---|---|---|---|---|
| | 08-JES-04 | 08-JES-07 | 08-JES-08 | 08-JES-10 | 08-JES-11 | 08-JES-19 | 08-JES-20 | 09-JES-08 |
| **Wt.%** | **Sill** | **Sill** | **Sill** | **Sill** | **Sill** | **Sill** | **Sill** | **F.Dyke** |
| $Fe_2O_3$ | 14.99 | 14.62 | 14.94 | 13.48 | 14.94 | 14.69 | 15.13 | 14.89 |
| MnO | 0.22 | 0.21 | 0.22 | 0.22 | 0.22 | 0.22 | 0.22 | 0.22 |
| MgO | 6.25 | 6.23 | 6.18 | 6.26 | 6.55 | 6.22 | 6.46 | 6.26 |
| CaO | 10.91 | 10.87 | 10.83 | 10.75 | 11.19 | 11.07 | 11.16 | 11.10 |
| $Na_2O$ | 2.45 | 2.37 | 2.39 | 2.32 | 2.33 | 2.34 | 2.32 | 2.32 |
| $K_2O$ | 0.34 | 0.36 | 0.32 | 0.57 | 0.30 | 0.26 | 0.31 | 0.23 |
| $P_2O_5$ | 0.22 | 0.22 | 0.22 | 0.21 | 0.20 | 0.22 | 0.21 | 0.22 |
| [a]LOI | 0.06 | 0.07 | -0.10 | 0.07 | 0.09 | -0.09 | -0.15 | -0.17 |
| Total | 100.67 | 99.44 | 100.01 | 100.65 | 100.04 | 100.56 | 100.15 | 100.10 |
| Ppm | | | | | | | | |
| Sr | 174 | 167 | 170 | 168 | 171 | 174 | 170 | 175 |
| Y | 37 | 37 | 38 | 36 | 35 | 36 | 36 | 37 |
| Zr | 138 | 139 | 141 | 135 | 125 | 141 | 134 | 142 |
| Nb | 11 | 10 | 10 | 8.9 | 9.2 | 10 | 10 | 11 |
| Ba | 88 | 88 | 96 | 101 | 95 | 84 | 90 | 79 |
| Sc | 43 | 44 | 43 | 44 | 44 | 45 | 45 | 45 |
| V | 426 | 419 | 426 | 427 | 413 | 432 | 418 | 425 |
| Cr | 59 | 63 | 60 | 66 | 66 | 62 | 72 | 58 |
| Ni | 58 | 64 | 61 | 61 | 60 | 64 | 63 | 66 |
| Cu | 236 | 243 | 236 | 221 | 208 | 257 | 219 | 250 |
| Zn | 93 | 98 | 101 | 95 | 91 | 101 | 95 | 95 |
| $Y/TiO_2$ | 17.46 | 18.89 | 18.04 | 17.61 | 17.28 | 17.08 | 17.25 | 17.11 |
| Zr/Y | 3.76 | 3.72 | 3.73 | 3.71 | 3.61 | 3.87 | 3.75 | 3.83 |
| Nb/Y | 0.29 | 0.27 | 0.26 | 0.25 | 0.27 | 0.28 | 0.29 | 0.29 |

| Sample | Morskranes Sill | | | | | Svínoy-Fugloy Sill | | |
|---|---|---|---|---|---|---|---|---|
| | 08-JMS-14 | 08-JMS-16 | 08-JMS-17 | 16-JMS-18 | 16-JMS-19 | 08-JFS-21 | 08-JSVS-22 | 08-JSVS-23 |
| **Wt.%** | **Sill** | **Sill** | **Sill** | **[c]Sill** | **[c]Sill** | **Sill** | **Sill** | **Sill** |
| $SiO_2$ | 48.73 | 48.87 | 47.65 | 48.30 | 47.90 | 48.37 | 48.49 | 48.58 |
| $TiO_2$ | 1.20 | 1.20 | 1.21 | 1.20 | 1.16 | 2.09 | 2.10 | 2.10 |
| $Al_2O_3$ | 15.19 | 14.48 | 13.83 | 14.60 | 14.30 | 13.89 | 13.54 | 13.86 |
| $Fe_2O_3$ | 14.85 | 12.33 | 12.66 | 12.50 | 12.50 | 12.83 | 14.37 | 14.22 |
| MnO | 0.21 | 0.20 | 0.21 | 0.21 | 0.19 | 0.21 | 0.21 | 0.20 |
| MgO | 7.06 | 8.09 | 8.22 | 7.25 | 7.81 | 7.00 | 7.07 | 6.95 |
| CaO | 13.26 | 12.86 | 11.86 | 12.60 | 12.50 | 11.74 | 11.66 | 11.77 |
| $Na_2O$ | 1.95 | 1.86 | 1.68 | 2.02 | 1.92 | 2.26 | 2.18 | 2.26 |
| $K_2O$ | 0.04 | 0.03 | 0.79 | 0.07 | 0.04 | 0.17 | 0.15 | 0.18 |
| $P_2O_5$ | 0.10 | 0.10 | 0.10 | 0.09 | 0.09 | 0.19 | 0.19 | 0.19 |
| [a]LOI | 0.64 | 0.61 | 2.01 | 1.03 | 0.86 | -0.22 | 0.00 | -0.22 |
| Total | 99.85 | 100.70 | 100.95 | 99.80 | 99.20 | 100.39 | 100.08 | 99.80 |
| Ppm | | | | | | | | |
| Sr | 88 | 86 | 94 | ----- | ----- | 215 | 213 | 214 |
| Y | 29 | 27 | 29 | ----- | ----- | 29 | 28 | 29 |
| Zr | 63 | 61 | 62 | ----- | ----- | 124 | 117 | 126 |
| Nb | 2.7 | 1.9 | 2 | ----- | ----- | 9.7 | 9.7 | 10 |
| Ba | 19 | 18 | 25 | ----- | ----- | 56 | 64 | 63 |
| Sc | 49 | 44 | 45 | ----- | ----- | 39 | 39 | 38 |
| V | 350 | 326 | 349 | ----- | ----- | 352 | 359 | 371 |
| Cr | 361 | 344 | 352 | ----- | ----- | 215 | 237 | 228 |
| Ni | 119 | 109 | 112 | ----- | ----- | 100 | 118 | 101 |
| Cu | 173 | 157 | 132 | ----- | ----- | 194 | 203 | 210 |
| Zn | 83 | 77 | 77 | ----- | ----- | 89 | 92 | 93 |
| $Y/TiO_2$ | 23.70 | 22.73 | 23.67 | ----- | ----- | 14.00 | 13.28 | 13.93 |
| Zr/Y | 2.22 | 2.25 | 2.17 | ----- | ----- | 4.23 | 4.2 | 4.32 |
| Nb/Y | 0.09 | 0.07 | 0.07 | ----- | ----- | 0.33 | 0.35 | 0.36 |

Major elements are in weight percent and trace elements are in parts per million. Total iron is given as $Fe_2O_3$. Sample 07-JSS-38 represents a weathered basaltic rock specimen. The abbreviation F. Dyke refers to feeder dyke. [a]LOI indicates loss on ignition. [b]Ey. S. refers to the Eysturoy Sill. [c]Sill refer to samples analysed at NGU, Norway.

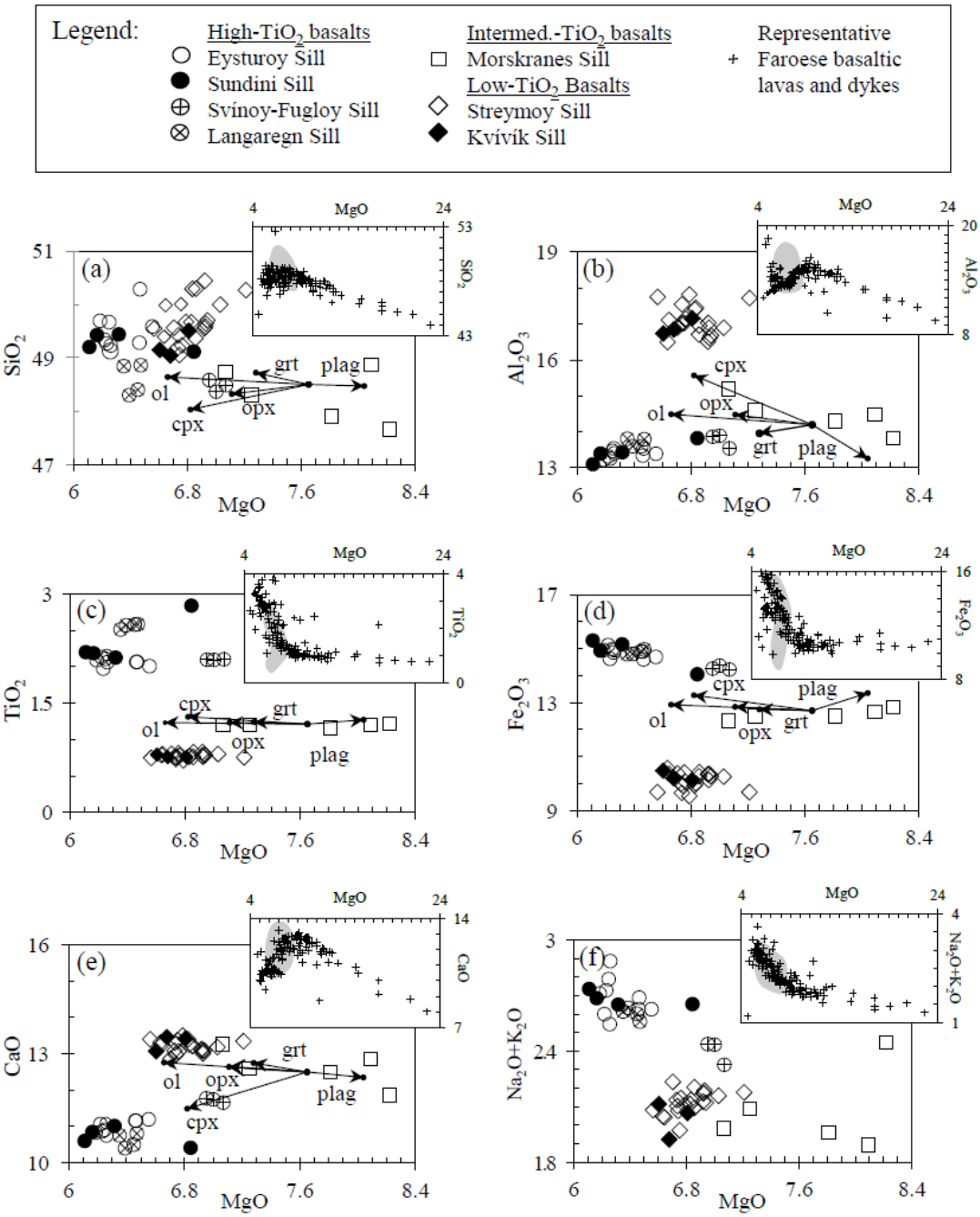


***Figure 2.*** *The diagrams show bivariate plots of major element data from Table 1. The Faroese sills define three main categories (high-$TiO_2$, intermediate-$TiO_2$ and low-$TiO_2$), albeit somewhat scattered for the intermediate $TiO_2$ and high-$TiO_2$ specimen. The vectors in sub-figures (a) to (e) represent calculated crystallisation trends with ol = 2 wt%, opx = 2 wt%, cpx = 10 wt%, plag = 5 wt% and grt = 3 wt% fractional crystallisation. Vector calculations are based on major element compositions from the compilation in [59]. Insets show major element compositions representing local lavas and dykes (black crosses) and range in compositions of Faroese sills (semi-transparent grey fields). Data on Faroese lavas and dykes are from [7, 8, 45, 46, 47] and from this study (see Supplement 3 [51] for host-rock data from this study). plag = plagioclase; other abbreviations are as shown in the ref. in caption to Figure 8 below. Datasets on calculated crystallisation trends are shown in the ref. as indicated in caption to Figure 6 below.*

#### *4.3.2. Selected Trace Elements*

Mantle-normalised trace element data from 17 representative sill samples (Table 2; Figure 3) define three main tendencies. The low-$TiO_2$ and high-$TiO_2$ sills generally display separate well-defined, relatively flat sub-parallel trends with the latter being comparatively more enriched in most elements; by contrast, the intermediate $TiO_2$ content sill generally exhibits a gradual depletion towards the most incompatible elements (Figure 3a). All sills display negative P anomalies and some samples of the intermediate $TiO_2$ sill are characterised by distinctive positive and moderately negative Rb and K anomalies. The low-$TiO_2$ sill samples display relatively uniform positive Ba, Rb, Th, K and Sr anomalies, whereas most of the high-$TiO_2$ sill samples exhibit negative anomalies for these same elements (Figure 3). It is clear however, that some relative differences in these

elements exist internally within the high-$TiO_2$ sills, where the Eysturoy and Sundini sills display slightly larger Sr and slightly smaller Ba, Rb, Th and K anomalies respectively compared to those of the Svínoy-Fugloy and Langaregn sills (Figure 3d; Figure 3e). Perhaps less conspicuous features are (i) the weak positive and moderately positive Nb and Ta anomalies exhibited in the Eysturoy and Sundini sills, and in the Svínoy-Fugloy and Langaregn sills respectively, and (ii) moderately negative Nb and Ta anomalies in the Streymoy and Kvívík sills (Figure 3a; Figure 3b; Figure 3d; Figure 3e). Local high-$TiO_2$ and intermediate-$TiO_2$ host-rock samples (analysed in this study and shown in Supplement 3 [51]) display mantle-normalised trace element trends that are broadly similar to those of most sills with similar $TiO_2$ contents, but local low-$TiO_2$ host-rocks (analysed in this study too) exhibit trends that are considerably more depleted in incompatible elements relative to those of comparable low-$TiO_2$ sills (insets in Figure 3a; Figure 3b).

***Table 2.*** *Whole rock ICP-MS data on trace elements representing basaltic sills of the Faroe Islands (Analyses guided by C. J. Ottley, DU, UK, and analyses by O. Nielsen, GEUS, DK).*

| Ppm | [a]Str. S. | | | | [b]Kv. S. | [c]Lr. S. | [d]Su. S. |
|---|---|---|---|---|---|---|---|
| | 07-JSS-26 | 07-JSS-40 | 07-JSS-52 | 07-JSS-09 | 07-JSS-49 | 07-JSS-50 | 08-JES-01 |
| Rb | 3.81 | 3.45 | 1.98 | 1.42 | 3.00 | 3.40 | 6.71 |
| Sr | 208 | 215 | 204 | 186 | 185 | 260 | 176 |
| Y | 18.8 | 17.1 | 18.7 | 19.4 | 18.2 | 34.9 | 38.9 |
| Zr | 50.8 | 46.3 | 50.9 | 47.4 | 45.2 | 173 | 144 |
| Nb | 2.87 | 2.61 | 2.81 | 2.65 | 2.47 | 13.98 | 11.89 |
| Ba | 59.3 | 53.8 | 62.8 | 47.7 | 44.9 | 64.9 | 77.4 |
| La | 4.24 | 3.62 | 4.24 | 3.50 | 3.28 | 11.37 | 10.37 |
| Ce | 10.28 | 8.74 | 10.20 | 8.55 | 8.04 | 29.7 | 25.7 |
| Pr | 1.60 | 1.36 | 1.57 | 1.34 | 1.28 | 4.80 | 3.99 |
| Nd | 7.40 | 6.39 | 7.39 | 6.48 | 6.09 | 22.76 | 18.80 |
| Sm | 2.04 | 1.78 | 2.03 | 1.86 | 1.79 | 6.00 | 4.98 |
| Eu | 0.757 | 0.663 | 0.744 | 0.719 | 0.674 | 1.973 | 1.642 |
| Gd | 2.57 | 2.25 | 2.65 | 2.57 | 2.41 | 7.03 | 6.14 |
| Tb | 0.457 | 0.403 | 0.484 | 0.464 | 0.440 | 1.10 | 1.02 |
| Dy | 2.84 | 2.46 | 2.95 | 2.93 | 2.77 | 6.11 | 6.15 |
| Ho | 0.634 | 0.540 | 0.647 | 0.654 | 0.604 | 1.20 | 1.28 |
| Er | 1.79 | 1.54 | 1.86 | 1.82 | 1.80 | 3.08 | 3.53 |
| Yb | 1.79 | 1.56 | 1.87 | 1.92 | 1.75 | 2.70 | 3.37 |
| Lu | 0.294 | 0.254 | 0.307 | 0.315 | 0.294 | 0.422 | 0.557 |
| Hf | 1.34 | 1.17 | 1.40 | 1.25 | 1.21 | 4.37 | 3.56 |
| Ta | 0.177 | 0.150 | 0.180 | 0.160 | 0.158 | 0.869 | 0.696 |
| Pb | 0.770 | 0.730 | 0.844 | 0.731 | 0.681 | 1.09 | 1.20 |
| Th | 0.525 | 0.439 | 0.526 | 0.421 | 0.374 | 0.854 | 0.961 |
| U | 0.140 | 0.127 | 0.138 | 0.112 | 0.111 | 0.262 | 0.287 |
| Nb/Ta | 16.21 | 17.37 | 15.63 | 16.53 | 15.61 | 16.09 | 17.09 |
| [h]$(Ce/Sm)_N$ | 1.25 | 1.19 | 1.20 | 1.12 | 1.11 | 1.21 | 1.27 |
| [h]$(Sm/Yb)_N$ | 1.24 | 1.26 | 1.19 | 1.09 | 1.10 | 2.38 | 1.59 |
| [h]$(Zr/Nd)_N$ | 0.82 | 0.86 | 0.82 | 0.87 | 0.88 | 0.91 | 0.91 |
| [h]$(Nb/Ce)_N$ | 0.71 | 0.76 | 0.70 | 0.79 | 0.78 | 1.20 | 1.18 |
| [h]Eu/Eu* | 1.05 | 1.05 | 1.01 | 1.05 | 1.05 | 0.97 | 0.97 |
| [h]Sr/Sr* | 1.73 | 2.09 | 1.71 | 1.82 | 1.92 | 0.73 | 0.58 |

***Table 2.*** *Continued.*

| Ppm | [e]Ey. S. | | | | [f]Mn. S. | | | | [g]Sv.-Fu. S. | |
|---|---|---|---|---|---|---|---|---|---|---|
| | 08-JES-08 | 08-JES-10 | 08-JES-11 | 08-JES-19 | 08-JMS-14 | 08-JMS-16 | 08-JMS-17 | 16-JMS-18 | 08-JFS-21 | 08-JSVS-22 |
| Rb | 7.03 | 10.34 | 7.14 | 4.83 | 0.367 | 0.321 | 24.04 | 1.07 | 3.50 | 3.19 |
| Sr | 176 | 174 | 174 | 180 | 87.0 | 85.5 | 97.9 | 87.4 | 220 | 217 |
| Y | 39.8 | 38.9 | 36.6 | 39.1 | 27.9 | 27.4 | 29.9 | 27.3 | 31.2 | 29.1 |
| Zr | 147 | 142 | 135 | 147 | 57.5 | 56.9 | 61.7 | 58.0 | 132 | 123 |
| Nb | 11.81 | 11.57 | 10.85 | 11.73 | 1.47 | 1.42 | 1.54 | 1.46 | 11.05 | 10.47 |
| Ba | 84.4 | 87.0 | 76.4 | 74.0 | 10.0 | 7.73 | 15.8 | 13.4 | 47.1 | 49.4 |
| La | 10.87 | 10.48 | 9.38 | 10.61 | 1.84 | 1.72 | 2.65 | 1.79 | 8.76 | 8.47 |
| Ce | 26.8 | 26.2 | 23.2 | 26.1 | 5.37 | 5.20 | 6.54 | 5.35 | 22.4 | 21.6 |
| Pr | 4.13 | 4.01 | 3.60 | 4.05 | 0.964 | 0.961 | 1.11 | 1.00 | 3.59 | 3.43 |
| Nd | 19.47 | 18.83 | 17.34 | 19.03 | 5.59 | 5.71 | 6.67 | 5.94 | 17.22 | 16.53 |
| Sm | 5.22 | 5.03 | 4.63 | 5.07 | 2.33 | 2.39 | 2.57 | 2.45 | 4.61 | 4.50 |
| Eu | 1.702 | 1.667 | 1.545 | 1.668 | 0.935 | 0.941 | 1.004 | 0.920 | 1.532 | 1.507 |
| Gd | 6.38 | 6.17 | 5.63 | 6.17 | 3.53 | 3.47 | 4.39 | 3.48 | 5.45 | 5.30 |
| Tb | 1.07 | 1.03 | 0.945 | 1.055 | 0.649 | 0.664 | 0.787 | 0.665 | 0.900 | 0.876 |
| Dy | 6.31 | 6.24 | 5.70 | 6.16 | 4.57 | 4.59 | 4.83 | 4.52 | 5.15 | 4.88 |
| Ho | 1.33 | 1.30 | 1.18 | 1.30 | 0.989 | 0.993 | 1.06 | 0.986 | 1.04 | 0.988 |

| Ppm | [e]Ey. S. | | | | [f]Mn. S. | | | | [g]Sv.-Fu. S. | |
|---|---|---|---|---|---|---|---|---|---|---|
| | 08-JES-08 | 08-JES-10 | 08-JES-11 | 08-JES-19 | 08-JMS-14 | 08-JMS-16 | 08-JMS-17 | 16-JMS-18 | 08-JFS-21 | 08-JSVS-22 |
| Er | 3.68 | 3.57 | 3.24 | 3.51 | 2.87 | 2.87 | 2.95 | 2.80 | 2.74 | 2.64 |
| Yb | 3.45 | 3.39 | 3.13 | 3.39 | 2.62 | 2.66 | 2.90 | 2.77 | 2.49 | 2.36 |
| Lu | 0.554 | 0.547 | 0.499 | 0.550 | 0.427 | 0.417 | 0.475 | 0.401 | 0.395 | 0.380 |
| Hf | 3.67 | 3.53 | 3.30 | 3.63 | 1.65 | 1.65 | 1.81 | 1.72 | 3.31 | 3.07 |
| Ta | 0.707 | 0.699 | 0.625 | 0.697 | 0.085 | 0.088 | 0.105 | 0.105 | 0.667 | 0.636 |
| Pb | 1.23 | 1.23 | 1.26 | 1.22 | 0.443 | 0.332 | 0.336 | 0.364 | 0.845 | 0.900 |
| Th | 0.993 | 0.949 | 0.854 | 0.944 | 0.153 | 0.152 | 0.171 | N0.163 | 0.692 | 0.661 |
| U | 0.287 | 0.285 | 0.252 | 0.284 | 0.050 | 0.044 | 0.050 | 0.041 | 0.216 | 0.208 |
| Nb/Ta | 16.70 | 16.55 | 17.36 | 16.84 | 17.33 | 16.08 | 14.70 | 16.47 | 16.57 | 16.47 |
| $^{h}(Ce/Sm)_N$ | 1.25 | 1.26 | 1.25 | 1.27 | 0.56 | 0.53 | 0.61 | 1.13 | 1.19 | 1.16 |
| $^{h}(Sm/Yb)_N$ | 1.61 | 1.61 | 1.60 | 1.61 | 0.97 | 0.98 | 1.00 | 2.06 | 1.97 | 2.02 |
| $^{h}(Zr/Nd)_N$ | 0.90 | 0.90 | 0.93 | 0.92 | 1.22 | 1.19 | 1.10 | 1.16 | 0.92 | 0.89 |
| $^{h}(Nb/Ce)_N$ | 1.12 | 1.12 | 1.19 | 1.14 | 0.70 | 0.70 | 0.60 | 0.69 | 1.26 | 1.23 |
| $^{h}Eu/Eu^*$ | 0.95 | N 0.93 | 0.99 | 0.96 | 0.99 | 1.00 | 0.95 | 0.96 | 0.99 | 0.97 |
| $^{h}Sr/Sr^*$ | 0.56 | 0.57 | 0.63 | 0.59 | 1.14 | 1.12 | 1.07 | 1.11 | 0.82 | 0.84 |

Trace elements in parts per million. [a]Str. S. = Streymoy Sill; [b]Kv. S. = Kvívík Sill; [c]Lr. S. = Langaregn Sill; [d]Su. S. = Sundini Sill; [e]Ey. S. = Eysturoy Sill; [f]Mn. S. = Morskranes Sill; [g]Sv.-Fu. S. = Svínoy-Fugloy Sill; [h]Normalised to primitive mantle [60]. Eu/Eu* = $(Eu)_N$ / ((Sm + Gd)$_N$ / 2) and Sr/Sr* = $(Sr)_N$ / ((Ce + Nd)$_N$ / 2). Samples 08-JMS-14, 08-JMS-16 and 16-JMS-18 were analysed at GEUS, DK. The rest were analysed at DU, UK.

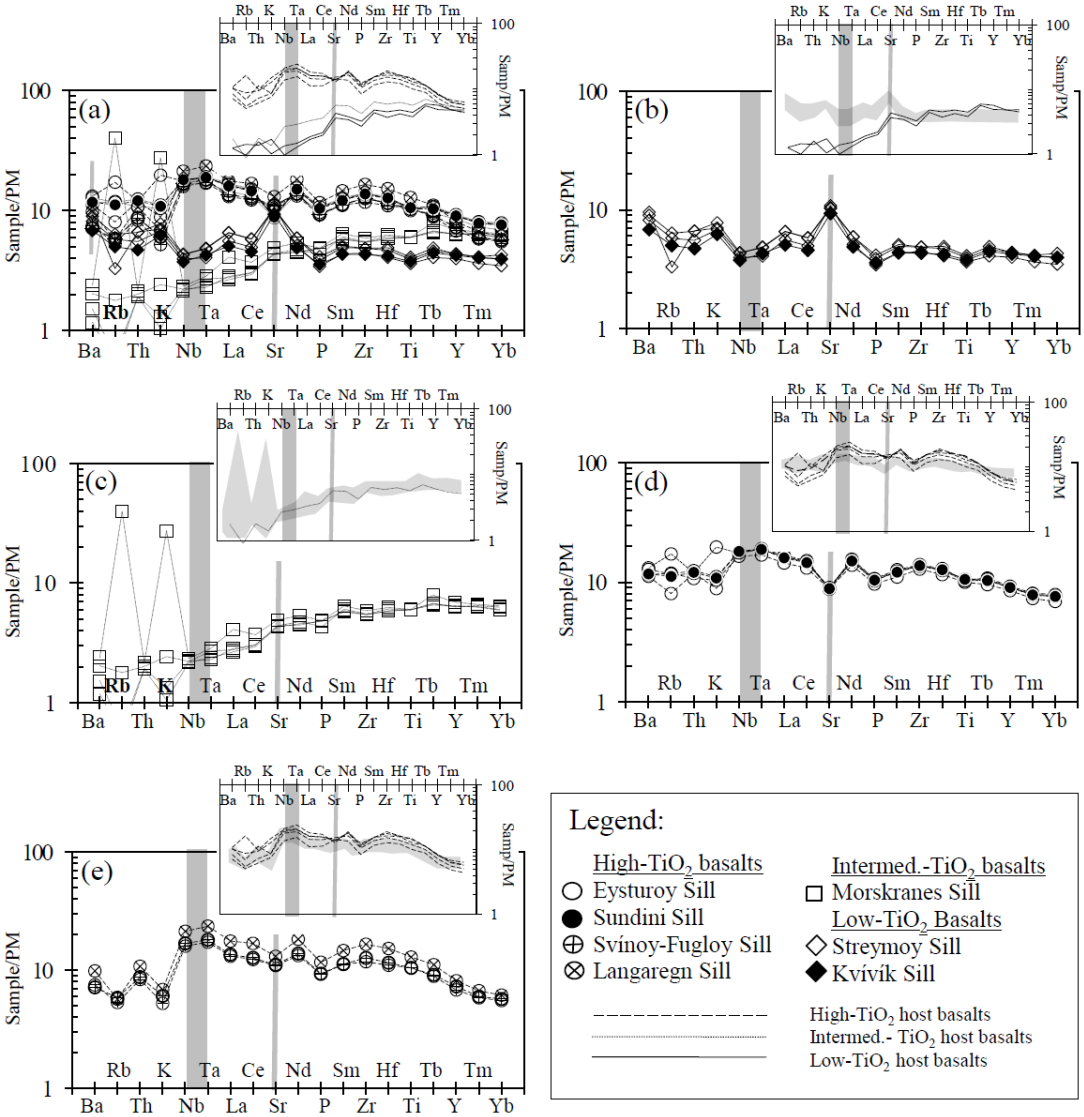


***Figure 3.*** *The diagrams show mantle normalised trace element data from Table 2. (a) All sills combined define three main trends. (b) Low-$TiO_2$ sill samples display strong positive Sr and moderately negative Nb and Ta anomalies. c) The intermediate-$TiO_2$ samples are generally depleted with respect to incompatible elements, but some samples display noticeable enrichment or depletion in Rb and K in particular. (d) Most samples from the high-$TiO_2$ Eysturoy and Sundini sills display negative Sr, Ba, Rb, Th and K anomalies and weak positive Nb and Ta anomalies. (e) Samples representing the high-$TiO_2$ Svínoy-Fugloy and Langaregn sills display moderately negative Sr and positive Nb and Ta anomalies, while their Ba, Rb, Th and K contents are depleted to various degrees. All sills display negative P anomalies. Trace elements of selected local host-rocks, as shown in Supplement 3 [51], are plotted in insets attached to the main plots, in where their $TiO_2$ contents are identical to those of their attached main sill plots. Semi-transparent grey fields in all insets represent multi-element ranges from the main diagrams. Normalising mantle values are from [60].*

### *4.3.3. REE*

Mantle-normalised REE data representing 17 sill samples (Table 2; Figure 4) define three main tendencies. The low-$TiO_2$ and high-$TiO_2$ sills (excluding the Langaregn Sill) display moderately negatively sloping LREE trends with $(Ce/Sm)_N$ ratios ranging from 1.11 to 1.27. The low-$TiO_2$ sills also display relatively flat negative HREE slopes with $(Sm/Yb)_N$ ratios ranging from 1.09 to 1.26. The samples representing the high-$TiO_2$ sills are characterised by steeper negative HREE slopes that can be further categorised into three sub-trends, where $(Sm/Yb)_N$ ratios for the Eysturoy and Sundini sills range from 1.59 to 1.61 and from 1.97 to 2.02 for the Svínoy-Fugloy Sill compared to 2.38 for the Langaregn Sill. The Morskranes Sill is LREE depleted with an average $(Ce/Sm)_N$ ratio of ~0.6, but displays a flat HREE trend with an average $(Sm/Yb)_N$ ratio of ~1. Local low-$TiO_2$ basaltic host-rock samples (analysed in this study) display relatively steep positive LREE and MREE slopes in contrast to the gentle negative slopes for these same elements representing comparable low-$TiO_2$ sill samples. Local high-$TiO_2$ host-rocks (analysed in this study and shown in Supplement 3 [51] display positive LREE slopes, which is slightly at odds with the relatively flat negative slopes for these same elements that represent comparable high-$TiO_2$ sill samples, when the Langaregn Sill is excluded (insets in Figure 4b; Figure 4e). The REE trends of the low-$TiO_2$ local host-rock samples analysed in this study are virtually identical to those of local MgO-rich (including picritic) low $TiO_2$ host-rock samples reported in earlier studies as outlined below, but are much more depleted in their LREE and MREE compared to the low-$TiO_2$ samples (Figure 4c). Intermediate-$TiO_2$ sill samples are almost identical to those of comparable local host-rocks (Figure 4d).

With respect to published REE data on local host-rocks, low-$TiO_2$ dykes (0.75-1.75 wt% $TiO_2$) generally display flat or MORB-like depleted trends with $(La/Sm)_N$ = 0.4-1.2 and $(Sm/Yb)_N$ = 0.5-1.15; intermediate-$TiO_2$ dykes (1.45-2.45 wt% $TiO_2$) display $(La/Sm)_N$ = 1.0 – 1.6 and $(Sm/Yb)_N$ = 1.35-2.35 while high-$TiO_2$ dykes (2.6-3.8 wt% $TiO_2$) display $(La/Sm)_N$ = 1.25-1.75 and $(Sm/Yb)_N$ = 1.95-2.65 [7]. Lava flows of the Beinisvørð Formation (exposed above sea level) and the Malinstindur Formation are LREE enriched ($(La/Yb)_N$ = 1.4-3.3) with a relatively wide range in overall REE concentrations, whereas some parts of the Enni Formation display depleted MORB-like LREE trends with $(La/Yb)_N$ = 0.45-0.62 [23].

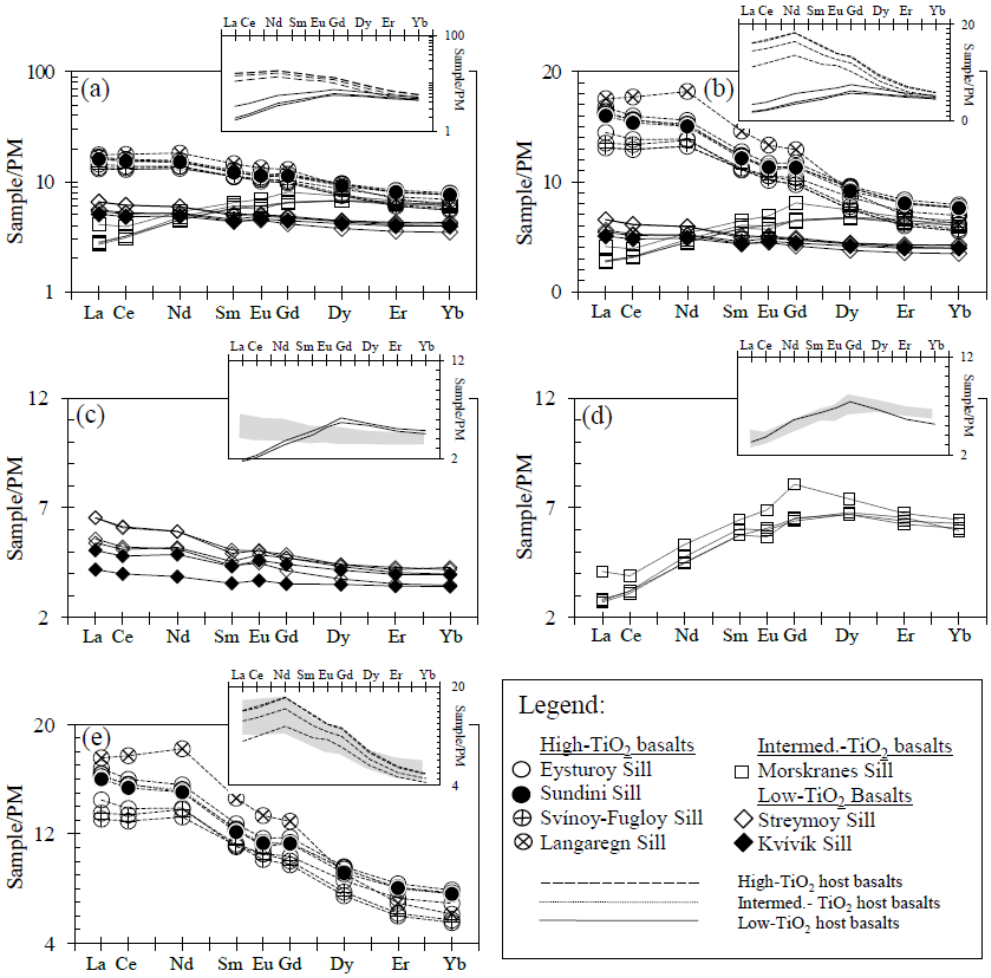


***Figure 4.*** *The diagrams show mantle normalised REE data from Table 2. (a) In these logarithmic plots, the REE data of Faroese sills define the same three main categories as those detected in Figure 2 and Figure 3. (b) Same as (a), but with linear scale on y axis. (c) Low-$TiO_2$ sill samples display very gentle negative REE slopes (linear scale on y axis). (d) Intermediate $TiO_2$ sill samples display depletion with respect to their LREE and MREE compositions (linear scale on Y axis). (e) MREE and HREE of high-$TiO_2$ Faroese sill samples display clear negative trends/slopesm while LREE of these same samles mostly display gentle negative trends (linear scale on y axis). Insets represent the same local host rocks from Supplement 3 [51]), as those shown in Figure 3. Semi-transparent grey fields in all insets of Figure 4, represent sill samples from the main diagrams, i.e. they possess $TiO_2$ compositions identical to those of the host-rocks. Normalising mantle values are from [60].*

### *4.4. Isotopes*

#### *4.4.1. Sr and Nd Isotopes*

Assuming that all sills were emplaced broadly contemporaneously and are slightly younger than the ~55 Ma determined for the upper parts of the host lava pile, the eight samples from seven sills analysed for Sr and Nd isotopes were age corrected to 54 Ma (Table 3; Figure 5). The $^{87}Sr/^{86}Sr(t)$ ratios of the sills range from 0.7028 to 0.7033, while their $^{143}Nd/^{144}Nd(t)$ ratios range from 0.512910 to 0.512976 (Nd(t) range from 6.7 to 7.9). When displayed graphically, these isotope data define a negative slope, plotting in two main clusters with two samples of the intermediate-$TiO_2$ sill displaying a $^{87}Sr/^{86}Sr(t)$ range from 0.7028 to 0.7029 and a $^{143}Nd/^{144}Nd(t)$ range from 0.512966 to 0.512976 compared to ranges of 0.7032 to 0.7033 and 0.51291 to 0.51296 respectively for the samples representing low-$TiO_2$ and high-$TiO_2$ sills (Figure 5a). These Sr and Nd isotope ranges plot within ranges for similar isotopes reported for samples representing other basaltic rocks of the Faroe Islands, and partly within those Sr and Nd isotopic ranges reported for Icelandic samples (inset in Figure 5a).

#### *4.4.2. Lead Isotopes*

Lead isotopes were determined on 13 samples representing 7 Faroese sills (Table 3; Figure 5). Total measured $^{206}Pb/^{204}Pb$ ratios range from ~17.89 to ~18.48, the measured total $^{207}Pb/^{204}Pb$ ratios range from ~15.39 to ~15.48 while total measured $^{208}Pb/^{204}Pb$ ratios span from ~37.85 to ~38.31. Similar to the Sr and Nd isotopes representing Faroese sills, lead isotope ratios of samples representing Faroese sills define two main fields, where the intermediate-$TiO_2$ Morskranes Sill defines one field and all the remaining Faroese sills define another field. The Morskranes Sill displays Pb isotope ratio ranges of $^{206}Pb/^{204}Pb$ = 17.89-17.98; $^{207}Pb/^{204}Pb$ = 15.39-15.45 and $^{208}Pb/^{204}Pb$ = 37.85-38.02 compared to ranges of $^{206}Pb/^{204}Pb$ = 18.23-18.48; $^{207}Pb/^{204}Pb$ = 15.43-15.48 and $^{208}Pb/^{204}Pb$ = 38.17-38.31 for the remaining sills, i.e. the Morskranes Sill displays larger spread in $^{207}Pb/^{204}Pb$ and $^{208}Pb/^{204}Pb$ ratios than all the remaining sills combined (Figure 5b; Figure 5c; Figure5d). Both of these two sill categories define perfectly linear (but different) trends in $^{206}Pb/^{204}Pb$ versus $^{208}Pb/^{204}Pb$ plots (Figure 5c), while some (three) samples of the Morskranes Sill in particular as well as samples representing the Eysturoy and Sundini sills are shifted towards higher $^{207}Pb/^{204}Pb$ ratios in $^{206}Pb/^{204}Pb$ versus $^{207}Pb/^{204}Pb$ and $^{207}Pb/^{204}Pb$ versus $^{208}Pb/^{204}Pb$ ratio plots (Figure 5b; Figure 5d). The values of lead isotope ratios of all Faroese sills combined generally plot within fields delineating similar isotope ratios representing other basaltic rocks of the Faroe Islands, E Greenland and Iceland (insets in Figure 5b; Figure 5c; Figure 5d). An overview on measured versus age corrected (at 54 Ma) lead isotopes from samples representing Faroese sills is presented in Supplement 4 [51].

***Table 3.*** *Whole rock MC-ICP-MS isotope data representing basaltic sills of the Faroe Islands (Analysed by Geoff Nowell, DU, UK, and Robert Frey, CU, DK).*

| Samples | $^{206/204}Pb$ | $^{207/204}Pb$ | $^{208/204}Pb$ | $^{208/206}Pb$ | Pb | Rb | Sr | $^{87/86}Sr$ |
|---|---|---|---|---|---|---|---|---|
| 08-JSVS-22 | [a]18.3736 | [b]15.4482 | [c]38.2266 | [d]2.0804 | 0.85 | 3.19 | 217 | [e]0.703306 |
| 07-JSS-49 | [i]18.4802 | [j]15.4765 | [k]38.3115 | [l]2.0731 | 0.68 | 3.00 | 185 | [e]0.703255 |
| 07-JSS-50 | [a]18.2326 | [b]15.4246 | [c]38.1692 | [d]2.0935 | 1.08 | 3.40 | 259 | [e]0.703266 |
| 07-JSS-52 | [a]18.4444 | [b]15.4756 | [c]38.2700 | [d]2.0749 | 0.85 | 1.98 | 203 | [e]0.703313 |
| 08-JES-01 | [a]18.2442 | [b]15.4493 | [c]38.1727 | [d]2.0922 | 1.19 | 6.71 | 176 | [e]0.703308 |
| 08-JES-10 | [a]18.2501 | [b]15.4493 | [c]38.1765 | [d]2.0919 | 1.28 | 10.30 | 174 | [e]0.703380 |
| 08-JMS-14 | [a]17.9131 | [b]15.4536 | [c]37.8876 | [d]2.1150 | 0.44 | 0.37 | 87 | [e]0.702895 |
| 16-JMS-14 | [i]17.8932 | [j]15.4525 | [k]37.8611 | [l]2.1160 | 0.44 | ----- | ----- | ---------- |
| 08-JMS-16 | [i]17.9314 | [j]15.3916 | [k]37.9184 | [l]2.1146 | 0.33 | ----- | ----- | ---------- |
| 08-JMS-17 | [a]17.9505 | [b]15.4086 | [c]37.9737 | [d]2.1153 | 0.32 | 24.00 | 98 | [e]0.703693 |
| 16-JMS-18 | [i]17.9825 | [j]15.4315 | [k]38.0194 | [l]2.1143 | 0.36 | ----- | ----- | ---------- |
| 16-JMS-19 | [i]17.9490 | [j]15.3901 | [k]37.9272 | ---------- | ----- | ----- | ----- | ---------- |
| 16-JMS-20 | [i]17.8862 | [j]15.3878 | [k]37.8542 | ---------- | ----- | ----- | ----- | ---------- |

***Table 2.*** *Continued.*

| Samples | $^{87}Rb/^{86}Sr$ | $^{87/86}Sr$ (t) | Sm | Nd | $^{143/144}Nd$ (0) | $^{147}Sm//^{144}Nd$ | $^{143/144}Nd$ (t) | εNd (t) |
|---|---|---|---|---|---|---|---|---|
| 08-JSVS-22 | [f]0.060346 | 0.703260 | 4.52 | 16.5 | [g]0.512987 | [h]0.211594 | 0.512912 | 6.7 |
| 07-JSS-49 | [f]0.066592 | 0.703204 | 1.79 | 6.09 | [g]0.513032 | [h]0.223383 | 0.512953 | 7.5 |
| 07-JSS-50 | [f]0.053838 | 0.703225 | 5.93 | 22.80 | [g]0.512999 | [h]0.201413 | 0.512928 | 7.0 |
| 07-JSS-52 | [f]0.039892 | 0.703282 | 2.06 | 7.39 | [g]0.513023 | [h]0.215840 | 0.512947 | 7.4 |
| 08-JES-01 | [f]0.156658 | 0.703188 | 4.93 | 18.80 | [g]0.512986 | [h]0.202623 | 0.512914 | 6.8 |
| 08-JES-10 | [f]0.244165 | 0.703193 | 5.02 | 18.80 | [g]0.512983 | [h]0.206201 | 0.512910 | 6.7 |
| 08-JMS-14 | [f]0.129173 | 0.702796 | 2.33 | 5.59 | [g]0.513086 | [h]0.312780 | 0.512976 | 7.9 |
| 16-JMS-14 | ---------- | ---------- | ----- | ----- | ---------- | ---------- | ---------- | ----- |
| 08-JMS-16 | ---------- | ---------- | ----- | ----- | ---------- | ---------- | ---------- | ----- |
| 08-JMS-17 | [f]1.008897 | 0.702919 | 2.62 | 6.67 | [g]0.513073 | [h]0.303742 | 0.512966 | 7.8 |
| 16-JMS-18 | ---------- | ---------- | ----- | ----- | ---------- | ---------- | ---------- | ----- |

| Samples | $^{87}Rb/^{86}Sr$ | $^{87/86}Sr$ (t) | Sm | Nd | $^{143/144}Nd$ (0) | $^{147}Sm/^{144}Nd$ | $^{143/144}Nd$ (t) | εNd (t) |
|---|---|---|---|---|---|---|---|---|
| 16-JMS-19 | ---------- | ---------- | ----- | ----- | ---------- | ---------- | ---------- | ----- |
| 16-JMS-20 | ---------- | ---------- | ----- | ----- | ---------- | ---------- | ---------- | ----- |

(t) refer to Sr and Nd isotopic ratios corrected back to 54 Ma; [a]2SE range from 0.0013 to 0.0053; [b]2SE range from 0.0015 to 0.0051; [c]2SE range from 0.0049 to 0.0190; [d]2SE range from 0.0001 to 0.0005; [e]2SE range from 0.000013 to 0.000023; [f]calculated ratios; [g]2SE range from 0.000006 to 0.000014; [h]calculated ratios; [i]2SE range from 0.0215 to 0.0314; [j]2SE range from 0.02 to 0.0277; [k]2SE range from 0.0515 to 0.0702; [l]2SE range from 0.0008 to 0.0013. Decay constants: $^{87}Rb \rightarrow {}^{87}Sr = 1.42\times10^{-11}$ yr$^{-1}$ [61] and $^{147}Sm \rightarrow {}^{143}Nd = 6.54\times10^{-12}$ yr$^{-1}$ [62]. The bulk of the analyses were carried out at Durham University, UK, while lead isotopes for samples 07-JSS-49, 16-JMS-14, 08-JMS-16, 16-JMS-18, 16-JMS-19 and 16-JMS-20 were analysed at Copenhagen University, DK.

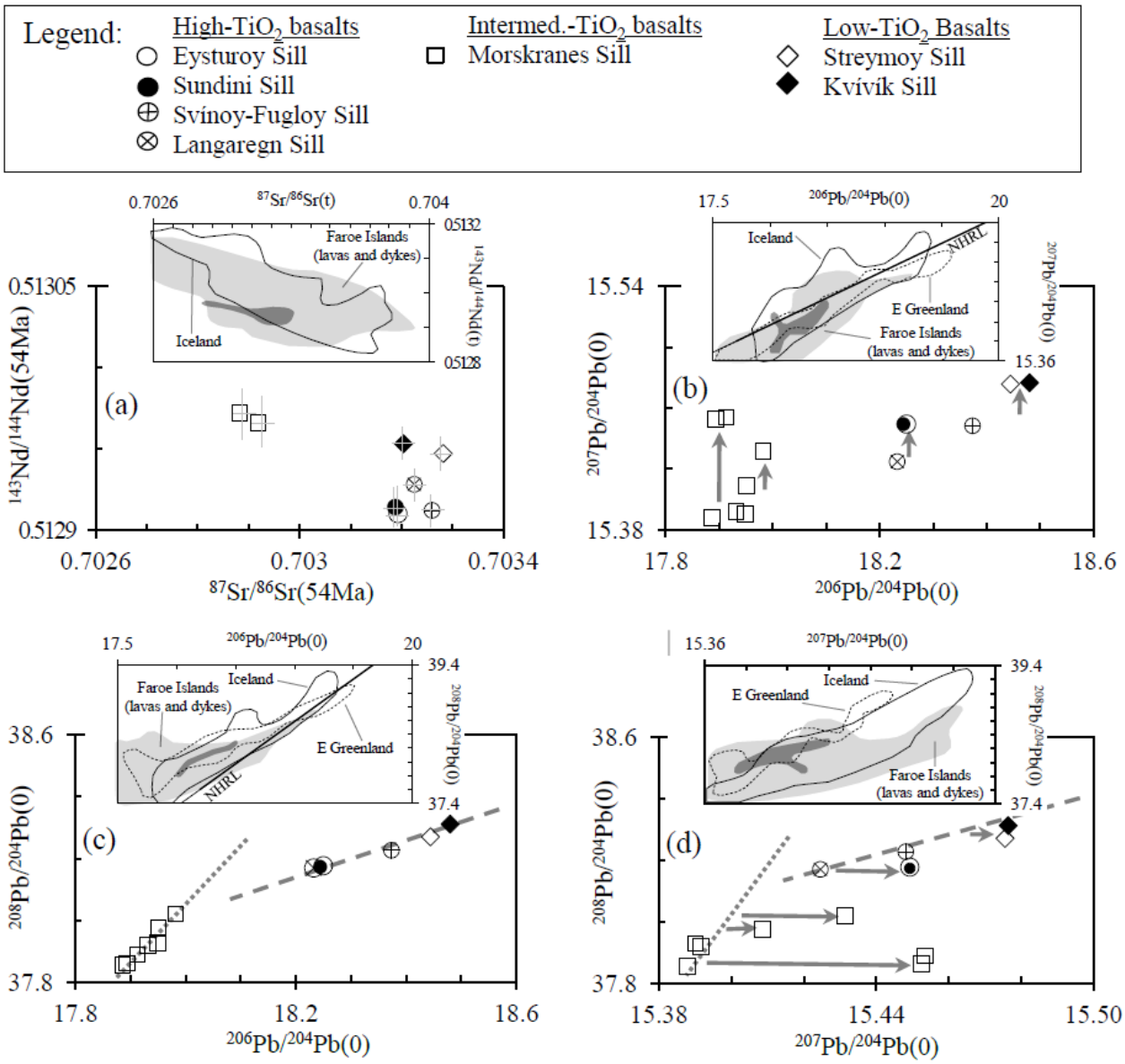


***Figure 5.*** *The diagrams show isotope data from Table 3. (a) Age-corrected (to 54 Ma) $^{87}Sr/^{86}Sr$ versus $^{143}Nd/^{144}Nd$ ratios, representing the actual sill samples, define two main clusters with high-$TiO_2$ and low-$TiO_2$ sill samples combined in one and intermediate-$TiO_2$ sill samples in another. 2SE analytical errors are indicated by vertical and horizontal semi-transparent bars. (b), (c) and (d) It is noticeable that, while Faroese sill samples define two perfectly linear trends in $^{206}Pb/^{204}Pb$ versus $^{208}Pb/^{204}Pb$ ratio plots for the same groups/clusters as shown in diagram (c), some samples of the Morskranes Sill and a few samples of the Eysturoy and Sundini sills display relative enrichments in $^{207}Pb/^{204}Pb$ ratios in (b) and (d) (see main text). The insets show isotopic compositions of Faroese sills (darker shaded fields) contrasted against those of other Faroese basaltic rocks [7, 8, 46], against those of Icelandic basaltic rocks [49, 63, 64] and against those of basaltic rocks from Central East Greenland [8]. (t) and (0) at diagram axes refer to age corrected and measured isotope ratios respectively.*

# 5. Discussion

### *5.1. Element Mobility*

The reliability of geochemical data as petrogenetic indicators must be evaluated carefully, as igneous rocks exposed at the Earth's surface commonly experience post-magmatic mineral break-down and associated mobilisation of major and trace elements, in addition to recrystallisation [65]. Major elements like Si, Mg and K and large ion lithophile elements (LILE) may be mobilised by low-grade metamorphism or weathering [66-68], while high field strength elements (HFSE) such as Th, Nb, Ta, Zr, Y and Ti commonly remain relatively unaffected during low or moderate grades of metamorphism [66-68].

Some of the investigated Faroese sill samples display

evidences of element mobilisation at the microscopic (single grain) scale, including minute olivine grains being partially or entirely altered to phyllosilicates (see details on petrography in Supplement 1 [51]. Greenish coatings occurring in <0.5 mm wide joints represent low-temperature hydrous minerals, and suggest element mobilisation at the whole-rock scale within some parts of these intrusions. For instance, comparison between the slightly jointed sill sample 07-JSS-38 and another fresh/intact sill sample 09-JSS-02 (Table 1), collected less than 100 metres apart within the Streymoy Sill, illustrates these effects of element mobilisation and geochemical modification. Sample 07-JSS-38 is relatively depleted in Si, Al, K, Sr and Ba and relatively enriched in Mg, Fe, Ti and Y. A relative enrichment in Ti and Y thus may indicate the relative immobility of Ti and Y in the more weathering-resistant mineral phases such as Fe-Ti oxides and/or clinopyroxene. Accordingly, for the purposes of petrogenetic investigation, only samples without signs of element mobilisation have been utilised in this work.

### *5.2. Crustal Contamination*

#### *5.2.1. Geochemical Constraints on Crustal Contamination*

The incorporation of crustal materials into magmas en-route to the upper crust is commonly attributed to bulk assimilation with concomitant fractional crystallisation or to net assimilation of the most fusible crustal materials [25, 69, 70].

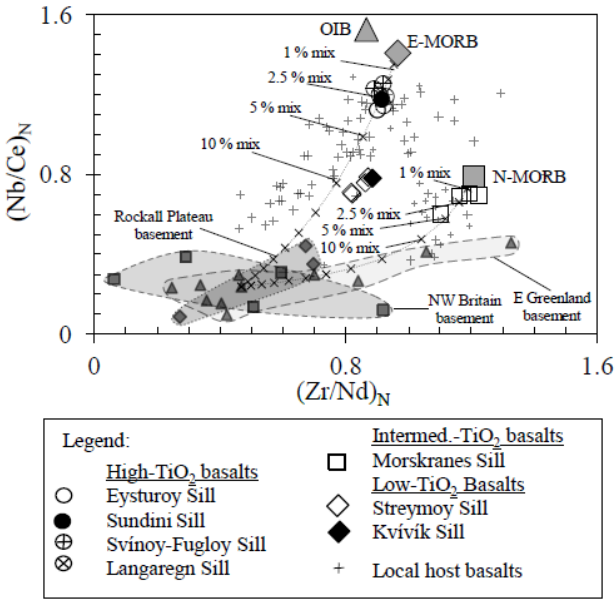


***Figure 6.*** *Intermediate-$TiO_2$ and high-$TiO_2$ sill samples plot close to representative N-MORB and E-MORB specimens respectively in this $(Zr/Nd)_N$ versus $(Nb/Ce)_N$ diagram. Around 1 to 2.5% contributions to the N-MORB with materials comparable to average N Atlandic basement could in theory account for most of the range in trace element ratios of the intermediate-$TiO_2$ sill shown in this diagram, while around 2 to 3% addition to the E-MORB with the same materials could in theory account for the range in the trace element ratios displayed by the high-$TiO_2$ sills. OIB, E-MORB and N-MORB data are from [71]; basement data on E Greenland from [72-74]; on NW Britain basement data from [75, 76, 70, 77]; on Rockall Plateau data from [78]. Data on Faroese host-rocks are from [7, 8, 45, 46] and from this study (Supplement 3 [51]). Normalising mantle values are from [60]. Datasets on calculated mixing trends are shown in [79].*

Since no geochemical data are available for the continental basement underneath the Faroese lava succession, samples representing Proterozoic/Archaean continental basements from NW Britain, the Rockall Plateau and E Greenland were utilised to evaluate potential crustal contamination of precursor melts to Faroese basaltic rocks. In theory, less than 4-5% bulk assimilation of material similar to average basement composition for E Greenland, NW Britain and the Rockall Plateau would be required in order to shift $(Zr/Nd)_N$ and $(Nb/Ce)_N$ ratios from those of typical N-MORB and E-MORB to those representing intermediate-$TiO_2$ and high-$TiO_2$ Faroese sills respectively (Figure 6). Substantially less assimilated basement material would be required to account for the internal variations in these elements displayed by the Faroese low-$TiO_2$ and high-$TiO_2$ sills. Around 5% crustal assimilation by Faroese sills appears quite unrealistic based on bulk geochemistry and would become apparent from additional isotopic evidences. The pronounced positive Rb and K anomalies displayed by one sample of the Morskranes Sill (Figure 3a; Figure 3c) seem to indicate selective enrichment in these elements. In theory, K-rich material could originate from residual mantle melts, or else from small-scale melting of suitable sources; but such melts also commonly tend to be $SiO_2$ and $Na_2O$ enriched. Given the relative depletion of these two major elements within this sample (Table 2) such scenario is unlikely. Hence, potential enrichment candidates may include net assimilation of crustal materials or perhaps LILE-rich metasomatic fluids leached from other adjacent basalts (i.e. secondary processes like the infilling of vesicles), which would also be in accordance with negative Rb and K anomalies displayed by many Faroese sill samples of all $TiO_2$ compositions (Figure 4).

#### *5.2.2. Isotopic Constraints on Potential Crustal Contamination*

The Pb isotopic compositions of presumed uncontaminated Faroese basaltic rocks compared with those of local contaminated basaltic lavas, of the Enni Formation, indicate involvement of two contamination sources characterised by different $^{208}Pb/^{204}Pb$ ratios in particular, but also with various $^{207}Pb/^{204}Pb$ ratios (Figure 7b, Figure 7c; Figure 7d). While the low $^{208}Pb/^{204}Pb$ contaminated samples could owe their Pb isotopic characteristics to assimilation of materials comparable to those reported for felsic and intermediate granulites or amphibolitic gneisses from E Greenland and NW Britain, the contaminated basalts with higher $^{208}Pb/^{204}Pb$ ratios most likely assimilated felsic or intermediate materials with Pb isotopic compositions corresponding to those of basement samples reported for E Greenland (Figure 7b, Figure 7c; Figure 7d). If precursor melts to the contaminated Faroese basalts (silicic basalts) originally possessed Sr and Nd isotopic compositions similar to those of the present-day MgO-rich Faroese dykes (e.g.

sample Sv-12 in [7]), then between 10 and 20% assimilation of materials similar to representative Proterozoic/Archean continental basement samples from E Greenland or NW Britain would be required in order to modify them to the isotopic range currently measured for these contaminated basalts (Figure 7a).

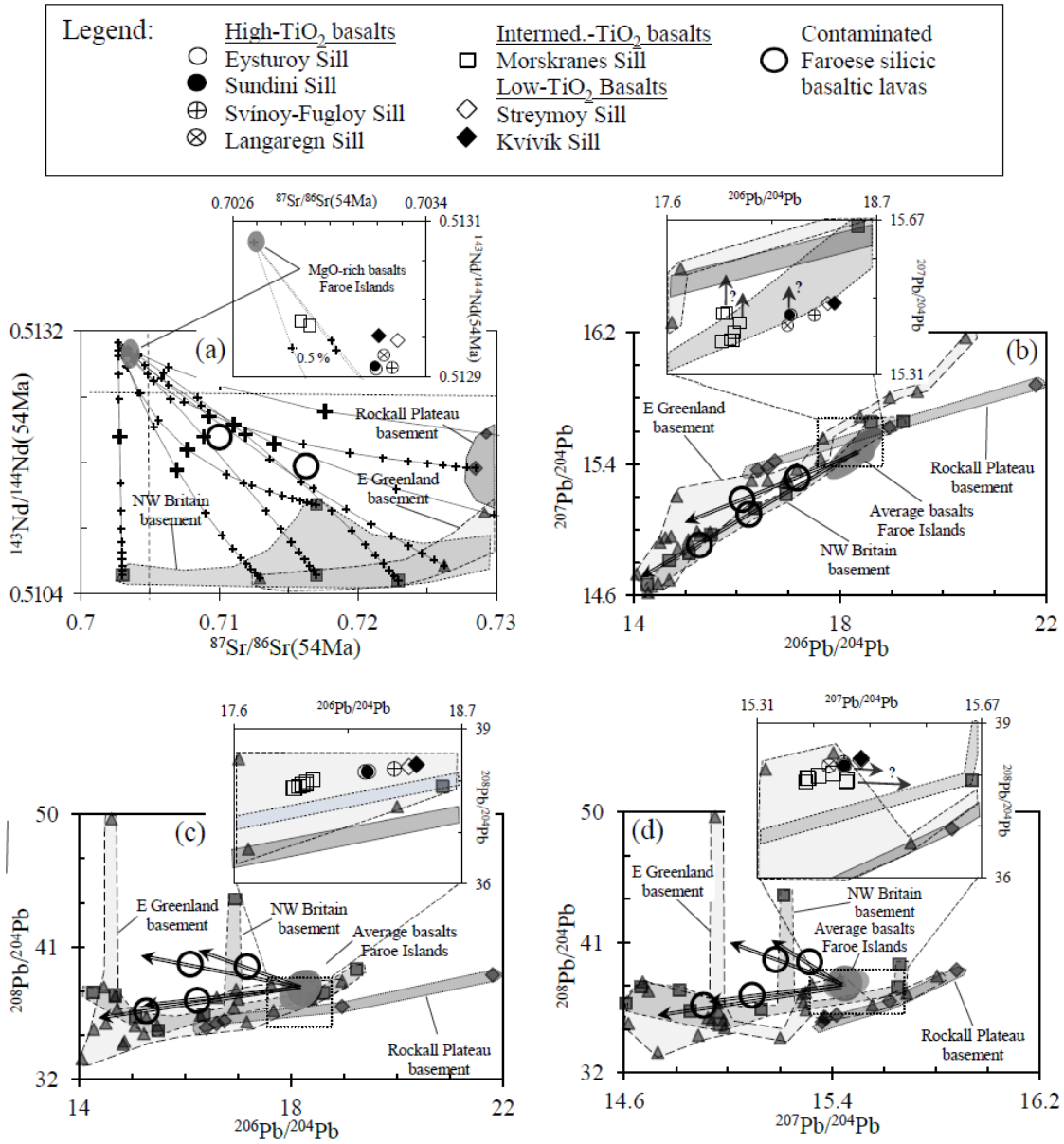


***Figure 7.*** *Sr, Nd and Pb isotopes, representing average Faroese basaltic rock samples, contaminated Faroese silicic basaltic samples as well as sill samples from this study (darkest shaded fields), are contrasted against Proterozoic/Archaean N Atlantic basement samples. (a) Age corrected (at 54 Ma) Sr and Nd isotopic ratios. Between 10 and 20% contributions from N Atlantic basement materials (NW Britain or E Greenland) to average Faroese basalts (dark shaded field) can explain the Sr and Nd isotopic compositions of local contaminated silicic basalts. Each of the large crosses on mixing curves indicates 10% contamination. Contributions with roughly 0.5% of average E Greenland and/or NW Britain basement sources to relatively primitive Faroese basalts could in theory explain some of the Sr and Nd isotopic variations of Faroese sill samples (inset). (b), (c) and (d) Measured Pb isotopic ratios. Two distinct contamination sources are required in order to explain the configuration of contaminated silicic basalts versus average Faroese basalts namely, one purely E Greenland-like basement source and one E Greenland-like and/or NW Britain-like basement source. Arrows point towards Pb isotope compositions of their probable contamination sources. Contamination with materials similar to those of the Rockall Plateau and those of E Greenland could explain variations of Pb isotope ratios of some samples of the Morskranes Sill, if these heterogeneities were not inherited from their mantle source (insets). Basement data for E Greenland are from [72, 83, 84]; NW Britain basement data are from [70, 76, 77, 85, 86, 87]; Rockall Plateau basement data are from [78]. Datasets on calculated mixing trends in a) are shown in [79].*

The enriched isotopic signatures of these contaminated Faroese basalts have previously been attributed to contamination with continental basement material possessing isotopic characteristics comparable to Lewisian amphibolites [7-23]. Other more resent studies have suggested that the isotopic compositions of these contaminated Faroese basalts reflected the probable existence of two distinct contamination sources beneath the archipelago, which possessed isotopic characteristics similar to basement material recorded for E Greenland [8]. Our own results presented above, suggesting 10 to 20% assimilation of crustal material for the entire isotopic range, displayed by these basalts, are in good accordance with the 12-13% assimilation of crustal material calculated for these contaminated basalt samples previously [8].

At present, it remains un-clear whether the noticeable variations in $^{207}Pb/^{204}Pb$ ratios between some samples of the small Morskranes Sill, as well as those within the Eysturoy and Sundini sills (Figure 5b, Figure 5d), reflect characteristics inherited from their mantle source(s), or if contamination with crustal materials is the most likely source. Indeed, noticeable differences in Pb isotopic compositions between melt inclusions and crystals versus their host phenocrysts and matrix respectively (thought to reflect isotopic heterogeneities at short length scales in their mantle sources) have been measured at a number of sites worldwide [80-81]. However, it is noticeable that samples of the Morskranes Sill with decreasing $^{207}Pb/^{204}Pb$ ratios also display increasing MgO contents (e.g. samples: 08-JMS-14 → 16-JMS-18 → 08-JMS-16 display increasing MgO contents and decreasing $^{207}Pb/^{204}Pb$ ratios in direction of arrows), i.e. Table 1; Table 3.

If assimilation indeed modified the Pb isotopic composition of the Morskranes Sill in particular and (to a lesser degree) that of the Eysturoy and Sundini sills, minor involvement of crustal materials with Pb isotopic compositions comparable to those of basement samples of the Rockall Plateau and of E Greenland could be an explanation (inset in Figure 7b). In this context, it is worth noting that isotopic compositions of Rockall granites led [82] to conclude that there existed an isotopic/genetic relationship between Rockall granites and alkali-rich intrusives of E Greenland. The inset in Figure 7d does not conclusively point to any particular of the three potential contamination sources, discussed in this sub-Sect.

If variations in Sr and Nd isotopic ratios of Faroese sill samples reflect assimilation of crustal material into their precursor melts, then less than 0.5% contamination with basement materials comparable to those of E Greenland and NW Britain would be required in order to shift the Nd isotopic compositions from those of the Faroese LREE depleted MgO-rich lava/dyke samples to those of LREE depleted samples of the Morskranes Sill (inset in Figure 7a). In theory, the Sr and Nd isotopic variations within high-$TiO_2$ and low-$TiO_2$ sills of this study, as well as Sr and Nd isotopic differences between high-$TiO_2$ and low-$TiO_2$ sills versus intermediate-$TiO_2$ sill samples, could have been generated by ≤ 0.25% assimilation of materials comparable to those of Proterozoic/Archean continental basement material from E Greenland, Rockall Plateau or NW Britain (e.g. Figure 7a including inset).

To summarise, the isotopic compositions of the contaminated silicic basalts of the Faroe Islands together with some samples of the Morskranes Sill in particular (if differences in their isotopic signatures are not source related) suggest that at least three distinct crustal contamination sources could have affected their precursor melts during ascent through the local palaeo crust (Figure 5; Figure 7).

#### *5.2.3. Implications from Mixing Calculations*

Calculations (not shown) show that basaltic rocks with initial Pb concentrations of ~0.5 ppm and initial average $^{208}Pb/^{204}Pb$ ratios of ~38 that experience ~0.5% assimilation of basement material with Pb concentrations of ~15 ppm and $^{208}Pb/^{204}Pb$ ratios being ~5 higher and lower respectively than those of the target basalts (i.e. $^{208}Pb/^{204}Pb$ ratios of ~43 and ~33 respectively) will experience an increase and decrease of ~0.65 in their $^{208}Pb/^{204}Pb$ ratios to ~38.65 and ~37.35 respectively. Accordingly, contributions with fractions of a percent of high or low $^{208}Pb/^{204}Pb$ basement materials comparable to some of those reported for E Greenland (e.g. samples KS 60 and 229642 in [72, 84] respectively) to melts comparable to Faroese dykes or lavas [7, 8] could account for the poor correlation between their $^{208}Pb/^{204}Pb$ ratio plots. The same would apply for basaltic rock samples from Iceland and E Greenland (e.g. insets in Figure 5c; Figure 5d). A relatively recent study based on geochemistry and isotopes suggested that low-$TiO_2$ tholeiitic Faroese lavas with the highest probabilities of contamination would require less than 1% contributions with crustal components if they assimilated local continental material [8]. Similar arguments on potential contamination in low-$TiO_2$ basalts of E Greenland have been inferred earlier [18]. Collectively, the results of this sub-Sect. suggest that parts of the Morskranes Sill could have been affected by crustal contamination, while it is somewhat more uncertain if the high-$TiO_2$ and low-$TiO_2$ sills were affected as well. Small-scale crustal contamination of these two latter sill categories would probably have resulted in slightly elevated La and Ce values, but assimilation of ≤ 1% crustal components would hardly be detectable in normalised REE diagrams [41] and cannot account for the observed differences between LREE in sills versus their host-rocks with similar $TiO_2$ compositions (e.g. Figure 4).

### *5.3. Fractional Crystallisation and Accumulation*

#### *5.3.1. Constraints on Faroese Tholeiite Formation from Fractional Crystallisation*

MgO-rich primary basaltic melts typically evolve to less magnesian varieties by fractional crystallisation of olivine [88]. Further melt modifications may occur in response to e.g. plagioclase, clinopyroxene or garnet fractionation [47-89]. Basaltic magmas can also evolve in response to complex RTF processes [15-90] (e.g. Sect. 1).

Around 15 wt% olivine fractionation combined with minor amounts of fractionated magnetite and ilmenite from MgO-rich melts, which are geochemically similar to selected Faroese picrites (MgO-rich [picrite] sample Ey-129 from [7], will generate tholeiitic melts with $SiO_2$, MgO and $K_2O$ values comparable to those of samples from the Morskranes Sill. Values for the other calculated major elements resemble those of low-$TiO_2$ and high-$TiO_2$ Faroese sills (Table 1; Table 4). Additional fractionation of clinopyroxene with typical $SiO_2$ values of 51 to 54 wt% [59, 91, 92] from the same MgO-rich magmas would result in silica depletion, thus requiring compensation by further Fe – Ti oxide fractionation, which in turn would result in unrealistically low $Fe_2O_3$ and $TiO_2$ values in the calculated melts. In addition, the average Sc concentrations in samples representing the Faroese sills are

broadly similar to the average concentrations of this element in local picrites and local MgO-rich olivine basaltic dykes. Hence, it is not likely that clinopyroxene was a dominating fractionating phase during early stages of magmatic evolution of melts that gave rise to most Faroese sills, if the geochemical compositions of their primary melts resembled those of local picrites. Moreover, the similarities in Sc concentrations between sills and local picrites also argue against any noticeable fractionation of garnet, provided that the picrites and primary melts that developed to the Faroese sills displayed matching compositions.

### *5.3.2. Trace Element Constraints on Fractional Crystallisation and Assimilation*

While the pronounced positive Sr anomalies displayed by samples of the low-$TiO_2$ Streymoy – Kvívík sills and the likewise conspicuous negative Sr anomalies of the high-$TiO_2$ Eysturoy - Sundini sills (Figure 3) clearly indicate the involvement of plagioclase at some point during melt evolution, there remains a slight uncertainty regarding the reliability of the weak Eu anomalies of samples from these same sills (Figure 4) given the small sizes of these compared to analytical error. Olivine fractionation and accumulation from/to modelled primitive basaltic melts (partition coefficients and the equation used are shown in Supplement 5 [51]) do not result in noticeable changes of their Sr/Sr* and Eu/Eu* ratios (definitions outlined in caption to Table 2), but around 15 wt% fractionated olivine in combination with minor amounts of fractionated magnetite and ilmenite would increase their Nb, Ta, Er and Y concentrations slightly. Similar calculations involving clinopyroxene fractionation from similar melts would not affect their Eu/Eu* ratios and would only result in very minor changes in their Sr/Sr* ratios. Addition of ~25 wt% plagioclase from external sources to magmas, generated by ~20% mantle melting (modelled), could explain much of the span in Sr/Sr* and Eu/Eu* ratios displayed by the low-$TiO_2$ Streymoy and Kvívík sills, while around 20 wt% plagioclase fractionation from magmas, generated by 10 to 12% mantle melting (modelled), could explain much of the range in the Sr/Sr* and Eu/Eu* ratios displayed by the Eysturoy and Sundini sills (Table 2; Figure 8). Plagioclase fractionation in the range 10 to ~20 wt% from magmas formed by ~10% mantle melting are required in order to recreate the Sr/Sr* and Eu/Eu* ratios of the Svínoy-Fugloy and Langaregn sills (Figure 8). The differences in calculated plagioclase accumulation and fractionation required to recreate Sr/Sr* versus Eu/Eu* ratios representing the Faroese sills, as shown in Figure 8, could in theory stem from either analytical error during analyses of Faroese sill samples, or the actual Sr/Sr* and Eu/Eu*ratios of these elements in their respective mantle sources differed from those used in the modelling. Around 20 wt% plagioclase accumulation and fractionation to/from liquids with geochemical compositions broadly similar to those of Faroese low-$TiO_2$ and high-$TiO_2$ sill samples would decrease/increase their overall REE concentrations respectively by amounts corresponding to around 2% larger/lesser degrees of partial melting of their respective mantle sources, while ~10 to ~15 wt% olivine fractionation would increase their overall REE concentrations by amounts corresponding to around 1% lesser degree of partial mantle melting (calculations not shown).

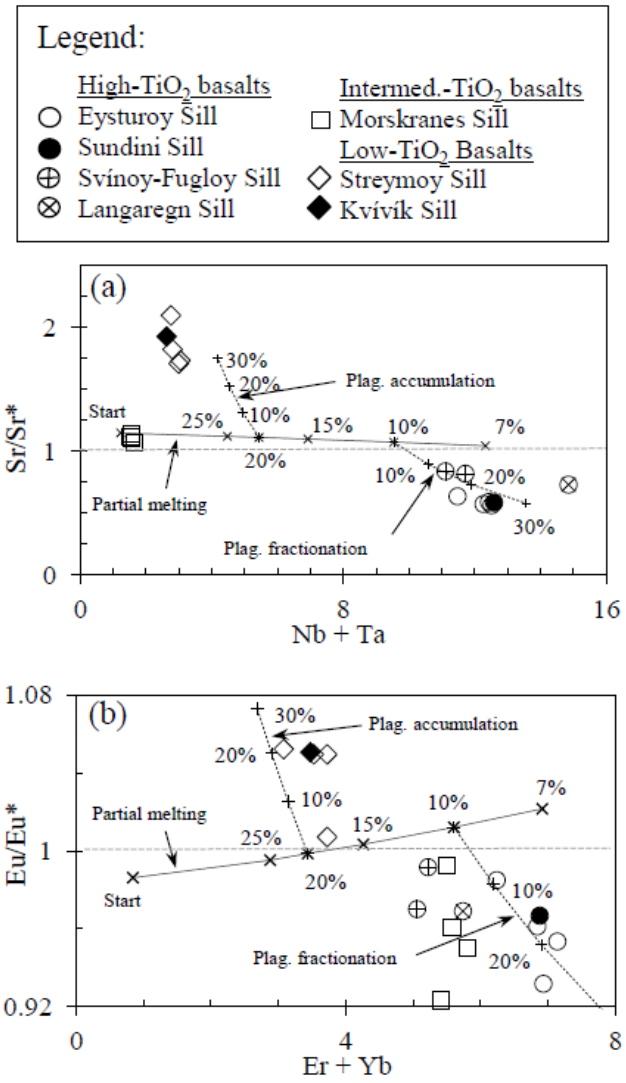


***Figure 8.*** *Trace element constraints on plagioclase fractionation and accumulation. (a) Partial melting calculations, utilising a selected initial mantle composition, are shown at 7, 10, 15, 20 and 25% melting intervals. Plagioclase accumulation and fractionation, shown at 10, 20 and 30 wt% intervals, are modelled from ~20% and ~10% calculated partial melts respectively. Initial selected fertile mantle composition: (Nb + Ta) = (1.2 + 0.025) and Sr/Sr* = 1.145, where Sr = 35, Ce = 2.6 and Nd = 1.9 [93]. Residual minerals during partial melting calculations were ~82% ol + 16% opx in addition to ~2% of mainly cpx and spl. (b) Same as in (a), but with (Er + Yb) = (0.42 + 0.42) and Eu/Eu* = 0.9862, where Eu = 0.182, Sm = 0.52 and Gd = 0.65 (i.e. [93]). Residual minerals were the same as in a). See Table 2 for definition of Sr/Sr* and Eu/Eu*. Mineral abbreviations are from [94]. Numbers along dotted lines indicate melting percentages and numbers along dashed lines indicate plagioclase fractionation/accumulation percentages. Datasets on calculated partial mantle melting, calculated fractionation and calculated accumulation of plagioclase are shown in [79].*

### *5.3.3. Constraints on Fractionation/Accumulation from Mass-balance Calculations*

Mass-balance calculations, involving all major elements

apart from MnO and $P_2O_5$, suggest that fractionation and accumulation of plagioclase from/to basaltic melts with compositions comparable to Faroese low-$TiO_2$ and high-$TiO_2$ sills chiefly affect their $Al_2O_3$, $Fe_2O_3$ and MgO compositions and to some degree their CaO and $TiO_2$ compositions, while the other major elements remain relatively unaffected (Table 4). If low-$TiO_2$ sills of this study evolved by ~25 wt% plagioclase accumulation, their precursor melts would possess significantly lower $Al_2O_3$ and higher $Fe_2O_3$ contents relative to values measured for these sills, while evolvement of their high-$TiO_2$ counterparts by ~20 wt% plagioclase fractionation would produce parental melts being significantly enriched with respect to their $Al_2O_3$ and depleted with respect to their $Fe_2O_3$ contents relative to values measured for these particular sills (Table 4). Consequently, in contrast with measured relative abundances of $Al_2O_3$ and $Fe_2O_3$ in Faroese high-$TiO_2$ sills versus low-$TiO_2$ sills, which define positive and negative slopes respectively when connected and plotted against MgO, the relative abundances of these major elements in their calculated parental melts would define negative and positive partial melting slopes respectively when connected and plotted against MgO (Figure 9a; Figure 9b). The scenario is different for the $TiO_2$ and CaO contents of the same samples, when exposed to the same accumulation/fractionation calculations as discussed above. Both these major elements in the calculated parental melts maintain their original graphical trends (i.e. negative and positive slopes respectively) when connected and plotted against MgO, but the gradients for their calculated parents are gentler than those of the measured samples (Figure 9c; Figure 9d; Table 4). Configurations of $Al_2O_3$, $Fe_2O_3$, $TiO_2$ and CaO versus MgO in calculated parents to low-$TiO_2$ and high-$TiO_2$ sills resemble results from previous experimental studies on partial mantle melting to produce low-$TiO_2$ and high-$TiO_2$ basaltic rocks [95-97] and would also support inferences in the discussion on trace elements above. Insets in Figure 9 illustrate similarities between calculated high-$TiO_2$ versus low-$TiO_2$ melts of this study and experimental basaltic melts, produced at roughly 5 to 20% melting and extrapolated to lower MgO contents in response to 12-15 wt% olivine fractionation. The differences in slopes and concentrations of experimental versus calculated melts are due to low pressures (1 GPa) and the hydrated nature of the experimental mantle materials. The discussion above strongly suggests that noticeable accumulation and fractionation of plagioclase in mid crustal staging chambers affected the melts, which eventually evolved to low-$TiO_2$ and high-$TiO_2$ Faroese sills.

***Table 4.*** *Mass-balance calculations on olivine and plagioclase fractionation, in addition to plagioclase accumulation.*

| Major elements | [a]olivine | [a]magnetite | [a]ilmenite | [b]MgO-rich magma | [c]calc. melts |
|---|---|---|---|---|---|
| $SiO_2$ | 41.85 | 0.27 | 0.10 | 45.89 | 48.50 |
| $Al_2O_3$ | 0.00 | 0.21 | 1.53 | 12.94 | 15.76 |
| $Fe_2O_3$ | 2.05 | 99.63 | 68.80 | 10.82 | 9.10 |
| MgO | 56.17 | 0.00 | 1.76 | 15.11 | 8.40 |
| CaO | 0.00 | 0.00 | 0.00 | 10.90 | 13.29 |
| $Na_2O$ | 0.00 | 0.00 | 0.00 | 1.53 | 1.87 |
| $K_2O$ | 0.00 | 0.00 | 0.00 | 0.05 | 0.06 |
| $TiO_2$ | 0.07 | 0.00 | 27.40 | 0.96 | 0.81 |

***Table 4.*** *Continued.*

| Major elements | [a]plag | [d]high-$TiO_2$ sill | [e]calc. parent 1 | [f]low-$TiO_2$ sill | [g]calc. parent 2 |
|---|---|---|---|---|---|
| $SiO_2$ | 49.60 | 50.28 | 50.04 | 50.29 | 50.59 |
| $Al_2O_3$ | 32.14 | 13.54 | 17.26 | 16.95 | 13.15 |
| $Fe_2O_3$ | 0.27 | 14.60 | 11.73 | 10.42 | 12.96 |
| MgO | 0.20 | 6.47 | 5.22 | 6.86 | 8.52 |
| CaO | 15.38 | 11.15 | 12.00 | 13.22 | 12.68 |
| $Na_2O$ | 2.57 | 2.36 | 2.40 | 2.00 | 1.86 |
| $K_2O$ | 0.17 | 0.33 | 0.30 | 0.20 | 0.21 |
| $TiO_2$ | 0.00 | 2.07 | 1.65 | 0.82 | 1.03 |

[a]Mineral compositions are from [59]. [b]Similar to Faroese MgO-rich (picrite) sample Ey-129 [7]. [c]Geochemical composition calculated by fractionation of 14.6 wt% olivine, 2.4 wt% magnetite and 1.0 wt% ilmenite from the MgO-rich magma. [d]High-$TiO_2$ Faroese sample 08-JES-03 from Table 1; [e]Geochemical composition of parent 1 from backtrack/reiteration calculations on the high-$TiO_2$ sill sample on the assumption that parent 1 represents its precursor melt prior to ~20 wt% plagioclase fractionation; [f]Low-$TiO_2$ Faroese sample 07-JSS-52 from Table 1; [g]Geochemical composition of parent 2 from backtrack/reiteration calculations on the low-$TiO_2$ sill sample on the assumption that parent 2 represents its precursor melt prior to ~25 wt% plagioclase accumulation.

A scenario where plagioclase, originating from different sites of storage and differentiation during magma ascent, accumulated in magmas, which subsequently evolved to the Faroese low-$TiO_2$ sills, would be in accordance with earlier studies on basaltic magmas of the NAIP [25]. More specifically, [98] suggested that three criteria must be fulfilled in order for melts containing accumulated plagioclase to reach the upper crust: 1) the initial plagioclase-free melt must pass through conduits in which plagioclase cumulates are present; 2) the ascent velocity of the magma within the conduit must be greater than the settling velocity of the entrained phenocrysts and 3) the magma must not travel through a conduit system containing an axial magma chamber, which would halt the upward ascent of the magma and allow denser plagioclase crystals to segregate.

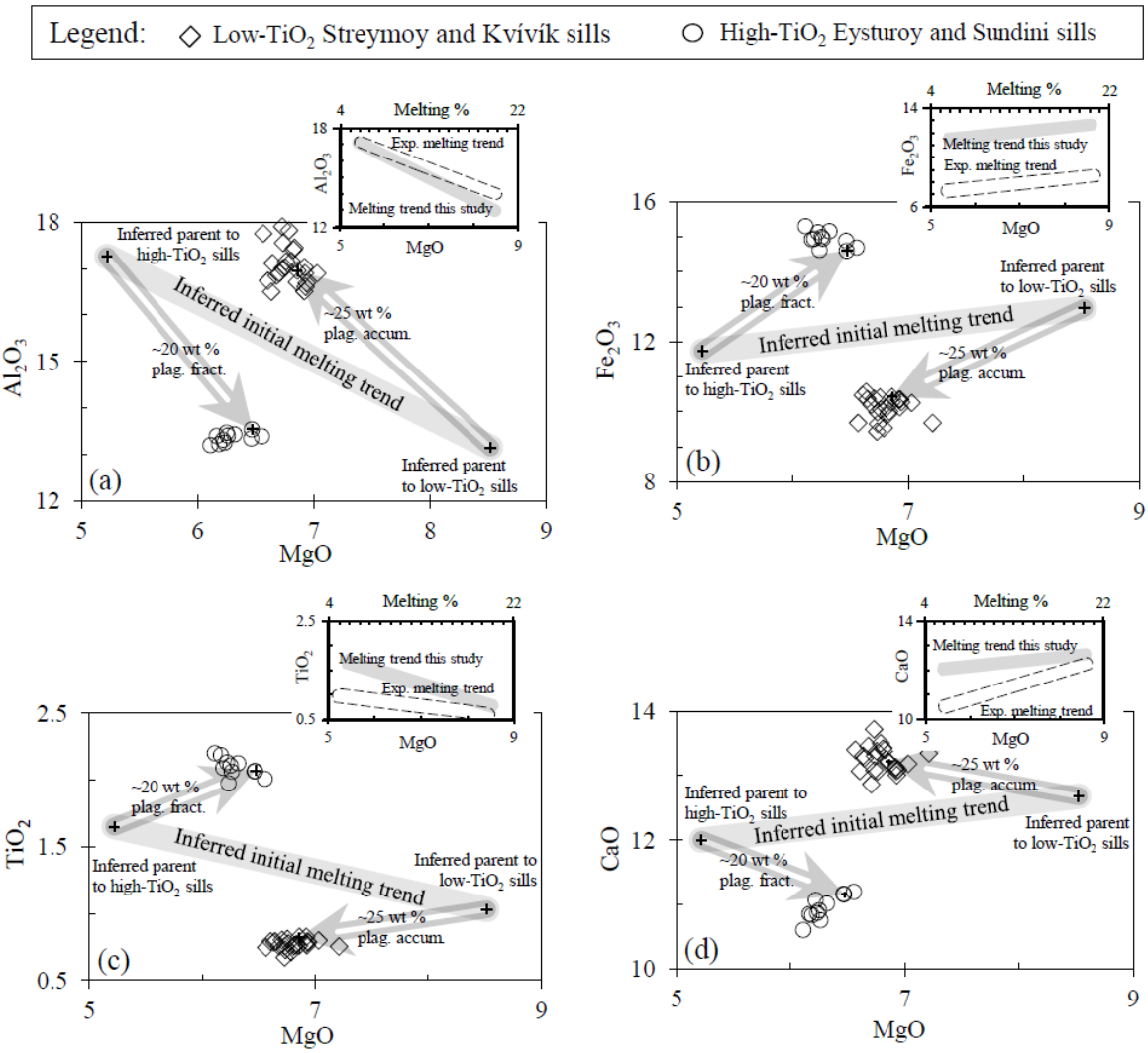


***Figure 9.*** *Calculated plagioclase fractionation (roughly 20 wt%) and accumulation (roughly 25 wt%) during the evolvement of precursor melts to Faroese sills (from Table 4). It is presumed that parental melts to Faroese high-$TiO_2$ and low-$TiO_2$ sills experienced roughly equal amounts of olivine fractionation from their primary melts on previous occasions. (a) Relative plots representing calculated parents to high-$TiO_2$ versus low-$TiO_2$ sills define a conspicuous negative trend/slope in a MgO versus $Al_2O_3$ diagram. (b) Relative plots showing calculated parents to high-$TiO_2$ versus low-$TiO_2$ sills define a clear positive trend/slope in a MgO versus $Fe_2O_3$ diagram. (c) Relative plots showing calculated parents to high-$TiO_2$ versus low-$TiO_2$ sills define a clear negative trend/slope in a MgO versus $TiO_2$ diagram. (d) Relative plots representing calculated parents to high-$TiO_2$ versus low-$TiO_2$ sills define a clear positive trend/slope in a MgO versus CaO diagram. The inset diagrams show calculated melting trends from the main diagrams versus trends from an experimental melting project [96], with melt percentages spanning from ~5 to ~20%. It is assumed that olivine fractionation shifted/extrapolated MgO contents in both calculated and experimental primary melts roughly horizontally to lower MgO values, as displayed in this figure. See main text and Table 4 for more details.*

### *5.4. Partial Melting*

#### *5.4.1. Constraints on Depths of Formation by Partial Melting*

Since the Faroese archipelago rests on top of an Archaean continental crust, the melts that gave rise to their olivine tholeiites must have formed beneath an ancient microcontinent [33-34]. Such olivine tholeiitic basaltic magmas may form by partial melting of a range of mantle compositions under various T and P [95, 97, 99, 100], but the lack of HREE depletion in Faroese low-$TiO_2$ and most high-$TiO_2$ sill samples points to formation of their precursor melts by partial melting outside the garnet stability field, i.e. at P ≤ ~2.8 GPa corresponding to depths of ≤ ~85 km. Moreover, as melting of plagioclase-bearing mantle material would produce quartz tholeiitic basalts [99-100], the olivine tholeiitic sills of the Faroe Islands probably formed at depths outside the plagioclase stability field too, i.e. at P ≥ ~0.9 GPa corresponding to depths of ≥ ~30 km [102-103], thus leaving mantle sources within the spinel stability field as their most likely origin.

#### *5.4.2. Batch Melting Calculations*

Batch melting calculations (partition coefficients and the equation used are shown in Supplement 5 [51]) were carried out in this work, in order to estimate melting percentages of suitable mantle sources, which gave rise to the different types of melts that ultimately evolved to the Faroese sills. In these calculations, only realistic existing figures for mantle compositions are used, which have been reported for various sites worldwide previously. In addition, shallow mantle sources of late melts are considered, as hypothesized in earlier studies [104].

Calculations in this study suggest that partial melting of

slightly LREE enriched mantle sources have the potential to reproduce the REE trends characterising Faroese low-$TiO_2$ and high-$TiO_2$ sills, while LREE and MREE depleted mantle sources are required in order to recreate the REE trend(s) of the intermediate-$TiO_2$ Morskranes Sill. Residual mineral assemblages utilised in these calculations are dominated by olivine (~80 to ~84%) and orthopyroxene (~8 to ~16%) that may be associated with minor amounts of clinopyroxene (0 to ~7%) and spinel (0 to ~1%), i.e in accordance with the mineralogy of many naturally occurring peridotites worldwide [105-108].

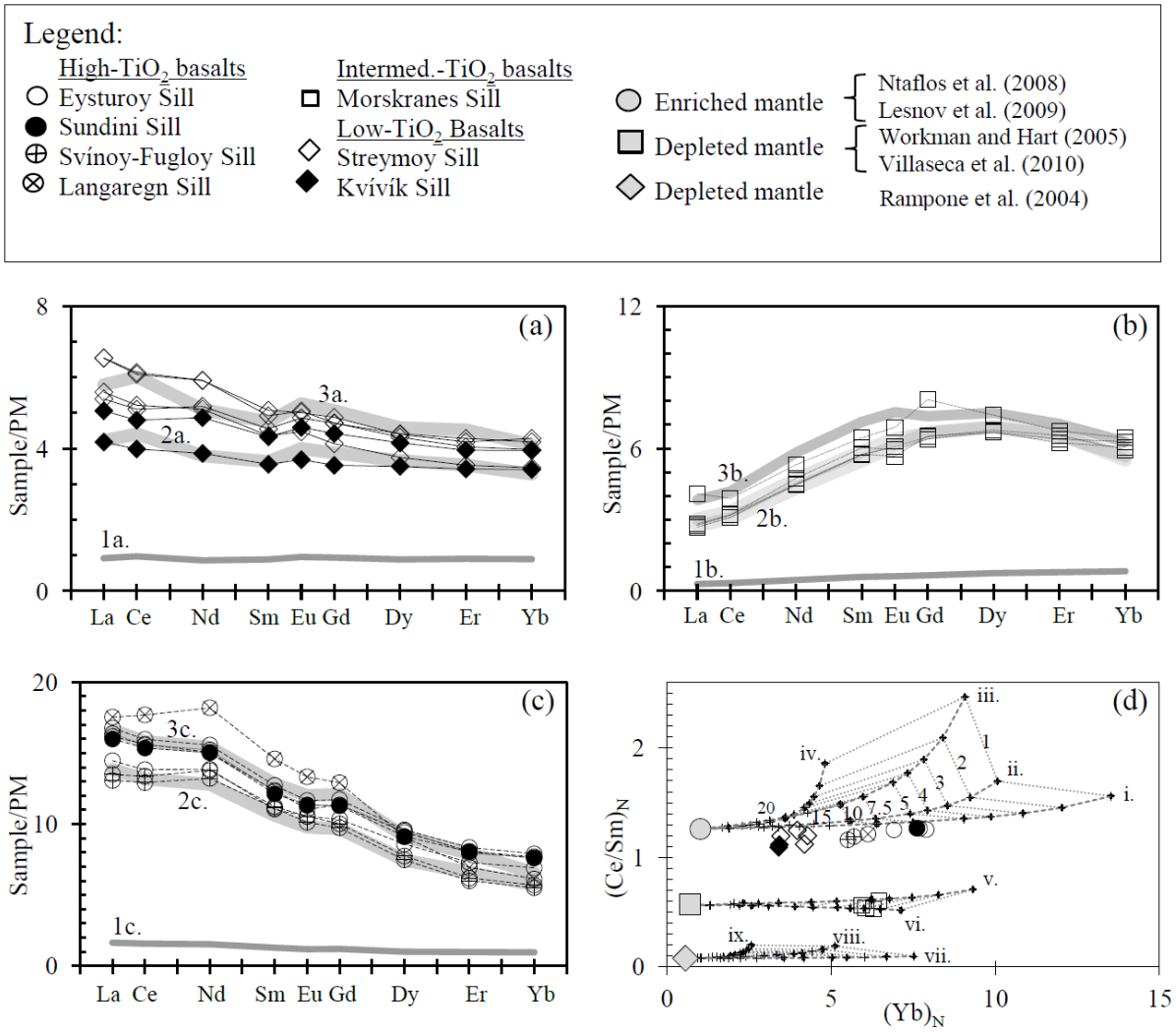


***Figure 10.*** *Partial melting calculations involving various mantle lithologies. The grey shaded trends in the mantle normalised REE diagrams (a), (b) and (c) indicate mantle sources (labelled 1.) and range in calculated melting percentages (labelled 2. and 3.). (a) Low-$TiO_2$ sills: 1a.= Spinel lherzolite sample VL 5-12 [110]; 2a.= around 20% melt of 1a. with 84% Ol + 8.5% Opx + 7% Cpx + 0.5% Spl residue; 3a.= around 15% melt of 1a. with 84% Ol + 8.5% Opx + 7% Cpx + 0.5% Spl residue. (b) Intermediate-$TiO_2$ sills: 1b.= average DMM [112]; 2b.= around 8% melt of 1b. with 84% Ol + 15 to 15.5% Opx + 0.5 to 1% Spl residue. 3b.= around 7% melt of 1b. with 84% Ol + 16% Opx residue. (c) High-$TiO_2$ sills: 1c.= average spinel lherzolite sample [93]; 2c.= around 10.5% melt of 1c. with 84% Ol + 15.75% Opx + 0.25% Spl residue; 3c.= around 8% melt of 1c. with 84% Ol + 15.5% Opx + 0.5% Spl residue. (d) The labelled curves in the $(Yb)_N$ versus $(Ce/Sm)_N$ diagram indicate partial melting trends calculated from three mantle sources (enriched, moderately depleted and strongly depleted). Numbers along curves ii. and iii. refer to melting percentages that also apply for all the other curves in the actual diagram. Normalising primitive mantle values in all four diagrams are from [60]. Mineral abbreviations are from [94]. See Supplement 5 [51] for partition coefficients and equation used in calculations and Supplement 6 [51] for details on mineral residues from calculations shown in (d), as well as similar calculations on the same sill samples using a Zr versus Y/$TiO_2$ diagram. Datasets on calculated melting trends are shown in [79].*

Trial partial melting calculations, performed in order to recreate measured REE trends of low-$TiO_2$ and most high $TiO_2$ sills, were carried out on a large number of mantle compositions from localities worldwide and from estimated average mantle values and include published material reported by e.g. [60, 93, 106, 107, 109, 110]. Melting percentages ranging from 15 to 20% of fertile mantle material from [110] and ranging from 8 to 10.5% of likewise fertile mantle material from [93] best reproduce the ranges in REE compositions of low-$TiO_2$ and high $TiO_2$ sills respectively (Figure 10a; Figure 10c). It is clear that the measured REE trend representing the Langaregn Sill doesn't quite fit in with those of the rest of the high-$TiO_2$ sills (Figure 4e; Figure 10c). Its actual REE trend can be recreated by ~7% partial melting of a fertile source (not shown), but it is likely that some garnet was a residual phase and that its source displayed slight depletion with respect to LREE when compared to sources to other local high-$TiO_2$ sills. Regarding measured (LREE depleted) REE in intermediate-$TiO_2$ sill samples, trial calculations included published material reported by e.g. [111-113], where 7 to 8% of average depleted mantle from [112] best recreate the REE

compositions of these samples (Figure 10b).

When the effects on REE compositions representing Faroese sills from supposed fractionation of olivine and plagioclase and accumulation of plagioclase (previous Sect.) are taken into account, partial melting percentages to produce melts that gave rise to the Faroese sills should be corrected slightly. With respect to the low-$TiO_2$ sills, olivine fractionation and plagioclase accumulation would shift the range of partial melting percentages in their source(s) by +1% from 15-20% to 16-21. With respect to the high-$TiO_2$ sills, olivine and plagioclase fractionation would shift the range of partial melting percentages in their source(s) by –3% from 8-10.5% to 5-7.5%, while the calculated melting for the Langaregn Sill should be shifted from ~7 to ~4%. With respect to the intermediate-$TiO_2$ sill, olivine fractionation would shift the range of partial melting percentages in its source by –1% from 7-8% to 6-7%.

Batch melting calculations based on selected REE, which are plotted in a binary $(Yb)_N$ versus $(Ce/Sm)_N$ diagram, are perhaps better suited to illustrate the effects of various residual mineralogies and general differences in source compositions on modelled melts. With respect to LREE-enriched mantle sources [93-110], the results shown in the binary REE plots support the inferences above regarding formation of the low-$TiO_2$ and high-$TiO_2$ sills by different degrees of partial melting of enriched sources that left residual mineralogies composed mainly of olivine and orthopyroxene (curves i-iv in Figure 10d). Similarly, partial melting of moderately LREE-depleted sources [112-113] with residual mineral assemblages dominated by olivine and orthopyroxene most realistically reproduces the REE composition of the intermediate-$TiO_2$ Morskranes Sill (curves v and vi in Figure 10d). In addition, strongly LREE depleted mantle sources [111] do not have the potential to reproduce REE compositions matching those of the Morskranes Sill, when exposed to partial melting, irrespective of which residual mineral assemblages are chosen (curves vii-ix in Figure 10d). More details on Figure 10d as well as additional modelling are shown in Supplement 6 [51].

#### *5.4.3. General Considerations*

Given that the mantle sources used in the partial melting calculations in this study were primarily selected because they best reproduce the REE trends representing the actual sills, the actual mantle sources to these sills could, in theory, have been less or more fertile relative to the chosen compositions; if so, then the outcome would require slightly lesser or greater degrees of partial melting relative to the calculated values. In cases where precursor melts to the actual sills experienced small-scale assimilation of felsic crustal materials upon ascent, it could have increased their LREE concentrations very slightly [41]. However, contamination with ≤ 1% crustal material would not have had noticeable effects on the modelling carried out in this work. Altogether, the partial modelling and trace element characteristics of actual sill samples combined (Figure 3; Figure 10) point to distinct mantle sources for intermediate-$TiO_2$ versus high-$TiO_2$ and low-$TiO_2$ sill samples. In turn, some heterogeneities probably exist between sources to high-$TiO_2$ and low-$TiO_2$ sill samples and probably also to some degree within sources to the high-$TiO_2$ sills themselves. Here the Eysturoy and Sundini sills, the Langaregn Sill and the Svínoy-Fugloy Sill respectively probably originated from three slightly different mantle sub-sources. These findings are in accordance with the isotopic characteristics recorded for the actual sills (Figure 5). Interestingly, four slightly different mantle sub-sources were inferred for high-$TiO_2$ lavas of the Faroese Enni and Malinstindur formations in a recent study [9].

Processes involving partial melting of sources, comparable to those reported for SCLM, to produce Faroese sills, as is suggested by our modelling above, are at odds with previous theories on formation of their host-rocks [7, 8, 46,].

### *5.5. Primary Melts*

Previous estimates on the MgO percentages present in primary magmas that evolved to basaltic rocks of the N Atlantic have come to various conclusions: 10.0-13.0 wt% and 17.0-18.5 wt% respectively for W Greenland [15-88]; 12.0-13.6 wt% and 16.6 wt% for E Greenland [17-121]; 13.0-15.0 wt% for NW Britain [122]; 13.5-17.7 wt% for Iceland and adjacent mid-ocean ridges [121] and 16.0-19 wt% MgO for the Faroe Islands [7-8]. MgO contents of 10-15 wt% have been calculated for primary magmas that gave rise to average global Ocean Ridge Basalts [119].

Based on the results from the partial melting modelling and presumed subsequent fractional crystallisation of olivine and plagioclase, as well as inferred plagioclase accumulation, melting percentages of ~16 to 21 and ~4 to 7.5% to produce primary melts that developed to Faroese low-$TiO_2$ and high-$TiO_2$ sills respectively appear to be reasonable estimates, if the following criteria are fulfilled: 1) fractionation of clinopyroxene did not play a major role during the early stages of their magmatic evolutions; 2) around 10 to 15 wt% olivine and minor amounts of magnetite and ilmenite fractionated from their primary melts, which contained ~15 wt% MgO and 3) ~15 to 20 wt% plagioclase fractionated from melts that gave rise to high-$TiO_2$ sills while about 15 to 25 wt% plagioclase accumulated in melts that evolved to the low-$TiO_2$ sills. The 16 to 21% partial melting range to produce precursor melts to the Faroese low-$TiO_2$ sills correspond roughly to earlier estimates on melting percentages for primary melts that developed to low-$TiO_2$ basaltic rocks of W Greenland [15] (Larsen and Pedersen, 2009), E Greenland [17], the Faroe Islands [7], southern Brazil [120] and global ocean ridge basalts [119]. The 4 to 7.5% partial melting range proposed for production of Faroese high-$TiO_2$ sills correspond roughly to melting percentages estimated for primary melts, which evolved to high-$TiO_2$ basaltic rocks of southern Brazil [120] and E Greenland [17], but reach slightly higher values than those estimated for primary melts that gave rise to other high-$TiO_2$ basalts of the Faroe Islands [7] and are slightly lower than

those inferred for global ocean ridge basalts [119]. However, as most sills of this study, being termed high-$TiO_2$ basaltic rocks, display $TiO_2$ compositions of only 2.0 to 2.5 wt% compared to 2.5 to 3.7 wt% for other high-$TiO_2$ basalts of e.g. the Faroe Islands [7-8], the proposed range in melting percentages for high-$TiO_2$ primary magmas in this study appear to be rather similar to other high-$TiO_2$ rocks within the N Atlantic area after all.

The 6-7% melting range calculated/estimated for the LREE depleted primary melts giving rise to the Morskranes Sill contrast somewhat with the higher degrees of melting thought to have generated comparable LREE depleted Central Mull Tholeiites from the British Tertiary Igneous Province (BTIP) and with the melting percentages measured for experimentally produced MORB-like rocks [100-114]. It should be noted however, that the basalts reported by these authors presumably formed at relatively low pressures, e.g. 1.5 GPa for the experimental rocks [100]. If the melts that evolved to the Morskranes Sill also experienced 10-15 wt% plagioclase fractionation, as could perhaps be suggested by its Eu/Eu* ratio (Figure 8b), then slightly higher range in melting percentages of 7-9% could be a more correct approximation. All the above estimated melting percentages rely on the assumption that crustal contamination did not significantly affect the overall trace element compositions used in the modelling.

### *5.6. Mantle Sources*

#### *5.6.1. Geochemical Implications from the Literature*

Depleted mantle materials probably represent residue(s) following earlier phases partial melting of primordial mantle reservoirs to produce basaltic melts [111, 112, 115, 116]. By contrast, fertile mantle materials could result from metasomatic processes, where primordial mantle materials were contaminated with ascending low-degree basaltic magmas or with fluids expelled from these [93, 115, 117, 118], or they could originate from assimilation of recycled oceanic crust [2, 88, 97, 121, 123]. Total normative Fe-oxide values of ≥ 13 wt% in basaltic rocks are at times interpreted in terms of derivation from mantle sources contaminated with recycled oceanic crustal components [97]. The Faroese high-$TiO_2$ sills display average measured $Fe_2O_3$ values of ~14.7 wt%, but their calculated parental melts contain less than 12 wt% of this oxide, compared to average measured $Fe_2O_3$ values of ~10 wt% for the Faroese low-$TiO_2$ sills and ~12.8 wt% for their calculated parental melts (Table 4; Figure 9b). The iron contents of the actual sills also plot well within ranges displayed by common mid-ocean ridge and ocean island tholeiites [124].

Previous studies have attributed the trace element characteristics displayed by Faroese basaltic lavas and dykes to an origin from a heterogeneous mantle plume comprising distinct geochemical zones [7-8], while asthenospheric and/or SCLM sources have been inferred for Faroese lavas by other authors [23]. Based chiefly on Zr, Nb and Y concentrations, [125] indicated an enriched plume component, a depleted astenospheric component and minor contributions from an additional EM 1- like component, entrained within the asthenosphere, as the main sources to Icelandic basalts. [126] demonstrated that an additional local depleted Iceland plume (DIP) component was required in order to adequately account for the Zr, Nb and Y characteristics of the Icelandic basalts combined. In theory, mantle sources broadly similar to those suggested by [125-126] for the Icelandic basalts could have been involved during formation of basaltic rocks of the Faroe Islands, as samples representing Faroese sills, lavas and dykes share many of the geochemical characteristics defined by the Icelandic basalts (Figure 11a).

Importantly, it is evident from the inset to Figure 11a that all Faroese low-$TiO_2$ and most high-$TiO_2$ sill samples combined define a "missing link" between fields outlining the bulk of Faroese low-$TiO_2$ and high-$TiO_2$ host-rocks, whilst the intermediate-$TiO_2$ Morskraness Sill and the high-$TiO_2$ Langaregn Sill plot within the fields for low-$TiO_2$ and high-$TiO_2$ host-rocks respectively. Overall, the bulk of Faroese basaltic rocks, including the local sills, define a trend quite comparable inn shape to average values reported for Iceland previously (i.e. the bold curve in Figure 11a, adopted from [125]), but which is relatively rotated by around 10° clockwise.

#### *5.6.2. Geochemical Implications on Metasomatised Mantle Sources*

Negative Nb and Ta anomalies in basaltic rocks have commonly been associated with mantle sources that were metasomatised previously with hydrous fluids, C-bearing fluids or low-degree basaltic melts, while positive Nb and Ta anomalies are commonly associated with residual dryer mantle materials from which the above-mentioned metasomatic agents were extracted previously [69-127]. Negative Nb and Ta anomalies in suites of low-$TiO_2$ flood basalts from the Siberian Traps, and from Central Nicaragua, being virtually identical to low-$TiO_2$ sills from this study; were previously attributed to an origin from metasomatised upper mantle sources in subduction-zone environments [10-12], while negative Nb and Ta anomalies in low-$TiO_2$ basaltic rocks from the Emeishan Igneous Province, SW China, are thought to reflect partial melting of enriched SCLM materials [11]. Basaltic rocks of the Emeishan Igneous Province with higher $TiO_2$ contents that display positive Nb and Ta anomalies are interpreted in terms of partial melting of mantle sources being significantly affected by plume-derived components [11], while relatively high-$TiO_2$ basaltic rocks from Central Nicaragua possessing positive Nb anomalies are thought to have developed from a mantle wedge comparable in composition to an enriched sub-oceanic mantle and unaffected by subduction zone processes [10].

Therefore, if the moderately negative Nb and Ta anomalies displayed by the Faroese low-$TiO_2$ sills resulted from melting of mantle sources affected by metasomatism, the moderately positive Nb and Ta anomalies of the high-$TiO_2$ sills (Figure 3) could indicate magma tapping from dryer Nb and Ta enriched residual mantle sources, from which metasomatic

agents were already extracted. The discussion above, suggesting formation of the Faroese low-$TiO_2$ sills by higher degrees of partial melting relative to the melting percentages required to produce their high-$TiO_2$ counterparts, would be in accordance with more metasomatised materials in sources to the former sills, as the presence of metasomatic agents supposedly enhance mantle melting [96, 104, 128]. However, as all the investigated Faroese high-$TiO_2$ sills, except for the Langaregn Sill, are LREE enriched (Figure 4), the formation of these sills by low-degree melting of a relatively dry Nb and Ta enriched source, which had already experienced a partial melting event, may appear to be problematic, if no other processes were involved, as the LREE within their source rocks would have been strongly partitioned into the first melts, leaving a relatively LREE depleted residue. Refertilisation of relatively dry mantle sources to the high-$TiO_2$ Faroese sills by other highly LREE enriched metasomatic agents could be a plausible explanation and would be in accordance with geochemical modification of upper mantle sources by multiple metasomatic events, as reported for other igneous regions previously [129]. Based on the gentle REE slopes of most high-$TiO_2$ and low-$TiO_2$ sill samples and the modelling above, in addition to their Nb and Ta characteristics, we propose that these sills originated from melting of variously metasomatised mantle materials with compositions comparable to those reported for SCLM materials previously. Formation of basaltic rocks by melting of such materials would fit tentative suggestions by [23] regarding petrogenesis of some of the Faroese lavas and would also fit inferences by [130] regarding origin of alkaline lavas from W Greenland, but would be at odds with earlier theories favouring magma supplies to Faroese lavas/dykes from a deep-rooted mantle plume [7-8].

#### *5.6.3. Geochemical Implications on Heterogeneous Mantle Sources*

While differences between some major elements of the low-$TiO_2$ Faroese sills in particular and local lavas/dykes (insets in Figure 2) could reflect post-melting processes where plagioclase was accumulated in precursor melts to the actual sills, some of the observed differences in trace element characteristics between data for Faroese lavas/dykes and those of the investigated sills (insets in Figure 3; Figure 4; Figure 11) most likely point to differences between their respective mantle sources.

The higher concentrations of LREE in high-$TiO_2$ sills and higher concentrations of LREE and MREE in low-$TiO_2$ sills relative to those of older local basaltic dykes and irregular intrusions with exactly similar $TiO_2$ contents (insets in Figure 4) could indicate a temporal enrichment of these elements in the local upper mantle in Early Cenozoic times, if all these intrusions originated at broadly similar mantle depths. Alternatively, the Faroese sills formed at relatively shallower depths from distinct mantle sources that may or may not have been geochemically affected/metasomatised by the earlier melting to produce melts parental to local dykes and irregular intrusions at deeper mantle levels. The scenario where the enrichment of LREE in high-$TiO_2$ sills and enrichment of LREE and MREE in low-$TiO_2$ sills relative to REEs in their host-rock counterparts with similar $TiO_2$ contents (i.e. Figure 4) could result from small-scale crustal contamination is not realistic, as this would require the contribution from at least a few percent of crustal materials [41]. The steeper HREE slopes in Faroese high-$TiO_2$ dykes and irregular intrusions relative to those of most high-$TiO_2$ sills could indicate some residual garnet or garnet fractionation during their formation, suggesting that they may indeed have developed at mantle levels deeper than those of the sill sources.

Evolution of the Faroese high-$TiO_2$ sills by RTF processes from local low-$TiO_2$ magmas, as suggested for Early Cenozoic basalts of e.g. W Greenland [15], could explain many of the differences in trace element concentrations between these two basalt groups. However, as Nb and Ta are not noticeably fractionated relative to e.g. La and Ce during common rock-forming processes, it is not likely that the moderately negative Nb and Ta anomalies in the Faroese low-$TiO_2$ sills developed to the moderately positive Nb and Ta anomalies, characterising many of the Faroese high-$TiO_2$ sill samples, by RTF processes.

All things considered, it is tentatively suggested that the compositional characteristics of Faroese low-$TiO_2$ and high-$TiO_2$ sills developed in response to tapping of fertile SCLM-like sources affected by metasomatism in various ways, which resulted in slight geochemical differences between the sources to these two categories and also to some degree internally within the high-$TiO_2$ category. There is abundant evidence that metasomatised lithosphere domains exist in other regions of the NAIP such as W Greenland too [130]. If some of the inferred metasomatic agents to low-$TiO_2$ and high-$TiO_2$ Faroese sill sources were not supplied from local Early Cenozoic mantle melting, geological activities associated with the complex geological history within this part of the North Atlantic area could be an alternative explanation. A potential alternative to metasomatic source enrichment would be magma mixing at deeper mantle levels involving recycled crustal materials. The origin of basaltic rocks within a fertile and metasomatised SCLM source during waning stages of regional magmatism, as we tentatively suggest for melts parental to Faroese low$TiO_2$ and high-$TiO_2$ saucer-shaped sills, would be in accordance with inferences regarding late stage magmatism in other LIPs too [104]. [104] pointed out that a thermal anomaly from some sort of a mantle plume at the base of the lithosphere in the Paraná-Etendeka province once provided the heat necessary for basaltic melt production within the overlying fertile metasomatised lithospheric mantle. He inferred melting at successively shallower lithospheric levels with time from the arrival of the presumed mantle plume, provided that overall lithospheric thicknesses exceeded 100 km. [130] inferred a slightly different scenario, where production of basaltic magmas within an enriched metasomatised W Greenland lithospheric mantle was triggered by hot asthenosphere-derived tholeiitic magmas traversing the lithosphere.

The intermediate-$TiO_2$ Morskranes Sill most probably

developed in response to melting of a distinct and geochemically depleted source and the similarity between its REE trend and those representing the local low-$TiO_2$ and intermediate-$TiO_2$ dykes and irregular intrusions analysed in this study (Figure 4) could indicate broadly similar geochemical compositions of their respective mantle sources.

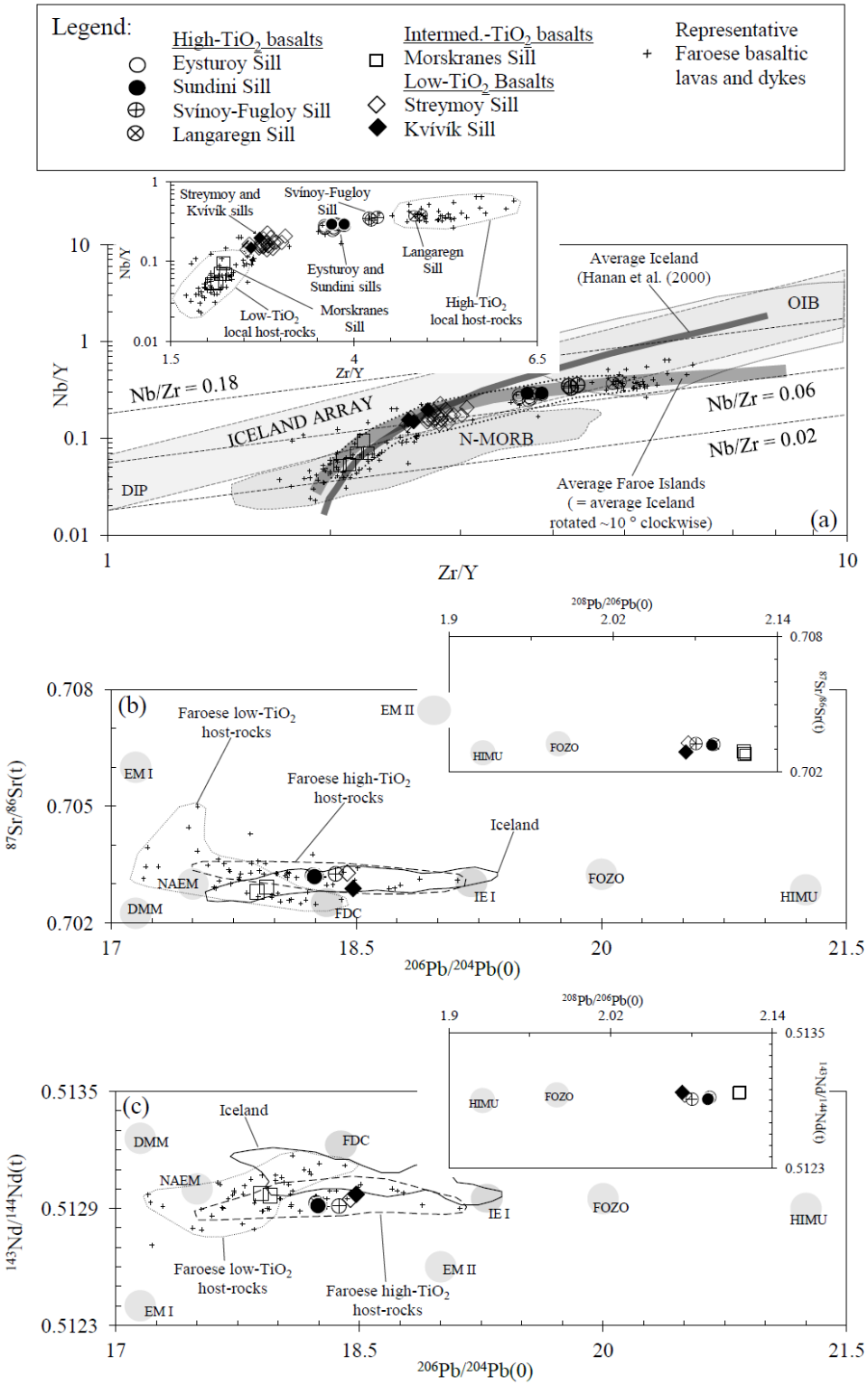


***Figure 11.*** *Geochemical and isotopic data of Faroese sills are compared with data of local basaltic lavas/dykes, Icelandic basaltic rocks and with data from various mantle reservoirs reported for the northern hemisphere. (a) Most Faroese low-$TiO_2$ and intermediate-$TiO_2$ basaltic samples, including sill samples of this study, plot slightly below the lower limit of the "Iceland Array" in a Zr/Y versus Nb/Y ratio diagram, while high-$TiO_2$ lavas/dykes/sills with relatively higher Zr/Y ratios straddle this same lower limit. Literature data in (a): "Iceland Array" field, OIB, DIP (Depleted Iceland Plume) and N-MORB are from [126]; Bold curve representing average Iceland is from [125]. (b) and (c) Samples representing the Faroese sills exhibit relatively well defined trends between end-member mantle reservoirs NAEM and FOZO (and IE 1) in both $^{206}Pb/^{204}Pb(0)$ versus $^{87}Sr/^{86}Sr(t)$ and $^{206}Pb/^{204}Pb(0)$ versus $^{143}Nd/^{144}Nd(t)$ ratio diagrams, but the low-$TiO_2$ and high-$TiO_2$ sill samples are skewed slightly towards the EM reservoirs. The same good correlation is maintained in $^{208}Pb/^{206}Pb$ versus $^{87}Sr/^{86}Sr(t)$ and $^{208}Pb/^{206}Pb$ versus $^{143}Nd/^{144}Nd(t)$ ratio plots (insets). It is noteworthy that Faroese low-$TiO_2$ sill samples together with Faroese high-$TiO_2$ sill samples all plot in the field for local high-$TiO_2$ host-rocks in (b) and (c). Literature data: Iceland, EM I and EM II [63]; HIMU and FOZO [131]; DMM [132]; IE 1 [49]; NAEM [8-22]; FDC [8]. (t) and (0) refer to age corrected and measured isotope ratios respectively. See text for more details.*

#### *5.6.4. NW Atlantic Isotopic Mantle Reservoirs from the Literature*

Isotopic and geochemical similarities between Faroese low-$TiO_2$ lavas and MORB led [23] to infer a depleted asthenospheric source for these lavas, while they attributed $^{87}Sr/^{86}Sr$ ratios of 0.7032 in local high-$TiO_2$ lavas to an origin from mantle materials comparable to sources inferred for ocean island basalts (OIB) within the sub-continental lithospheric mantle or from partial melting of deep mantle "blobs". The source to LREE depleted Faroese low-$TiO_2$ picritic dykes displaying very low $\varepsilon_{Sr}$ and high $\varepsilon_{Nd}$ has previously been interpreted to represent a true depleted end-member composition that may originate from deeper mantle levels when compared to sources to depleted recent basalts of the Reykjanes Ridge and Neogene-recent lavas from Iceland [7]. The Pb isotopic compositions of Faroese high-$TiO_2$ magnesian dykes are thought to reflect mixing between this depleted source and a high $^{208}Pb/^{204}Pb$ end-member source comparable to the one that gave rise to Icelandic samples with the most radiogenic Pb [7]. These authors ascribed the higher $^{208}Pb/^{204}Pb$ ratios at low $^{207}Pb/^{204}Pb$ ratios in most of the other Faroese high-$TiO_2$ dykes relative to those of e.g. comparable basaltic rocks from Iceland, to a main plume component possessing Pb isotopic characteristics that were particular for the Faroese mantle. According to a more recent study, Faroese low-$TiO_2$ basaltic lavas owe their isotopic variations to mixing between a primitive end-member component ($^{206}Pb/^{204}Pb$ = 17.5; $^{87}Sr/^{86}Sr$ = 0.703; $^{143}Nd/^{144}Nd$ = 0.5131), a Faroese depleted component (FDC, $^{206}Pb/^{204}Pb$ = 18.2; $^{87}Sr/^{86}Sr$ = 0.7025; $^{143}Nd/^{144}Nd$ = 0.5132) and an enriched EM-type component [8]. These authors further stated that enriched Faroese high-$TiO_2$ lavas developed from two enriched mantle reservoirs similar to the IE1 and IE2 end-member mantle components proposed as sources to some Icelandic basaltic rocks [49].

[49] suggested five end-member mantle components that could explain the entire isotopic range displayed by the basaltic rocks of Iceland, while [133] invoked a model based on three end-member mantle components/reservoirs *d*, *p* and *e* in order to explain the isotopic range of Icelandic volcanic rocks. [63] attributed the impressive correlation in radiogenic Pb isotope ratios of Icelandic basalts to contributions from HIMU-like components to a main primitive end-member source possessing Pb isotopic compositions comparable to Theistareykir picrites, probably with slight involvement of an additional EM I-like component too, i.e. a mechanism that resembles the model proposed earlier for the BTIB and Faroese lavas respectively [8-22]. A more recent study suggested that involvement of isotopically enriched HIMU mantle components in NAIP mantle sources could be problematic, as these represent extreme isotopic compositions reported only in the southern hemisphere, whereas less enriched FOZO components are thought to occur widely in the mantle on both hemispheres [131]. The isotopic NAEM component ($^{206}Pb/^{204}Pb$ = ~17.5, $^{207}Pb/^{204}Pb$ = ~15.4 and $^{208}Pb/^{204}Pb$ = ~37.4), invoked as a common primitive end-member reservoir throughout the NAIP [22], possesses isotopic composition broadly similar to a depleted end-member NAIP mantle component proposed earlier [8].

#### *5.6.5. Faroese Sill Samples Relative to NW Atlantic Isotopic Mantle Reservoirs*

Altogether, the Faroese sill samples define a rough trend between the isotopic mantle reservoirs NAEM and FOZO, but low-$TiO_2$ and high-$TiO_2$ sills are also skewed slightly towards EM-like mantle reservoirs, when plotted in $^{206}Pb/^{204}Pb$ versus $^{87}Sr/^{86}Sr$ and $^{143}Nd/^{144}Nd$ diagrams (Figure 11b; Figure 11c). The differences in Nd isotopic compositions between samples representing high-$TiO_2$, intermediate-$TiO_2$ and low-$TiO_2$ Faroese sill samples relative to those that outline Icelandic basalts (Figure 11c) suggest that some of their end-member mantle sources differed with respect to their Nd isotopes in particular. The lead isotope signatures displayed by the LREE enriched samples of Faroese low-$TiO_2$ and high-$TiO_2$ sills differ noticeable from those of LREE depleted NAEM-like Faroese low-$TiO_2$ lavas/dykes and Icelandic low-$TiO_2$ lavas from the Theistareykir area, whilst samples of the LREE depleted Morskranes Sill plot closer to the NAEM (Figure 11b; Figure 11c). As the Faroese sill samples do not display any clear association with DMM and FDC isotopic end-member reservoirs (apart from a sample of the Kvívík Sill in Figure 11b), inferred to have influenced the isotopic compositions in Icelandic and Faroese low-$TiO_2$ lavas (Figure 11b; Figure 11c), these are unlikely to have contributed noticeable to the general isotopic characteristics displayed by the actual sill samples. Samples of the Faroese low-$TiO_2$ and high-$TiO_2$ sills in general could originate from mantle sources that displayed moderate isotopic enrichment towards IE 1 or FOZO-like reservoirs (Figure 11b; Figure 11c), a scenario that would be in accordance with the moderately fertile sources we infer to have resulted in their gentle negative REE slopes. The relatively low $^{87}Sr/^{86}Sr(t)$, $^{206}Pb/^{204}Pb$ and (to a lesser degree) $^{207}Pb/^{204}Pb$ ratios in samples representing the small Morskranes Sill relative to samples representing the other local sills point to (a) more depleted mantle source(s) for this small sill relative to those inferred for the other sills, perhaps related to the NAEM isotope reservoir (Figure 5; Figure 11).

On the one hand, samples representing low-$TiO_2$ and high-$TiO_2$ sills combined, as well as all samples representing the intermediate-$TiO_2$ Morskranes Sill, define two almost perfect linear trends when plotted in a $^{206}Pb/^{204}Pb$ versus $^{208}Pb/^{204}Pb$ ratios diagram (Figure 5c). On the other hand, at least three samples representing the Morskranes Sill and two samples representing the Eysturoy and Sundini sills (and perhaps also two samples representing the Streymoy and Kvívík sills) are shifted

towards higher $^{207}Pb/^{204}Pb$ ratios relative to other local sill samples in diagrams, where these lead isotope ratios are plotted against $^{208}Pb/^{204}Pb$ and $^{206}Pb/^{204}Pb$ ratios (Figure 5b; Figure5d). The lead isotope particularities of these Faroese sills could stem either from tapping from mantle reservoirs displaying isotopic heterogeneities (at short length scales in the case of the Morskranes Sill), or they could implicate crustal contamination (i.e. discussion in sub-Sect. 5.2 above).

*[13] suggested a link between increasing $TiO_2$ contents in OIBs worldwide and relative enrichments of their Sr and Nd isotopes, due to decreasing degrees of partial mantle melting of eclogite-bearing peridotites (~1 to ~10% eclogite) with increasing mantle depths, in accordance with the lid effect [13, 14, 120]. The lid effect has also been considered as an important process in parts of the NAIP [8, 9, 16, 17, 18]. The distinct $TiO_2$ compositions, displayed by samples representing the various Faroese sills, could in theory have evolved in response to similar mantle processes, but no clear systematic Sr and Nd isotopic enrichments exist for Faroese high-$TiO_2$ versus low-$TiO_2$ sills (although the low $TiO_2$ sills display slightly elevated $^{143}Nd/^{144}Nd$ ratios relative to all high-$TiO_2$ sills). Also, the limited Sr and Nd isotopic data available for these sills (Figure 5a) render it difficult to assess with any certainty whether they developed in accordance with the lid effect. If these sills indeed formed broadly contemporaneously according to the lid effect, it would imply a very steep or discontinuous local lithospheric base, as lateral distances between most low-$TiO_2$ and high-$TiO_2$ Faroese sills only range from 10 to 15 km (Figure 1). A discontinuous local lithospheric base in the Faroese area could have developed in response to previous regional or provincial tectonic activity. Alternatively, some of the magmas may have experienced noticeable lateral transport, like it has been suggested in recent studies for other low-$TiO_2$ Faroese lavas and during recent volcanic eruptions in Bali, Indonesia [9-134].

# 6. Summary and Concluding Remarks

The basaltic sills of the Faroe Islands can be grouped into three main categories according to their $TiO_2$ contents. The Streymoy and Kvívík sills define a low-$TiO_2$ category, the Eysturoy, Sundini, Langaregn and Svínoy-Fugloy sills define a high-$TiO_2$ category, while samples of the Morskranes Sill are intermediate-$TiO_2$ between these two. It is likely that the high-$TiO_2$ sills developed from three slightly dissimilar mantle sub-sources, i.e. the Eysturoy and Sundini sills, the Langaregn Sill and the Svínoy-Fugloy Sill respectively tapped mantle reservoirs of slightly different geochemical compositions Calculations suggest that differences in $Al_2O_3$, $Fe_2O_3$, $TiO_2$, CaO, MgO, Sr, Eu compositions in particular within the actual intrusions can be explained by various degrees of partial melting, olivine fractionation, as well as plagioclase fractionation and accumulation. Moderately positive and negative Nb and Ta anomalies in some of the sills seem to suggest that their mantle sources were affected by the addition or extraction of metasomatic agents at some point. The inferred petrogenetic sequences for the actual sills can briefly be summarised as follows:

1. The Streymoy and Kvívík sills evolved by fractional crystallisation of mainly olivine (~15 wt%) and net accumulation of plagioclase (15 to 25 wt%) upon ascent. Their REE compositions can be explained by 16 to 21% melting of a moderately fertile mantle at depths of ≤ 85 km and (e.g. Figure 12a).
2. The Eysturoy, Sundini, Svínoy-Fugloy and Langaregn sills evolved by fractional crystallisation of mainly olivine (~15 wt%) and plagioclase (15 to 20 wt%), while en-route to the upper crust. The REE compositions of the first three sills can be accounted for by 5 to 7.5% melting of a moderately fertile mantle at depths of ≤ 85 km, while ~4% melting of a slightly different mantle composition(s) at deeper levels is required for the Langaregn Sill (Figure 12b; Figure 12c).
3. The primary magmas, which eventually evolved to the Morskranes Sill by fractional crystallisation of mainly olivine (~15 wt%) and perhaps some plagioclase (≤ 10 wt%) during ascent, most likely formed by 6 to 7% melting of a moderately depleted mantle at depths of ≤ 85 km (Figure 12d). Isotopic constraints suggest that parts of the Morskranes Sill have experienced slight crustal contamination, or their mantle source(s) displayed slight isotopic heterogeneities a short length scales. Such a contaminant would be of similar composition to that reported earlier for the Rockall Plateau basement and/or E Greenland basement (please see captions Figure 7 for references).
4. The Pb isotope range of local contaminated silicic lavas can be explained in terms of assimilation of materials comparable to those reported for E Greenland, while part of this isotope range could be explained by contamination with materials comparable in isotope compositions to those reported for NW Britain basement. Hence, E Greenland-type basement is apparently ubiquitous beneath the Faroe Islands (please see captions Figure 7 for references).

Based on the limited data of this work, isotopic compositions of most Faroese sill samples can probably be explained in terms of the two well-known isotopic mantle reservoirs NAEM and FOZO, where low-$TiO_2$ and high-$TiO_2$ sills probably also contain slight amounts of materials originating from an EM-like mantle component. Hence, it is likely that at least three main end-member isotopic mantle reservoirs contributed to the isotopic characteristics displayed by the Faroese sills. It is proposed that melt generation to produce the Faroese sills occurred at relatively shallow mantle levels during the waning stages of basaltic magmatism in the NAIP, much similar to what has been envisaged previously for some Early Cretaceous Paraná-Etendeka flood basalts [104].

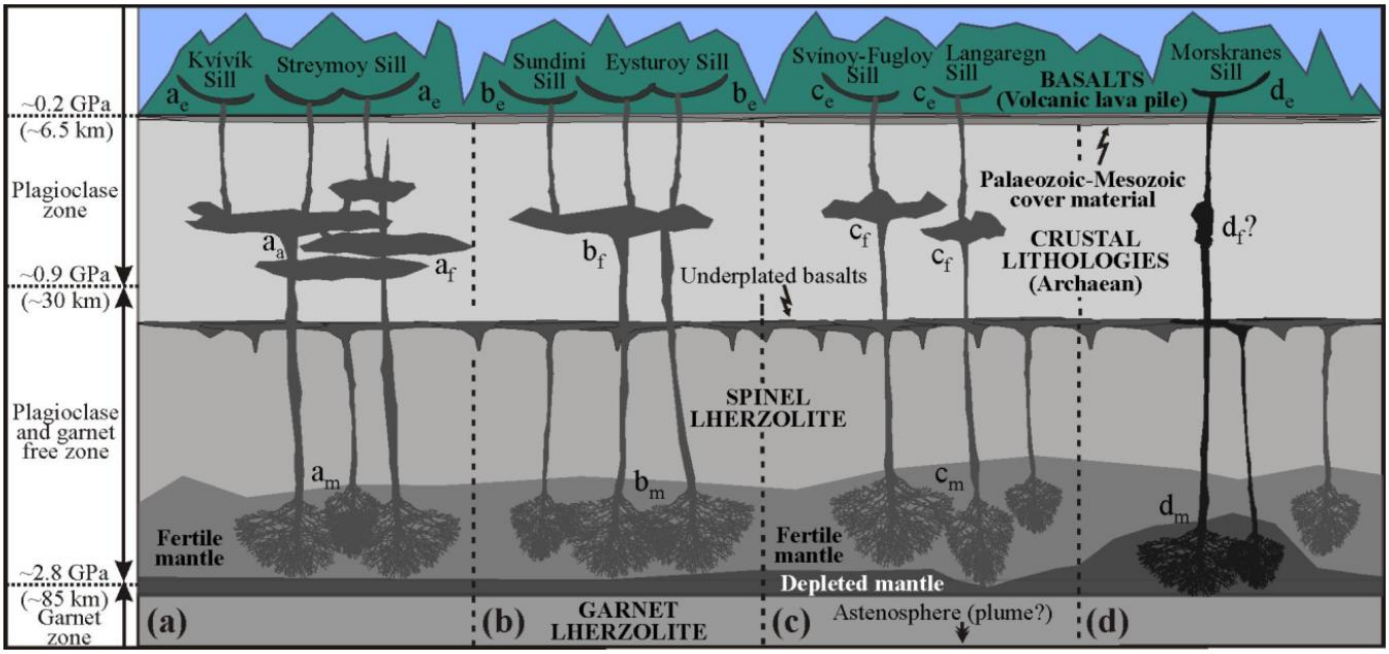


***Figure 12.*** *The simplified profile summarises the inferred petrogenetic processes in action during formation of the Faroese sills. Vertical distances are drawn at arbitrary scales. (a) The Streymoy and Kvívík sills. (b) The Eysturoy and Sundini sills. (c) The Svínoy-Fugloy and Langaregn sills. (d) The Morskranes Sill. The garnet stability field is from [101, 102]. The plagioclase stability field is from [103, 102]. Abbreviations where x represents the letters a-d are: $x_m$ = partial melting; $x_a$ = plagioclase accumulation; $x_f$ = mineral fractionation; $x_e$ = sill emplac ement. See main text for a more detailed explanation.*

*Data availability.* All information on international and/or in-house standard geological samples, used in association with analyses related to this research (i.e. as mentioned in Supplement 2 [51], are available at the actual laboratories: at the Open University, Milton Keynes, UK, and at NGU, Trondheim, NO, for XRF analyses; at Durham University, Durham, UK, and at GEUS, Copenhagen, DK, for the ICP-MS analyses; at Durham University, Durham, UK, and at the Copenhagen University (KU), Copenhagen, DK, for the MC-ICP-MS analyses.

Data on results from calculations/modelling performed in this study can be accessed via Hansen et al. (2019b) via the link: DOI: 10.17632/47fzntf2b3.1

*Author contributions.* The actual manuscript is based upon a relatively recent Ph.D. thesis in geology, defended at Durham University in 2012 by the first author. The actual research and writing/preparation was performed by the first author Jógvan Hansen. All listed co-authors have acted as supervisors at various stages of thesis and paper preparation. In addition, Dougal Jerram initiated the actual research project at Durham University, while Mike Widdowson and Christopher Ottley ran XRF and ICP-MS laboratories at the Open University and at Durham University respectively, where the actual analyses were performed.

*Competing interests.* The authors declare that they have no conflict of interest.

*Disclaimer.* The authors declare that they have nothing to disclaim.

*Acknowledgements.* This manuscript is to a large degree based on data from a previous research project at Durham University, funded by BP, Chevron and Geysir Petroleum, via Jarðfeingi (Faroese Geological Survey). In addition, key data and fieldwork, funded privately by the first author, are of utmost importance for the current version of this paper. AV Faroe Islands is appreciated for provision of basic living costs for the first author during the production of parts of this work. Isotope analyses carried out at the Arthur Holmes Isotope Laboratory, Department of Earth Sciences, Durham University by Dr. Geoff M. Nowell are greatly appreciated. Dougal Jerram acknowledges the support from the Research Council of Norway through its Centres of Excellence funding scheme, project 22372 (CEED - Centre for Eath Evolution and Dynamics). Earlier versions of this paper benefited from reviews by Tod Waight and an anonymous reviewer, while the current manuscript version benefited from reviews by anonymous reviewers at Earth Sciences. Costs associated with the publication of this paper were provided by the Faroese Research Council and are greatly appreciated. The authors of this manuscript are indebted to fellow author Jon Davidson, Durham University, who sadly passed away in 2016, for his thorough work on earlier versions of this paper.

# References

[1] Svensen, H. H., Jerram, D. A., Polozov, A. G., Planke, P., Neal, C. R., Augland, L. E. and Emeleus, H. C. (2019). Thinking about LIPs: a brief history of ideas of large igneous province research, Tectonophysics 760, 229-251. https://doi.org/10.1016/j.tecto.2018.12.008

[2] Meyer, R., Van Wijk, J. and Gernigon, L. (2007). The North Atlantic Igneous Province: A review of models for its formation, Geol. Soc. Am. Spec. Pap. 430, 525-552.

[3] Waagstein, R. (1988). Structure, composition and age of the Faeroe basalt plateau, Geol. Soc. London, Spec. Publ. 39, 225-238.

[4] Gibson, S. A., Thompson, R. N., Dickin, A. P. and Leonardos, O. H. (1995). High-Ti and low-Ti mafic potassic magmas: Key to plume-lithosphere interactions and continental flood-basalt genesis, Earth Plan. Sci. Lett. 136, 149-165.

[5] Peate, D. W. and Hawkesworth, C. J. (1996). Lithospheric to asthenospheric transition in Low-Ti flood basalts from southern Paraná, Brazil, Chem. Geol. 127, l-24.

[6] Jerram, D. A., Single, R. T., Hobbs, R. W. and Nelson, C. E. (2009). Understanding the offshore flood basalt sequence using onshore volcanic facies analogues: an example from the Faroe–Shetland basin, Geol. Mag. 146 (3), 353-367.

[7] Holm, P. M., Hald, N. and Waagstein, R. (2001). Geochemical and Pb-Sr-Nd isotopic evidence for separate hot depleted and Iceland plume mantle sources for the Paleogene basalts of the Faroe Islands, Chem. Geol. 178, 95-125.

[8] Søager, N. and Holm, P. M. (2011). Changing compositions of the Iceland plume; Isotopic and elemental constraints from the Paleogene Faroe flood basalts, Chem. Geol. 280, 297-313.

[9] Millett, J. M., Hole, M. J., Jolley, D. W. and Passey, S. R. (2017). Geochemical stratigraphy and correlation within Large Igneous Provinces: The final preserved stages of the Faroe Islands Basalt Group, Lithos 286–287 1-15.

[10] Walker, J. A., Carr, M. J., Feigenson, M. D. and Kalamarides, R. I. (1990). The petrogenetic significance of interstratified high- and low-Ti basalts in central Nicaragua, J. Petrol. 31 (5), 1141-1164.

[11] Xiao, L., Xu, Y. G., Mei, H. J., Zheng, Y. F., He, B. and Pirajno, F. (2004). Distinct mantle sources of low-Ti and high-Ti basalts from the western Emeishan large igneous province, SW China: implications for plume-lithosphere interaction. Earth Plan. Sci. Lett. 228, 525-546.

[12] Ivanov, A. V., Demonterova, E. I., Rasskazov, S. V. and Yasnygina, T. A. (2008). Low-Ti melts from the southeastern Siberian Traps Large Igneous Province: Evidence for a water-rich mantle source, J. Earth. Syst. Sci. 117 (1), 1-21.

[13] Prytulak, J. and Elliott, T. (2007). $TiO_2$ enrichment in ocean island basalts, Earth Plan. Sci. Lett. 263, 388-403.

[14] Niu, Y., Wilson, M., Humphreys, E. R. and O'Hara, M. J. (2011). The origin of intra-plate ocean island basalts (OIB): the Lid Effect and its geodynamic implications, J. Petrol. 52 (7&8), 1443-1468.

[15] Larsen, L. M., and Pedersen, A. K. (2009). Petrology of the Paleocene Picrites and Flood Basalts on Disko and Nuussuaq, West Greenland, J. Petrol. 50 (9), 1667-1711.

[16] Tegner, C., Lesher, C. E., Larsen, L. M. and Watt, W. S. (1998). Evidence from the rare-earth-element recordof mantle melting for cooling of theTertiary Iceland Plume, Nature 395, 591-594.

[17] Momme, P., Tegner, C., Brooks, C. K. and Keays, R. R. (2006). Two melting regimes during Paleogene flood basalt generation in East Greenland: combined REE and PGE modelling, Contrib. Mineral. Petrol. 151, 88-100.

[18] Waight, T. E. and Baker, J. A. (2012). Depleted basaltic lavas from the Proto-Iceland Plume, Central East Greenland, Journal of Petrology 53 (8), 1569-1596.

[19] Hanghøj, K., Storey, M. and Stecher, O. (2003). An isotope and trace element study of the East Greenland Tertiary dyke swarm: constraints on temporal and spatial evolution during continental rifting, J. Petrol. 44 (11), 2081-2112.

[20] Peate, D. W. and Stecher, O. (2003). Pb isotope evidence for contributions from different Iceland mantle components to Palaeogene East Greenland flood basalts, Lithos 67, 39-52.

[21] Kitagawa, H., Kobayashi, K., Makishima, A. and Nakamura, E. (2008). Multiple pulses of the Mantle Plume: Evidence from Tertiary Icelandic Lavas, J. Petrol. 49 (7), 1365-1396.

[22] Ellam, R. M. and Stuart, F. M. (2000). The sub-lithospheric source of north Atlantic basalts: evidence for, and significance of, a common end-member, J. Petrol. 41 (7), 919-932.

[23] Gariépy, C., Ludden, J. and Brooks, C. (1983). Isotopic and trace element constraints on the genesis of the Faeroe Lava pile, Earth Plan. Sci. Lett. 63, 257-272.

[24] Fram, M. S. and Lesher, C. E. (1997). Generation and polybaric differentiation of East Greenland Early Tertiary flood basalts, J. Petrol. 38 (2), 231-275.

[25] Font, L., Davidson, J. P., Pearson, D. G., Nowell, G. M., Jerram, D. A. and Ottley, C. J. (2008). Sr and Pb IsotopeMicro-analysis of Plagioclase Crystals from Skye Lavas: an Insight into Open-systemProcesses in a Flood Basalt Province, J. Petrol. 49 (8), 1449-1471.

[26] Hald, N. and Waagstein, R. (1983). Silicic basalts from the Faeroe Islannds: evidence of crustal contamination, In: Bott MHP, Saxov S, Talvani M, Thiede J (eds) Structure and development of the Greenland-Scotland Ridge. New methods and concepts. Plenum New York 343-349, 1983.

[27] Hansen, J., Jerram, D. A., McCaffrey, K. J. W. and Passey, S. R. (2011). Early Cenozoic saucer-shaped sills of the Faroe Islands: an example of intrusive styles in basaltic lava piles, J. Geol. Soc. London 168 (1), 159-178.

[28] Jerram, D. A. and Widdowson, M. (2005). The anatomy of Continental Flood Basalt Provinces: geological constraints on the processes and products of flood volcanism, Lithos 79, 385-405.

[29] Hansen, J., Jerram, D. A., McCaffrey, K. J. W. and Passey, S. R. (2009). The onset of the North Atlantic Igneous Province in a rifting perspective, Geol. Mag. 146 (3), 309-325.

[30] Upton, B. G. J. (1988). History of Tertiary igneous activity in the N Atlantic borderlands, Geol. Soc. London, Spec. Publ. 39, 429-453.

[31] Saunders, A. D., Fitton, J. G., Kerr, A. C., Norry, M. J. and Kent, R. W. (1997). The North Atlantic Igneous Province, Geophys. Monogr. 100, 45-93.

[32] Passey, S. R. and Jolley, D. W. (2009). A revised lithostratigraphic nomenclature for the Palaeogene Faroe Islands Basalt group, NE Atlantic Ocean, Earth and Environmental Science Transactions of the Royal Society of Edinburg 99, 127-158.

[33] Bott, M. H. P., Sunderland, J., Smith, P. J., Casten, U. and Saxov, S. (1974). Evidence for continental crust beneath the Faeroe Islands. Nature 248, 202-204.

[34] Richardson, K. R., Smallwood, J. R., White, R. S., Snyder, D. B. and Maguire, P. K. H. (1998). Crustal structure beneath the Faroe Islands and the Faroe-Iceland Ridge, Tectonophys. 300, 159-180.

[35] Raum, T., Mjelde, R., Berge, A. M., Paulsen, J. T., Digranes, P., Shimamura, H., Shiobara, H., Kodaira, S., Larsen, V. B., Fredsted, R. and Harrison, D. J. (2005). Sub-basalt structures east of the Faroe Islands revealed from wide-angle seismic and gravity data, Petrol. Geosci. 11 (4), 291-308.

[36] Sammarco, C., Cornwell, D. G. and Rawlinson, N. (2017). Ambient noise tomography reveals basalt and sub-basalt velocity structure beneath the Faroe Islands, North Atlantic, Tectonophys. 721, 1-11.

[37] Rasmussen, J. and Noe-Nygaard, A. (1969). Beskrivelse til geologisk kort over Færøerne i målestok 1: 50000, Geol. Surv. Denm. 1. Series No. 24.

[38] Rasmussen, J. and Noe-Nygaard, A. (1970). Geology of the Faeroe Islands, Geol. Surv. Denm. I. Series No. 25, 1-142.

[39] Passey, S. R. and Bell, B. R. (2007). Morphologies and emplacement mechanisms of the lava flows of the Faroe Islands Basalt Group, Faroe Islands, NE Atlantic Ocean, Bull. Volc. 70, 139-156.

[40] Noe-Nygaard, A. and Rasmussen, J. (1968). Petrology of a 3, 000 metre sequence of basaltic lavas in the Faeroe Islands, Lithos 1, 286-304.

[41] Hansen, J. (2011). Petrogenetic Evolution, Geometries and Intrusive Styles of the Early Cenozoic Saucer-Shaped Sills of the Faroe Islands. Doctoral thesis, Durham University. Available at Durham E-Theses Online http://etheses.dur.ac.uk/3631/.

[42] Waagstein, R., Guise, P. and Rex, D. (2002). K/Ar and $^{39}Ar/^{40}Ar$ whole-rock dating of zeolite facies metamorphosed flood basalts: the upper Paleocene basalts of the Faroe Islands, NE Atlantic, Geol. Soc. London, Spec. Publ. 197, 219-252.

[43] Storey, M., Duncan, R. A. and Tegner, C. (2007). Timing and duration of volcanism in the North Atlantic Igneous Province: implications for geodynamics and links to the Iceland hotspot, Chem. Geol. 241, 264-281.

[44] Ellis, D., Bell, B. R., Jolley, D. W. and O'Callaghan, M. (2002). The Stratigraphy, environment of eruption and age of ther Faroes Lava Group, NE Atlantic Ocean, Geol. Soc. London, Spec. Publ. 197, 253-269.

[45] Hald, N. and Waagstein, R. (1984). Lithology and chemistry of a 2-km sequence of Lower Tertiary tholeiitic lavas drilled on Suðuroy, Faeroe Islands (Lopra-1), In: Berthelsen O., Noe-Nygaard A. and Rasmussen J. (eds) The deep drilling project 1980-1981 in the Faeroe Islands. Annales Societatis Scientiarum Færoensis, Tórshavn, Supplementum IX 15-38.

[46] Søager, N. and Holm, P. M. (2009). Extended correlation of the Paleogene Faroe Islands and East Greenland plateau basalts, Lithos 107, 205-215.

[47] Hald, N. and Waagstein, R. (1991). The dykes and sills of the Early Tertiary Faeroe Island basalt plateau, Trans. Royal Soc. Edinburg: Earth Sci. 82, 373-388.

[48] Jolley, D. W., Passey, S. R., Hole, M. and Millett, J. (2012). Large-scale magmatic pulses drive plant ecosystem dynamics, J. Geol. Soc. 169 (6), 03-711.

[49] Thirlwall, M. F., Gee, M. A. M., Taylor, R. N. and Murton, B. J. (2004). Mantle components in Iceland and adjecent ridges investigated using douple-spike Pb isotope ratios, Geochim. Cosmochim. Acta 68 (2), 361-386.

[50] Larsen, L. M., Waagstein, R., Pedersen, A. K. and Storey, M. (1999). Trans-Atlantic correlation of the Palaeocene volcanic successions in the Faeroe Islands and East Greenland, J. Geol. Soc. London 156, 1081-1095.

[51] Hansen, J., Jerram, D. A., Ottley, C. J. and Widdowson, M. (2019a). Supplements related to the paper: "Contrasting $TiO_2$ compositions in Early Cenozoic mafic sills of the Faroe Islands: an example of basalt formation from distinct melting regimes". Mendeley Data, DOI: 10.17632/s895tync87.2.

[52] Turner, S. R., Platt, J. P., George, R. M. M., Kelley, S. P., Pearson, D. G. and Nowell, G. M. (1999). Magmatism associated with orogenic collapse of the Betic–Alboran domain, SE Spain, J. Petrol. 40, 1011–1036.

[53] Ottley, C. J., Pearson, D. G. and Irvine, G. J. (2003). A routine method for the dissolution of geological samples for the analysis of REE and trace elements via ICP –MS, In: Plasma Source Mass Spectrometry, Applications and Emerging Technologies, (J. G. Holland, S. D. Taner, Eds.). Royal Soc. Chem. 221–230.

[54] Dowall, D. P., Nowell, G. M. and Pearson, D. G. (2003). Chemical pre-concentration procedures for high-precision analysis of Hf-Nd-Sr isotopes in geological materials by plasma ionisation multi-collector mass spectrometry (PIMMS) techniques, In: Holland J. G. and Tanner S. D. Eds. Plasma Source Mass Spectrometry: Applications and Emerging Technologies, The R. Soc. Chem. Cambridge 321-337.

[55] Charlier, B. L. A., Ginibre, C., Morgan, D., Nowell, G. M., Pearson, D. G., Davidson, J. P. and Ottley, C. J. (2006). Methods for the microsampling and high precision analysis of strontium and rubidium isotopes at single crystal scale for petrological and geochronological applications, Chem. Geol. 232, 114-133.

[56] Frei, R., Villa, I. M., Nägler, Th. F., Kramers, J. D., Pryzbylowicz, W. J., Prozesky, V. M., Hofmann, B. A. and Kamber, B. S. (1997). Single mineral dating by Pb–Pb step-leaching method; assessing the mechanisms, Geochim. Cosmochim. Acta 61, 393–414.

[57] Schaller, M., Steiner, O., Suder, I., Frei, R. and Kramers, J. D. (1997). Pb stepwise leaching (PbSL) dating of garnet—addressing the inclusion problem. Schweiz, Min. Pet. Mitt. 77, 113–121.

[58] Todt, W., Cliff, R. A., Hanser, A. and Hofmann, A. W. (1993). Re-calibration of NBS lead standards using $^{202}Pb$ + $^{205}Pb$ double spike, Terra Abstract 5, 396.

[59] Deer, W. A., Howie, R. A. and Zussman, J. (1992). An introduction to the rock forming minerals. Second edition., Longman pp. 696.

[60] McDonough, W. F. and Sun, S.-s. (1995). The composition of the Earth, Chem. Geol. 120, 223-253.

[61] Steiger, R. H. and Jäger, E. (1977). Subcommission on geochronology: convention of the use of decay constants in geo- and cosmochronology, Earth Plan. Sci. Lett. 36, 359-362.

[62] Lugmair, G. W. and Marti, K. (1978). Lunar initial $^{143}Nd/^{144}Nd$: differential evolution of the lunar crust and mantle, Earth Plan. Sci. Lett. 39, 349-357.

[63] Stracke, A., Zindler, A., Salters, V. J. M., McKenzie, D., Blichert-Toft, J., Albaréde, F. and Grønvold, K. (2003). Theistareykir revisited, Geochem. Geophys. Geosyst. 4 (2), pp. 49.

[64] Kokfeldt, T. F., Hoernle, K., Hauff, F., Fiebig, J., Werner, R. and Schônberg, D. G-S. (2006). Combined Trace Element and Pb-Nd–Sr-O Isotope Evidence for Recycled Oceanic Crust (Upper and Lower) in the Iceland Mantle Plume, J. Petrol. 47 (9), 1705-1749, 2006.

[65] Rollinson, H. (1998). Using geochemical data: evaluation, presentation, interpretation, Longman, pp. 352.

[66] Wood, D. A., Gibson, I. L. and Thompson, R. N. (1976). Elemental mobility during zeolite facies metamorphism of the Tertiary basalts of eastern Iceland, Contrib. Mineral. Petrol. 55, 241-254.

[67] Higgins, N. C., Solomon, M. and Varne, R. (1985). The genesis of the Blue Tier Batholith, northeastern Tasmania, Lithos 18, 129-149.

[68] Babechuk, M. G., Widdowson, M. and Kamber, B. S. (2014). Quantifying chemical weathering intensity and trace element release from two contrasting basalt profiles, Deccan Traps, India, Chem. Geol. 363, 56-75.

[69] Thompson, R. N., Morrison, M. A., Dickin, A. P. and Hendry, G. L. (1983). Continental flood basalts... Arachnids Rule OK?, In: Hawkesworth C. J., Norry M. J. (eds) Continental flood basalts and mantle xenoliths, Shiva, Nantwick, UK 158-185.

[70] Kerr, A. C., Kempton, P. D. and Thompson, R. N. (1995). Crustal assimilation during turbulent magma ascent (ATA); new isotopic evidence from the Mull Tertiary lava succession, N. W. Scotland, Contrib. Mineral. Petrol. 119, 142-154.

[71] Sun, S.-s and McDonough, W. F. (1989). Chemical and isotopic systematics of oceanic basalts: implications for mantle composition and processes, Geol. Soc. London, Spec. Publ. 42, 313-345, doi: 10.1144/GSL. SP.1989.042.01.19

[72] Kays, M. A., Goles, G. G. and Grover, T. W. (1989). Precambrian sequence bordering the Skaergaard Intrusion, J. Petrol. 30 (2), 321-361.

[73] Kalsbeek, F. (1995). Geochemistry, tectonic setting, and poly-orogenic history of Palaeoproterozoic basement rocks from the Caledonian fold belt of North-East Greenland, Precamb. Res. 72, 301-315.

[74] Thrane, K. (2002). Relationships between Archaean and Palaeoproterozoic crystalline basement complexes in the southern part of the East Greenland Caledonides: an ion microprobe study, Precamb. Res. 113, 19-42.

[75] Weaver, B. L. and Tarney, J. (1980). Rare earth geochemistry of Lewisian granulite-facies gneisses, northwest Scotland: implications for the petrogenesis of the Archaean lower continental crust, Earth Plan. Sci., Lett. 51, 279-296.

[76] Thompson, R. N., Morrison, M. A., Dickin, A. P., Gibson, I. L. and Harmon, R. S. (1986). Two contrasting styles of interaction between basic magmas and continental crust in the British Tertiary Igneous Province, J. Geophys. Res. 91 (B6), 5985-5997.

[77] Meyer, R., Nicoll, G. R., Hertogen, J., Troll, V. R., Ellam, R. M. and Emelius, C. H. (2009). Trace element and isotope constraints on crustal anatexis by upwelling mantle melts in the North Atlantic Igneous Province: an example from the Isle of Rum, NW Scotland, Geol. Mag. 146 (3), 382-399.

[78] Morton, A. C. and Taylor, P. N. (1991). Geochemical and isotopic constraints on the nature and age of basement rocks from Rockall Bank, NE Atlantic, J. Geol. Soc. London 148, 631-634.

[79] Hansen, J., Davidson, J. P., Jerram, D. A., Ottley, C. J. and Widdowson, M. (2019b). Data sets showing calculations/modelling on basaltic rocks of the Faroe Islands. Mendeley, 2019, DOI: 10.17632/47fzntf2b3.1.

[80] Saal, A. E., Hart, S. R., Shimizu, N., Hauri, E. H. and Layne, G. D. (1998). Pb isotopic variability in melt inclusions from oceanic island basalts, Polynesia, Science 282, 1481-1484.

[81] Bryce, J. G. and DePaolo, D. J. (2004). Pb isotopic heterogeneity in basaltic phenocrysts. Geochim. Cosmochim. Acta 68 (21), 4453-4468.

[82] Faure, G. (2001). Origin of igneous rocks: the isotopic evidence, Springer Verlag. Berlin, Heidelberg, New York pp. 495.

[83] Blichert-Toft, J., Lesher, C. E. and Rosing, M. T. (1992). Selectively contaminatcd magmas of the Tertiary East Greenland macrodyke complex, Contrib. Mineral. Petrol. 110, 154-172.

[84] Taylor, P. N., Kalsbeek, F. and Bridgwater, D. (1992). Discrepancies between neodymium, lead and strontium model ages from the Precambrian of southern East Greenland: Evidence for a Proterozoic granulite-facies event affecting Archaean gneisses, Chem. Geol. 94, 281-291.

[85] Dickin, A. P. (1981). Isotope geochemistry of Tertiary igneous rocks from the Isle of Skye., J. Petrol. 22, 155-189.

[86] Geldmacher, J., Haase, K. M., Devey, C. W. and Garbe-Schönberg, C. D. (1998). The petrogenesis of Tertiary cone-sheets in Ardnamurchan, NW Scotland: petrological and geochemical constraints on crustal contamination and partial melting, Contrib Mineral Petrol. 131, 196-209.

[87] Troll, V. R., Donaldson, C. H. and Emeleus, C. H. (2004). Pre-eruptive magma mixing in ash-flow deposits of the Tertiary Rum Igneous Centre, Scotland, Contrib Mineral Petrol. 147, 722-739.

[88] Yaxley, G. M. (2000). Experimental study of the phase and melting relations of homogeneous basalt + peridotite mixtures and implications for the petrogenesis of flood basalts, Contrib. Mineral. Petrol. 139, 326-338.

[89] Bernstein, S. (1994). High-pressure fractionation in rift-related basaltic magmatism: Faeroe plateau basalts, Geology 22, 815-818.

[90] O'Hara, M. J. and Mathews, R. E. (1981). Geochemical evolution in an advancing, periodically replenished, periodically tapped, continuously fractionated magma chamber, J. Geol. Soc. London 138, 237-277.

[91] Falloon, T. J., Green, D. H., Danyushevskyi, L. V. and Faul, U. H. (1999). Peridotite Melting at 1·0 and 1·5 GPa: an Experimental Evaluation of Techniques using Diamond Aggregates and Mineral Mixes for Determination of Near-solidus Melts, J. Petrol. 40 (9), 1343-1375.

[92] Dasgupta, R., Hirschmann, M. M. and Smith, N. D. (2007). Partial melting experiments of peridotite + $CO_2$ at 3 GPa and genesis of alkalic ocean island basalts. J. Petrol. 48 (11), 2093-2124.

[93] Lesnov, F. P., Koz'menko, O. A., Nikolaeva, I. V. and Palesskii, S. V. (2009). Residence of incompatible trace elements in a large spinel lherzolite xenolith from alkali basalt of Shavaryn Tsaram-1 paleovolcano (western Mongolia), Russ. Geol. Geophys. 50, 1063–1072.

[94] Kretz, R. (1983). Symbols for rock-forming minerals, Am. Mineral. 68, 277-279.

[95] Hirose, K. and Kushiro, I. (1993). Partial melting of dry peridotites at high pressures: Determination of compositions of melts segregated from peridotite using aggregates of diamond, Earth Plan. Sci. Lett. 114, 477-489.

[96] Hirose, K. and Kawamoto, T. (1995). Hydrous partial melting of lherzolite at 1 GPa: The effect of $H_2O$ on the genesis of basaltic magmas, Earth Plan. Sci. Lett. 133, 463-473.

[97] Kogiso, T., Hirose, K. and Takahashi, E. (1998). Melting experiments on homogeneous mixtures of peridotite and basalt: application to the genesis of ocean island basalts, Earth Plan. Sci. Lett. 162, 45-61.

[98] Lange, A. E., Nielsen, R. L., Tepley, III. F. J. and Kent, A. J. R. (2013). The petrogenesis of plagioclase-phyric basalts at mid-ocean ridges, Geochem. Geophys. Geosyst. 14 (8), 3282-3296.

[99] Kushiro, I. (1996). Partial melting of a fertile mantle peridotite at high pressures: An experimental study using aggregates of diamond, Geophys. Monogr. 95, 109-122.

[100] Kushiro, I. (2001). Partial melting experiments on peridotite and origin of mid-ocean ridge basalts, Ann. Rev. Earth Plan., Sci. 29, 71-107.

[101] Robinson, J. A. C. and Wood, B. J. (1998). The depth of the spinel to garnet transition at the peridotite solidus, Earth Plan. Sci. Lett. 164, 277-284.

[102] Presnall, D. C., Gudfinnsson, G. H. and Walters, M. J. (2002). Generation of mid-ocean ridge basalts at pressures from 1 to 7 GPa. Geochim. Cosmochim. Acta, 66 (120), 2073-2090. https://doi.org/10.1016/S0016-7037 (02) 00890-6

[103] Borghini, G., Fumagalli, P. and Rampone, E. (2010). The stability of plagioclase in the upper mantle: Subsolidus experiments on fertile and depleted lherzolite. J. Petrol. 51 (1-2), 229-254.

[104] Peate, D. W. (1997). The Parana-Etendeka Province. Large Igneous Provinces: Continental, Oceanic, and Planetary Flood Volcanism, Geophys. Monogr. 100, 217-245.

[105] Obata, M. and Morten, L. (1987). Transformation of Spinel Lherzolite to Garnet Lherzolite in Ultramafic Lenses of the Austridic Crystalline Complex, Northern Italy, J. Petrol. 28 (3), 599-623.

[106] Ionov, D. A., Bodinier, J-L., Mukasa, S. B. and Zanetti, A. (2002). Mechanisms and sources of mantle metasomatism: major and trace element compositions of peridotite xenoliths from Spitsbergen in the context of numerical modelling, J. Petrol. 43 (12), 2219-2259.

[107] Downes, H., MacDonald, R., Upton, B. G. J., Cox, K. G., Bodinier, J-L., Mason, P. R. D., James, D., Hill, P. G. and Hearn, B. C. (2004). Ultramafic xenoliths from the Bearpow Mountains, Montana, USA: Evidence for multiple metasomatic events in the lithospheric mantle beneath the Wyoming Craton, J. Petrol. 45 (8), 1631-1662.

[108] Choi, S. H. and Kwon, S-T. (2005). Mineral chemistry of spinel peridotite xenoliths from Baengnyeong Island, South Korea, and its implications for the paleogeotherm of the uppermost mantle, The Island Arc 14, 236-253.

[109] McDonough, W. F. (1994). Chemical and isotopic systematics of continental lithospheric mantle, In: H. O. A. Meyer and O. H. Leonardos (Editors), Proc. 5th Int. Kimberlite Conf., CPRM (Comp. Pesq. Recurs. Miner.), Brasilia pp. 478-485.

[110] Ntaflos, T., Tschegg, C., Coltorti, M., Akinin, V. V. and Kosler, J. (2008). Asthenospheric signature in fertile spinel lherzolites from the Viliga Volcanic Field in NE Russia, From: Coltorti M. and Gregoire M. (eds) Metasomatism in Oceanic and Continental Lithospheric Mantle. Geol. Soc., London, Spec. Publ. 293, 57–81.

[111] Rampone, E., Romairone, A. and Hofmann, A. W. (2004). Contrasting bulk and mineral chemistry in depleted mantle peridotites: evidence for reactive porous flow, Earth Plan. Sci. Lett. 218, 491-506.

[112] Workman, R. K. and Hart, S. R. H. (2005). Major and trace element composition of the depleted MORB mantle (DMM), Earth Plan. Sci. Lett. 231, 53-72.

[113] Villaseca, C., Ancochea, E., Orejana, D. and Jeffries, T. E. (2010). Composition and evolution of the lithospheric mantle in central Spain: inferences from peridotite xenoliths from the Cenozoic Calatrava volcanic field, From: Coltorti, M., Downes, H., Gregoire, M. & O'Reilly, S. Y. (eds) Petrological Evolution of the European Lithospheric Mantle, Geol. Soc. London, Spec. Publ. 337, 125–151.

[114] Kerr, A. C. (1995). The geochemistry of the Mull-Morvern Tertiary lava succession, NW Scotland: an assessment of mantle sources during plume-related volcanism, Chem. Geol. 122 (1-4), 43-58.

[115] Wood, D. A. (1979). A variably veined suboceanic upper mantle – Genetic significance for mid-ocean ridge basalts from geochemical evidence, Geology 7, 499-503.

[116] Hofmann, A. W. (2003). Treatise on Geochemistry, Volume 2. Editor: Richard W. Carlson. Executive Editors: Heinrich D. Holland and Karl K. Turekian, pp. 568, ISBN 0-08-043751-6, Elsevier 61-101.

[117] Dupuy, C., Mével, C., Bodinier, J-L. and Savoyant, L. (1991). Zabargad peridotite: Evidence for multistage metasomatism during Red Sea rifting, Geology 19, 722-725.

[118] Grégoire, M., Bell, D. R. and Le Roex, A. P. (2003). Garnet lherzolites from the Kaapvaal Craton (South Africa): trace element evidence for a metasomatic history, J. Petrol. 44 (4), 629-657.

[119] Klein, E. M. and Langmuir, C. H. (1987). Global correlations of ocean ridge basalt chemistry with axial depth and crustal thickness, J. Geophys. Res. 92 (B8), 8089-8115.

[120] Fodor, R. V. (1987). Low- and high-$TiO_2$ flood basalts of southern Brazil: origin from picritic parentage and a common mantle source, Earth Plan. Sci. Lett. 84, 423-430.

[121] Korenaga, J. and Kelemen, P. B. (2000). Major element heterogeneity in the mantle source of the North Atlantic Igneous Province, Earth Plan. Sci. Lett. 184, 251-268.

[122] Scarrow, J. H. and Cox, K. G. (1995). Basalts generated by decompressive adiabatic melting of a mantle plume: A case study from the Isle of Skye, NW Scotland, J. Petrol. 36, 3-22.

[123] Kogiso, T., Hirschmann, M. M. and Pertermann, M. (2004). High-pressure partial melting of mafic lithologies in the mantle, J. Petrol. 45 (12), 2407-2422, 2004.

[124] Blatt, H. and Tracy, R. J. (1995). Petrology, Igneous, Sedimentary, and Metamorphic, Second edition. W. H. Freeman and Company, New York pp. 529.

[125] Hanan, B. B., Blichert-Toft, J., Kingsley, R. and Schilling, J-G. (2000). Depleted Iceland mantle plume geochemical signature: artifact of multicomponent mixing?, Geochem. Geophys. Geosyst. 1 (1), pp. 19.

[126] Fitton, J. G., Saunders, A. D., Kempton, P. D. and Hardarson, B. S. (2003). Does depleted mantle form an intrinsic part of the Iceland plume?, Geochem. Geophys. Geosyst. 4 (3), pp. 14.

[127] Zhang, P-F., Tang, Y-J., Hu, Y., Zhang, H-F., Su, B-X., Xiao, Y. and Santosh, M. (2012). Review of melting experiments on carbonated eclogite and peridotite: insights into mantle metasomatism, Int. Geol. Rev. 54 (12), 1443-1455.

[128] Green, D. H. and Falloon, T. J. (2005). Primary magmas at mid-ocean ridges, "hotspots," and other intraplate settings: Constraints on mantle potential temperature, in Foulger GR, Natland J H, Presnall D C, Anderson D L, eds., Plates, plumes, and paradigms: Geol. Soc. of Am. Spec. Paper 388, 217-247.

[129] Peccerillo, A. (1999). Multiple mantle metasomatism in central-southern Italy: geochemical effects, timing and geodynamic implications, Geology 27 (4), 315-318.

[130] Larsen, L. M., Pedersen, A. K., Sundvoll, B. and Frei, R. (2003). Alkali picrites formed by melting of old metasomatized lithospheric mantle: Manîtdlat Member, Vaigat Formation, Palaeocene of West Greenland, J. Petrol. 44 (1), 3-38.

[131] Stracke, A., Hofmann, A. W. and Hart, S. T. (2005). FOZO, HIMU, and the rest of the mantle zoo, Geochem. Geophys. Geosyst. 6 (5), pp. 20.

[132] Zindler, A. and Hart, S. (1986). Chemical geodynamics, Ann. Rev. Earth Plan. Sci. 14, 493-571.

[133] Hanan, B. B. and Schilling, J-G. (1997). The dynamic evolution of the Iceland mantle plume: the lead isotope perspective, Earth Plan. Sci. Lett. 151, 43-60.

[134] Albino, F., Briggs, J. and Syahbana, D. K. (2019). Dyke intrusion between neighbouring arc volcanoes responsible for 2017 pre-eruptive seismic swarm at Agung, Nature Com. 10, 748, https://doi.org/10.1038/s41467-019-08564-9.